


Date: 8-Mar-19	Deliverable	
Project: Life4Fish project	University of Liege (ULiege) Hydraulics in environmental and civil engineering (HECE)	
Version: V1	Quartier Polytech 1, Allée de la Découverte 13 Bât. B52/3 - B-4000 Liège 1 (Belgique) ☎ + 32 (4) 366 95 96 - 📠 + 32 (4) 366 95 58 s.erpicum@uliege.be - <a href="http://www.hece.ulg.ac.be">www.hece.ulg.ac.be</a>	Contact name: Sébastien Erpicum

# DOWNSTREAM FISH MIGRATION ALONG THE LOW MEUSE RIVER



## Action A3

Modelling of the passages through the hydraulic works in order to design the solutions

***Deliverable – Numerical and physical hydraulic models of the pilot sites + design of the fish passages (Actions C1 & C2)***





Révision				
Ind.	Date	Published by	Checked by	Remarks
0	4/01/19	Epicum S./ Archambeau P.	Pirotton M.	First version
1	8/03/19	Epicum S.	Epicum S.	Update of deliverable format given project template

## TABLE OF CONTENTS

<b>I.</b>	<b>Introduction.....</b>	<b>11</b>
<b>II.</b>	<b>Fish monitoring and hydrodynamic data .....</b>	<b>12</b>
II.1	Data filtering .....	12
II.2	Smolts.....	14
II.2.1	Monitoring data .....	14
II.2.1.1	Temporal analysis .....	14
II.2.1.2	Spatial analysis .....	15
II.2.2	Hydraulic variables during monitoring period .....	17
II.2.2.1	Free surface levels at the upstream reach of the mobile dams .....	17
II.2.2.2	Discharges of the Meuse river .....	17
II.2.2.3	Operation of the facilities .....	18
II.2.3	Guidelines for the prescription of the hydrodynamic conditions.....	19
II.3	Eels .....	20
II.3.1	Monitoring data .....	20
II.3.1.1	Temporal analysis .....	20
II.3.1.2	Spatial analysis .....	21
II.3.2	Hydraulic variables during monitoring period .....	23
II.3.2.1	Free surface levels at the upstream reach of the mobile dams .....	23
II.3.2.2	Discharges of the Meuse river .....	23
II.3.2.3	Operation of the facilities .....	24
II.3.3	Discharge distribution at the passage of eels .....	25
II.4	Guidelines for the prescription of the hydrodynamic conditions.....	28
<b>III.</b>	<b>Setup of the Numerical modelling.....</b>	<b>29</b>
III.1	Flow solver WOLF2D .....	29
III.1.1	The WOLF package .....	29
III.1.2	The solver WOLF2D .....	29
III.1.3	Reproduction of the bottom friction .....	30
III.2	Topographic modelling .....	30
III.2.1	Grands-Malades .....	30
III.2.2	Ivoz-Ramet .....	31
III.3	Hydraulic conditions.....	32
III.3.1	Boundary conditions .....	32

III.3.2	Influence of the reproduction of the surface beam.....	32
<b>IV.</b>	<b>Influence of the mesh resolution and turbulence activation .....</b>	<b>34</b>
IV.1	Influence of the turbulence activation.....	34
IV.2	Influence of the mesh resolution.....	35
IV.3	Conclusion.....	37
<b>V.</b>	<b>Correlations between the hydraulic parameters and smolt monitoring data .....</b>	<b>38</b>
V.1	Smolts at Grands-Malades .....	39
V.1.1	Hydrodynamic scenarios representative of the period of observation .....	39
V.1.2	Density maps and maps of hydrodynamic parameters .....	42
V.1.3	Probability density functions .....	45
V.2	Smolts at Ivoz-Ramet .....	47
V.2.1	Hydrodynamic scenarios representative of the period of observation .....	47
V.2.2	Density maps and maps of hydrodynamic parameters .....	47
V.2.3	Probability density functions .....	49
V.3	Conclusion.....	50
<b>VI.</b>	<b>Velocity fields corresponding to eels passing through the turbines .....</b>	<b>52</b>
VI.1	Impact of discharges at the dam on the attraction of the eels at Grands-Malades.....	52
VI.2	Configuration with eel passages either through the turbines or through the dam at Ivoz-Ramet	53
VI.3	Conclusion.....	54
<b>VII.</b>	<b>Numerical design of the fish passages.....</b>	<b>55</b>
VII.1	Design assumptions .....	55
VII.2	Velocity distribution for the actual configuration.....	55
VII.3	Numerical simulations of fish passage configurations.....	56
VII.3.1	Overview of the configurations.....	56
VII.3.2	Fish passage on a gate of the mobile dam (full width of the gate) (configurations G0 and I0)	57
VII.3.3	Fish passage at the upstream of the pier between the hydropower plant and the mobile dam at Grands-Malades (G1 and G2) .....	58
VII.3.4	Fish passage in the Meuse river side of the pier between the hydropower plant and the mobile dam at Ivoz-Ramet (I1 and I2) .....	59
VII.3.5	Fish passage at the downstream of the pier between the hydropower plant and the mobile dam at Grands-Malades (G3).....	60
VII.3.6	Detailed design at Grands-Malades (G4 and G5).....	60
VII.3.7	Detailed design at Ivoz-Ramet (I3 and I4) .....	61





VII.4	Conclusion .....	62
<b>VIII.</b>	<b>Characteristics of the physical scale models .....</b>	<b>63</b>
VIII.1	Model extent and upstream boundary condition.....	63
VIII.1.1	Configurations.....	63
VIII.1.2	Grands-Malades pilot site .....	64
VIII.1.3	Ivoz-Ramet pilot site .....	66
VIII.2	Similitude .....	67
VIII.3	Scale factor .....	68
VIII.4	Scale model layout .....	68
VIII.5	Water supply system.....	69
VIII.6	Materials .....	70
VIII.7	Boundary conditions .....	70
VIII.8	Measurement devices.....	70
VIII.9	Drawings.....	70
VIII.10	Views of the scale models.....	71
<b>IX.</b>	<b>Geometry of the fish passages intakes .....</b>	<b>73</b>
IX.1	Methodology.....	73
IX.2	Grands Malades pilot site .....	73
IX.2.1	Initial geometry .....	73
IX.2.2	Optimized geometry .....	76
IX.3	Ivoz Ramet pilot site.....	77
IX.3.1	Initial geometry .....	77
IX.3.2	Modified geometry .....	80
IX.4	Conclusion .....	81
<b>X.</b>	<b>General conclusions .....</b>	<b>82</b>

## TABLES

Table 1: Number of 2D coordinates, redundant data and filtered data with the different filtering methods.	13
Table 2 : Tracking of smolts at the sites of Grands Malades and Ivoz-Ramet.	14
Table 3 : Tracking of eels at the sites of Grands Malades and Ivoz-Ramet.	20
Table 4: Correlation C and error E coefficients between the distributions of unit discharges $q$ in the x- and y-directions computed with or without a turbulence model at Grands-Malades.	35
Table 5: Correlation C and error E coefficients between the distributions of unit discharges $q$ in the x- and y-directions computed with a mesh resolution of 50 cm and with mesh resolutions of 2 m and 4 m.	36
Table 6 : Discharge at the turbines of the hydropower plant at Grands-Malades during the fish tracking and fraction of fish coordinates corresponding to different combinations of turbine operation.	41
Table 7 : Number of smolts observed for the different combinations of turbine operation.	41
Table 8 : Correlation and error coefficients for the unit discharge distribution resulting from the computation of the designs 1 to 3 of the laboratory model compared to the results obtained for the numerical model – Grands-Malades.	65
Table 9 : Correlation and error coefficients for the unit discharge distribution resulting from the computation of the designs 1 to 3 of the laboratory model compared to the results obtained for the numerical model – Ivoz-Ramet.	67

## FIGURES

Figure II-1: Values of the Dilution of Precision (DOP) parameter as a function of the raw absolute fish velocity.	14
Figure II-2 : Number of smolts detected at Grands-Malades and Ivoz-Ramet over the entire period of tracking.	15
Figure II-3 : Number of smolts detected at Grands-Malades and Ivoz-Ramet over the three first days of tracking.	15
Figure II-4: Density maps at Grands-Malades with a mesh resolution of 2.5 m and threshold absolute velocities of 1 m/s and 1.5 m/s.	16
Figure II-5: Density maps at Ivoz-Ramet with a mesh resolution of 5 m and threshold absolute velocities of 1 m/s and 1.5 m/s.	16
Figure II-6: Density maps at Ivoz-Ramet during the lock operation with a mesh resolution of 5 m and a threshold absolute velocity of 1 m/s.	17
Figure II-7 : Evolution of the free surface levels at Grands-Malades and Ivoz-Ramet during the monitoring of the smolts.	17
Figure II-8 : Localisation of the gauging station of Amay.	18
Figure II-9 : Discharge of the Meuse river at Amay during the monitoring period of the smolts.	18
Figure II-10 : Discharge at the mobile dams and hydropower plants. The grey areas represent the time periods for which smolts are detected.	19
Figure II-11: Cumulative number of lock operation cycles. The grey areas represent the time periods for which smolts are detected.	19
Figure II-12 : Number of eels detected at Grands-Malades and Ivoz-Ramet over the entire period of tracking.	21
Figure II-13: Density maps at Grands-Malades and Ivoz-Ramet with a mesh resolution of 5 m.	21

Figure II-14: Density maps at Grands-Malades and Ivoz-Ramet for the eels passing through the turbines.	22
Figure II-15: Density maps at Grands-Malades and Ivoz-Ramet for the eels passing through the dams.	22
Figure II-16 : Evolution of the free surface levels at Grands-Malades and Ivoz-Ramet during the monitoring of the eels.	23
Figure II-17 : Discharge of the Meuse river at the upstream of Grands-Malades and Amay during the monitoring period of the eels.	23
Figure II-18 : Discharge of the Meuse river at the upstream of Grands-Malades and Amay during the period of observation of eels going through the turbines.	24
Figure II-19 : Discharge at the mobile dams during the total period of observation of eels and identification of the ways of passage of the eels.	24
Figure II-20 : Discharge at the hydropower plants during the total period of observation of eels and identification of the ways of passage of the eels.	25
Figure II-21 : Number of opened turbines during the period of observation of eels passing through the turbines.	25
Figure II-22 : Discharge in the Meuse river, at the dams and at the turbines at the last detection time of eels passing through the turbines and the dams. The square represents the mean discharge while the extreme values represent the maximum range of variation (minimum and maximum values).	26
Figure II-23 : Relations between the discharges at the dams and at the turbines at the last detection time of eels passing through the turbines and the dams.	27
Figure II-24 : Relations between the dam opening coefficient and the discharge at the turbines at the last detection time of eels passing through the turbines and the dams.	28
Figure III-1: Topographic modelling of the upstream of the site of Grands-Malades.	31
Figure III-2: Topographic modelling of the water intake of the hydropower plant at Grands-Malades.	31
Figure III-3: Topographic modelling of the upstream of the site of Ivoz-Ramet.	32
Figure III-4: Topographic modelling of the water intake of the hydropower plant at Ivoz-Ramet.	32
Figure III-5: Profile AA' for the extraction of the absolute velocities.	33
Figure III-6: Absolute velocity distribution along the profile AA' of Figure III-5.	33
Figure IV-1: Distribution of the absolute unit discharge ( $\text{m}^2/\text{s}$ ) nearby the hydropower plants of Grands-Malades without (left) and with (right) a turbulence model.	34
Figure IV-2: Distribution of the absolute unit discharge ( $\text{m}^2/\text{s}$ ) nearby the hydropower plants of Ivoz-Ramet without (left) and with (right) a turbulence model.	35
Figure IV-3: Distribution of the absolute unit discharge ( $\text{m}^2/\text{s}$ ) nearby the hydropower plants of Grands-Malades at different mesh resolutions.	36
Figure IV-4: Normal unit discharge in the water intake with different mesh resolutions.	36
Figure V-1: Illustration of the quantitative analysis of the distribution of the hydrodynamic parameters in the presence of fishes.	39
Figure V-2: Temporal distribution of 2D detections of smolts at Grands-Malades.	40
Figure V-3: Discharge at the turbines of the hydropower plant at Grands-Malades during the fish tracking.	40
Figure V-4: Density maps at Grands-Malades for the different combinations of turbine openings.	43
Figure V-5: Absolute velocity distributions at Grands-Malades for the different combinations of turbine openings.	43
Figure V-6: Absolute unit discharge distributions at Grands-Malades for the different combinations of turbine openings.	44

Figure V-7: Turbulent viscosity distributions at Grands-Malades for the different combinations of turbine openings.	44
Figure V-8: Velocity gradient distributions at Grands-Malades for the different combinations of turbine openings.	44
Figure V-9: Topography of the zone of interest for the computation of the correlations between the fish locations and the hydrodynamic parameters at Grands-Malades.	45
Figure V-10: Probability density distributions (a) in the zone of interest, (b) in the presence of smolts and (c) attractiveness of absolute velocity, absolute discharge, 2D turbulent viscosity and velocity gradient for the smolts at Grands-Malades	46
Figure V-11: Density maps at Ivoz-Ramet with a mesh resolution of 5 m.	47
Figure V-12: Absolute velocity distributions at Ivoz-Ramet	48
Figure V-13: Absolute discharge distributions at Ivoz-Ramet	48
Figure V-14: Velocity gradient distributions at Ivoz-Ramet	48
Figure V-15: Probability density distributions (a) in the zone of interest, (b) in the presence of smolts and (c) attractiveness of absolute velocity, absolute discharge and velocity gradient for the smolts at Ivoz-Ramet for the scenario with a turbine opening on the <b>left</b> side.	49
Figure V-16: Probability density distributions (a) in the zone of interest, (b) in the presence of smolts and (c) attractiveness of absolute velocity, absolute discharge and velocity gradient for the smolts at Ivoz-Ramet for the scenario with a turbine opening on the <b>right</b> side.	50
Figure VI-1: Velocity fields at Grands-Malades for a discharge of 130 m <sup>3</sup> /s at the turbines and different values of the discharge at the single dam opening on the right side.	52
Figure VI-2: Velocity fields at Ivoz-Ramet for a discharge of 95 m <sup>3</sup> /s at the turbines and a discharge of 600 m <sup>3</sup> /s at the dam.	53
Figure VI-3: Velocity fields at Ivoz-Ramet for a discharge of 190 m <sup>3</sup> /s at the turbines and a discharge of 300 m <sup>3</sup> /s at the dam.	54
Figure VII-1: Velocity distribution at the site of Grands-Malades for the actual configuration and for the design hydrodynamic conditions.	55
Figure VII-2: Velocity distribution at the site of Ivoz-Ramet for the actual configuration and for the design hydrodynamic conditions.	56
Figure VII-3: Configurations of fish passages at Grands-Malades.	57
Figure VII-4: Configurations of fish passages at Ivoz-Ramet.	57
Figure VII-5: Velocity field for the configurations G0 and I0 with a fish passage through a valve of the mobile dam with the maximum equipped discharge (equipped discharge of 7.3 m <sup>3</sup> /s at Grands-Malades and 7.1 m <sup>3</sup> /s at Ivoz-Ramet).	58
Figure VII-6: Field of change of absolute velocity for the configurations G0 and I0 with a fish passage through a valve of the mobile dam with the maximum equipped discharge (equipped discharge of 7.3 m <sup>3</sup> /s at Grands-Malades and 7.1 m <sup>3</sup> /s at Ivoz-Ramet).	58
Figure VII-7: Velocity fields for the configuration G1 with a fish passage at the upstream of the pier between the hydropower plant and the mobile dam at Grands-Malades (discharge of 7.3 m <sup>3</sup> /s).	59
Figure VII-8: Velocity fields for the configuration I1 with a fish passage in the river Meuse side of the pier between the hydropower plant and the mobile dam at Ivoz-Ramet (discharge of 7.1 m <sup>3</sup> /s).	59
Figure VII-9: Velocity fields for the configuration G3 with a fish passage at the downstream of the pier between the hydropower plant and the mobile dam at Grands-Malades (discharge of 7.3 m <sup>3</sup> /s).	60
Figure VII-10: Velocity fields for the configurations G4 and G5 designed by Arcadis at Grands-Malades.	61
Figure VII-11: Velocity fields for the configurations I3 and I4 designed by Arcadis at Ivoz-Ramet.	62

Figure VIII-1: Numerical and laboratory models at Grands-Malades and Ivoz-Ramet.	63
Figure VIII-2: Design of laboratory models at Grands-Malades. The grey lines represent the water supply zones.	64
Figure VIII-3: Design of laboratory models at Ivoz-Ramet. The grey lines represent the water supply zones.	64
Figure VIII-4: Unit discharge distributions for the numerical and laboratory models at Grands-Malades.	65
Figure VIII-5: Absolute values of the unit discharge at the entrance of the water intake of Grands-Malades (from the right side to the left side of the water intake).	66
Figure VIII-6: Unit discharge distributions for the numerical and laboratory models at Ivoz-Ramet.	66
Figure VIII-7: Absolute values of the unit discharge at the entrance of the water intake of Ivoz-Ramet (from the right side to the left side of the water intake).	67
Figure VIII-8: Scale model layout on the real site for Grands Malades site	68
Figure VIII-9: Scale model layout on the real site for Ivoz Ramet site	69
Figure VIII-10: plan view of the scale models	69
Figure VIII-11: Separation wall on Grands Malades model made using high-density foam (yellow material)	70
Figure VIII-12: General view of the scale models	71
Figure VIII-13: General view of Grands Malades scale model	71
Figure VIII-14: General view of Ivoz Ramet scale model	72
Figure IX-1: Floats used for surface currents characterization (left) and example of instantaneous location of floats in the Grands Malades model (right)	73
Figure IX-2: Initial geometry of fish passage intake at Grands Malades	74
Figure IX-3: Elevations for 3D flow velocities measurement at Grands Malades	74
Figure IX-4: Horizontal flow velocity components on Grands Malades scale model	75
Figure IX-5: Floats trajectories without fish passage at Grands Malades (fish passage closed)	75
Figure IX-6: Floats trajectories for initial geometry of fish passage at Grands Malades (fish passage opened)	76
Figure IX-7: Modified geometry of fish passage at Grands Malades	76
Figure IX-8: Floats trajectories for modified geometry of fish passage at Grands Malades	77
Figure IX-9: Initial geometry of fish passage intake at Ivoz Ramet	77
Figure IX-10: Elevations for 3D flow velocities measurement at Ivoz Ramet	78
Figure IX-11: Horizontal flow velocity components on Ivoz Ramet scale model	78
Figure IX-12: Floats trajectories without fish passage at Ivoz Ramet (fish passage closed)	79
Figure IX-13: Floats trajectories for initial geometry of fish passage at Ivoz Ramet (fish passage opened)	80
Figure IX-14: Modified geometry of fish passage intake at Ivoz Ramet	80
Figure IX-15: Floats trajectories for modified geometry of fish passage at Ivoz Ramet	81



LIFE16 NAT/BE/000807 LIFE4FISH



## I. Introduction

In general terms, first part of the Action A3 of the Life for Fish project was dedicated to the development of hydraulic models and their application to the two pilot sites (Grands Malades and Ivoz Ramet) in order to design the solutions aiming at improving the safe downstream passage of fishes arriving upstream of the powerplants. Hydraulic modelling of the sites has been done using the two complementary approaches of numerical and experimental modelling (hybrid modelling). Results of hydraulic modelling have been used to analyse the possible correlation between hydraulic parameters and fishes' behaviour and designing the downstream passage solutions.

Data to set up the hydraulic models came from Service Public de Wallonie and EDF Luminus (topographic data, general flow conditions, dams, locks and turbines operation...) and ProFish (fishes data). For the latter, a monitoring of downstream migrating fishes (smolts and eels) was performed by the society Profish along a reach of the low Meuse River including 6 hydropower plants (from Grands Malades to Lixhe). In particular, a network of hydrophones was used to determine the instantaneous two-dimensional (2D) coordinates of the fishes at the upstream of the hydropower plants of Grands Malades and Ivoz-Ramet (pilot sites).

This report presents all the works performed by ULiege-HECE team within Action A3 of the Life for Fish project during the first year of the project.

In section II, the hydrodynamic variables (water level, discharge, turbines operation,...) in the Meuse river during the fishes monitoring process are analysed. Section III presents the set-up of the numerical models of the sites of Grands-Malades and Ivoz-Ramet in terms of topography and hydraulic conditions. A sensitivity analysis of the turbulence activation and the mesh resolution on the accuracy of the results is done in section IV to identify the most suitable trade-off between computation efficiency and computational time.

Based on the results of section II, the hydrodynamic numerical models are used to compute the Meuse river hydrodynamic characteristics during the fishes passage. Then, correlations between the 2D locations of smolts and hydrodynamic parameters are investigated in section V using an original methodology. The velocity field at times corresponding to eels passing to the turbines are discussed in section VI.

In section VII, the numerical models are used to analyse varied locations and designs for downstream passages. Section VIII describes the characteristics of the physical scale models used in section IX to optimize the design of the downstream passage.

Section X presents the conclusions of this first year of work in the scope of the Life for fish project.

## II. Fish monitoring and hydrodynamic data

The objective of this chapter is the characterization of the hydraulic variables in the Meuse river during the monitoring of the fishes behaviour at the two sites of Grands Malades and Ivoz-Ramet (Profish reports). This will help for the selection of a suitable hydrodynamic modelling for the reproduction of the flow during the period of monitoring.

In section II.1, an original filtering method of the 2D fish coordinates, based on considerations on absolute fish velocities, is presented and compared with the method based on the value of the Dilution of Precision (DOP), as used by Profish.

For the smolts and the eels (respectively sections II.2 and II.3), the data resulting from the fish monitoring are analysed regarding the temporal period of observation (sections II.2.1.1 and II.3.1.1) and the spatial distribution of the fish locations (sections II.2.1.2 and II.3.1.2). Based on identification of the temporal period of the fish monitoring in sections II.2.1.1 and II.3.1.1, hydrodynamic variables during this temporal period are discussed in sections II.2.2 and II.3.2. This provides guidelines (sections II.2.3 and II.4) for the prescription of the hydrodynamic conditions for the hydrodynamic modelling.

### II.1 Data filtering

At the site of Grands-Malades, the 2D coordinates corresponding to the smolts IDs 15117 and 22551 are not considered since these two smolts were identified as being dead. The number of 2D coordinates tracked for the smolts is around one order of magnitude higher than for the eels (Table 1). Among these data, some give different 2D coordinates for a same fish at a same time (*redundant data* in Table 1). The number of redundant data is around 10% at the site of Grands-Malades and around 5% at Ivoz-Ramet.

Based on the 2D coordinates of a fish corresponding to a same approach (an approach is defined as a group of successive detections whose time interval is lower than 1h), the absolute velocities of the fish is computed. A set of  $n-1$  absolute fish velocities  $V_{abs, fish}$  are computed for each set of  $n$  approaches ( $n > 1$ ) based on the times  $t$  and the coordinates  $X$  and  $Y$  in the  $x$ - and  $y$ - directions as follow:

$$V_{abs, fish} = \frac{\sqrt{(X_i - X_{i-1})^2 + (Y_i - Y_{i-1})^2}}{t_i - t_{i-1}}$$

with  $i-1$  and  $i$  two successive detections.

Profish filtered the raw 2D coordinates based on the concept of Dilution of Precision (DOP) (see Profish report, 15<sup>th</sup> December 2017, in French). In their filtering process, the coordinates for which the value of a DOP parameter is higher than a threshold value of 2 are removed from the dataset. This leads to a removal of 9% to 16% of the raw data (Table 1). However, as depicted in Figure II-1 showing the relations between the absolute fish velocities lower than 10 m/s and the corresponding DOP values, this method maintains some unrealistic values of the absolute fish velocities.

For this reason, a new filtering method of the 2D coordinates is considered in this report by considering the absolute fish velocities. The new methodology, based on a threshold value of the absolute fish velocity  $V_{max, fish}$ , is the following:

1. For the redundant data, i.e. two different 2D coordinates of a fish for a same time:
  - a. If only one 2D coordinate leads to a fish velocity higher than  $V_{max, fish}$ , this coordinate is removed from the dataset.
  - b. Otherwise, the choice of the single 2D coordinate to maintain in the dataset is based on the minimum value of the DOP.



2. The  $n-1$  absolute fish velocities of the  $n$  2D coordinates are computed for each approach of each fish.
3. The absolute fish velocities higher than  $V_{max, fish}$  are removed from the dataset.
4. Updated absolute fish velocities are computed from the updated dataset.
5. Operations 3 and 4 are repeated until all the absolute fish velocities are lower than  $V_{max, fish}$ .

The percentages of 2D coordinates filtered from the raw dataset are shown in Table 1 for different threshold values of the absolute fish velocity. The fraction of removal with the new methodology is systemically and significantly higher than the one resulting from the DOP threshold used by Profish. Additionally, the number of 2D coordinates removed from the dataset is systemically higher for the eels than for the smolts.

Among the data removed by the different filtering, some 2D coordinates are not realistic since they are located outside the zone occupied by water. For the site of Grands-Malades, the percentage of the filtered 2D coordinates located within the Meuse river is specified by the grey numbers in brackets. The number of unrealistic 2D coordinates for the smolts (22-23%) is higher than for the eels (7-14%).

	Smolts		Eels	
	Grands-Malades	Ivoz-Ramet	Grands-Malades	Ivoz-Ramet
<b>Number of raw 2D coordinates</b>	18,916	53,078	2,444	3,026
<b>Redundant data</b>	9%	3%	11%	6%
<b>Data retained by Profish</b>	84% (77%)	89%	84% (86%)	91%
<b>Data retained by the new methodology with <math>V_{max, fish} = 1</math> m/s</b>	62% (78%)	56%	49% (92%)	48%
<b>Data retained by the new methodology with <math>V_{max, fish} = 1.5</math> m/s</b>	69% (77%)	75%	58% (93%)	60%

Table 1: Number of 2D coordinates, redundant data and filtered data with the different filtering methods.

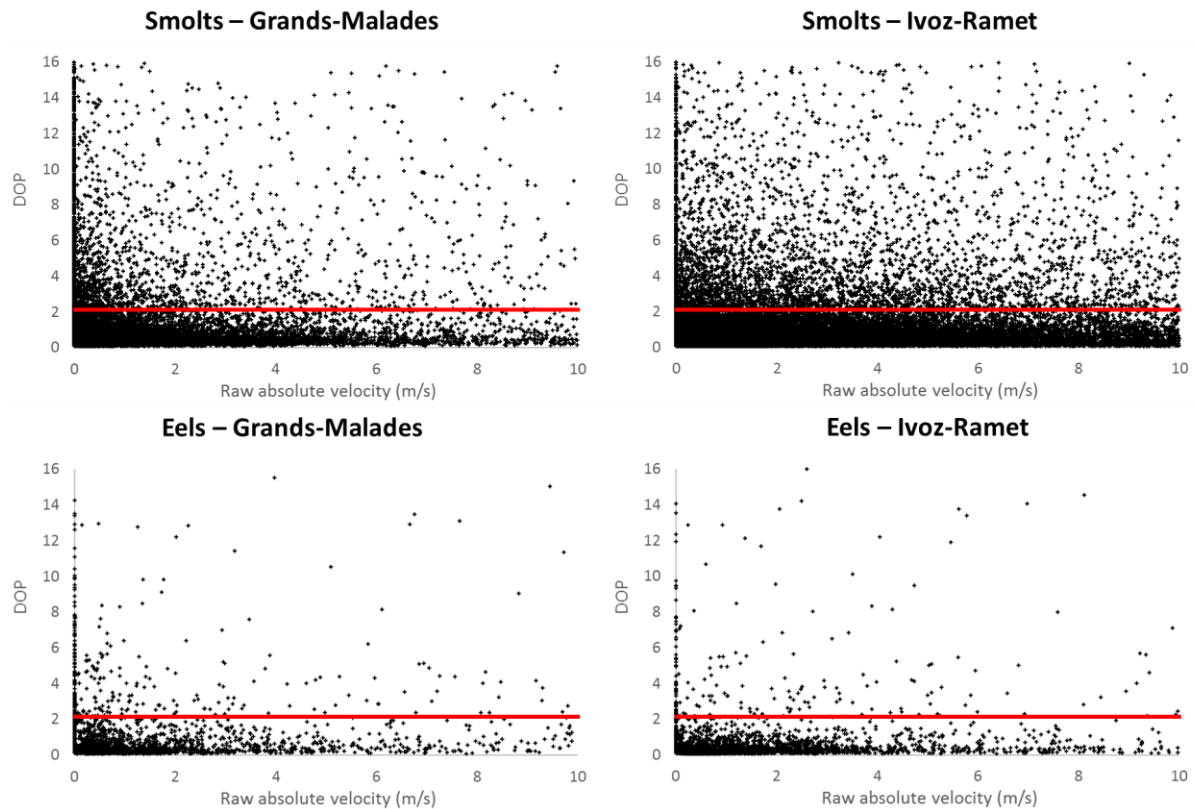


Figure II-1: Values of the Dilution of Precision (DOP) parameter as a function of the raw absolute fish velocity.

## II.2 Smolts

### II.2.1 Monitoring data

#### II.2.1.1 Temporal analysis

Smolts were tracked at the sites of Grands Malades and Ivoz-Ramet respectively from April 14<sup>th</sup> to May 22<sup>th</sup> 2017 (38 days) and from April 21<sup>th</sup> to May 03<sup>rd</sup> 2017 (12 days) (Table 2). The average residence times of the smolts in the monitoring zone are around 42 minutes at Grands Malades and 1h10 at Ivoz-Ramet with a high variability from one smolt to another.

The temporal distributions of the number of smolts detected at the two pilot sites are presented in Figure II-2 over the entire monitoring period. Smolts are mainly detected at the beginning of the monitoring period (Figure II-3). Indeed, respectively 95% and 86% of the total number of detections at Grands-Malades and Ivoz-Ramet occur during the first three days of monitoring.

	Grands Malades	Ivoz-Ramet
<b>Number of smolts</b>	47	14
<b>Start of the detection</b>	April 14 <sup>th</sup> , 2017	April 21 <sup>th</sup> , 2017
<b>End of the detection</b>	May 22 <sup>th</sup> , 2017	May 03 <sup>th</sup> , 2017
<b>Average residence time</b>	42 minutes	70 minutes

Table 2 : Tracking of smolts at the sites of Grands Malades and Ivoz-Ramet.

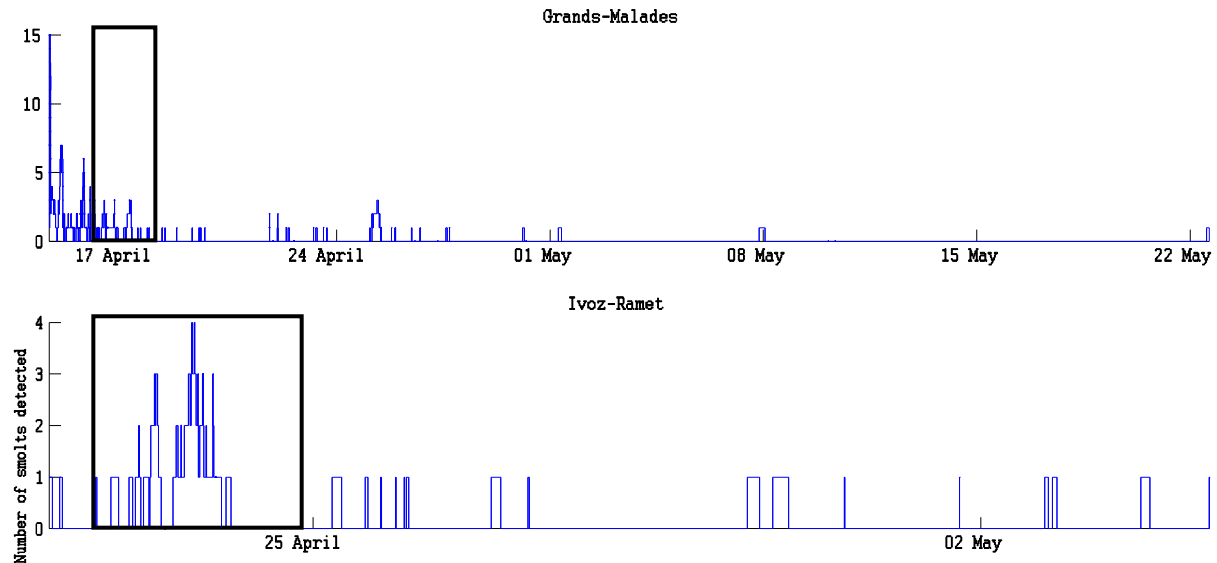


Figure II-2 : Number of smolts detected at Grands-Malades and Ivoz-Ramet over the entire period of tracking.

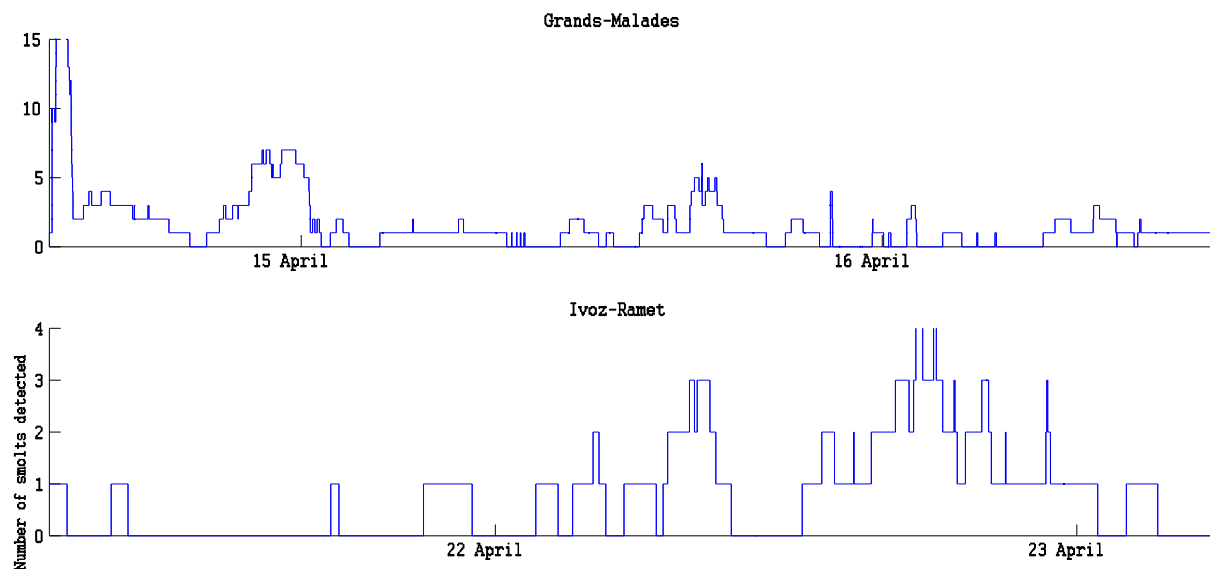


Figure II-3 : Number of smolts detected at Grands-Malades and Ivoz-Ramet over the three first days of tracking.

### II.2.1.2 Spatial analysis

A network of hydrophones was used by the society Profish to determine the 2D coordinates of the fish locations in a zone of detection. The zone of detection of smolts at the site of Grands-Malades is mainly located within the water intake while, at the site of Ivoz-Ramet, the zone of detection mainly covers the upstream of the topographic step at the entrance of the water intake (area just upstream of the surface beam).

Based on these 2D coordinates of smolt locations, a *density map* is built to quantify the density of presence of fishes at the upstream of the hydropower plant. The density maps are built on a Cartesian grid in which the value assigned to each cell is computed by the summation of the number of fishes observed within this cell at any time.

The resulting density maps for the site of Grands-Malades are shown in Figure II-4 with a mesh resolution of 250 cm. All these density maps show that the fish density is higher on the left half side

of the water intake. At the site of Ivoz-Ramet (Figure II-5), the smolts are mainly located around the central part of the entrance of the water intake of the hydropower plant. Hence, at Ivoz-Ramet, the surface beam at the entrance of the water intake acts as a barrier for the smolts from the Meuse river side. Comparing the density maps for the two threshold absolute velocities  $V_{max,fish}$  (1 m/s and 1.5 m/s), it appears that the influence of the value of this threshold on the distribution of the smolt coordinates in the monitoring zones is low. In the following of the report, the value of this threshold is fixed at 1 m/s for the two sites.

At the site of Grands-Malades, only around 1% of the filtered 2D coordinates were measured during a lock operation while, at the site of Ivoz-Ramet, this ratio rises up to 17%. In Figure II-6, the density map is computed at Ivoz-Ramet by considering only the 2D coordinates measured during a lock operation. The map indicates that smolts remain mainly located at the entrance of the water intake although the density distribution is more evenly distributed than in Figure II-5. Lock operation has thus little effect on the density map at Ivoz Ramet site.

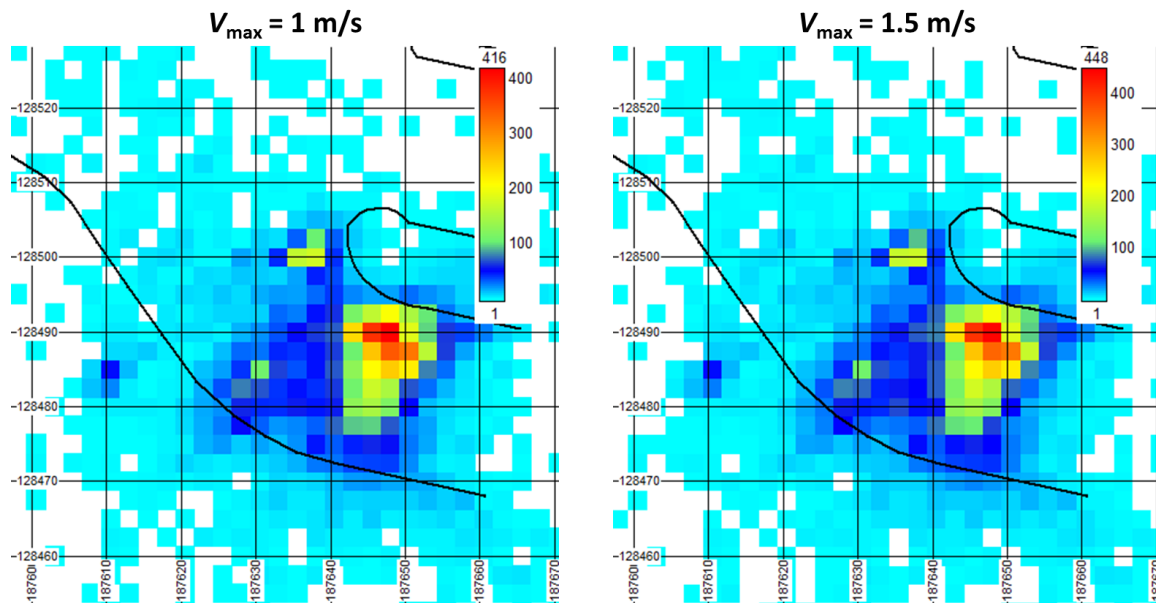


Figure II-4: Density maps at Grands-Malades with a mesh resolution of 2.5 m and threshold absolute velocities of 1 m/s and 1.5 m/s.

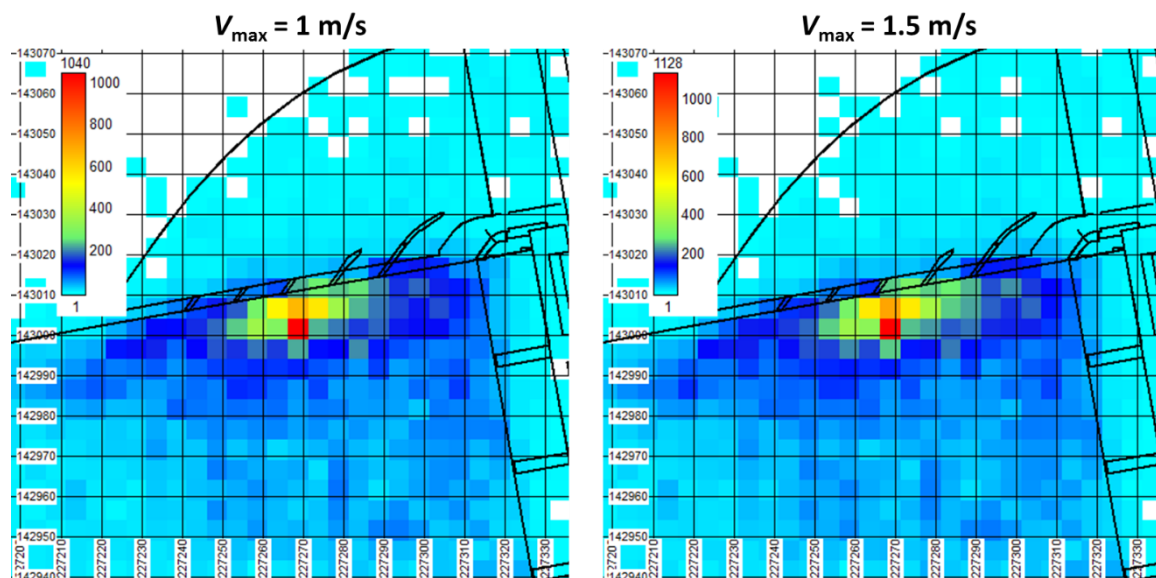


Figure II-5: Density maps at Ivoz-Ramet with a mesh resolution of 5 m and threshold absolute velocities of 1 m/s and 1.5 m/s.

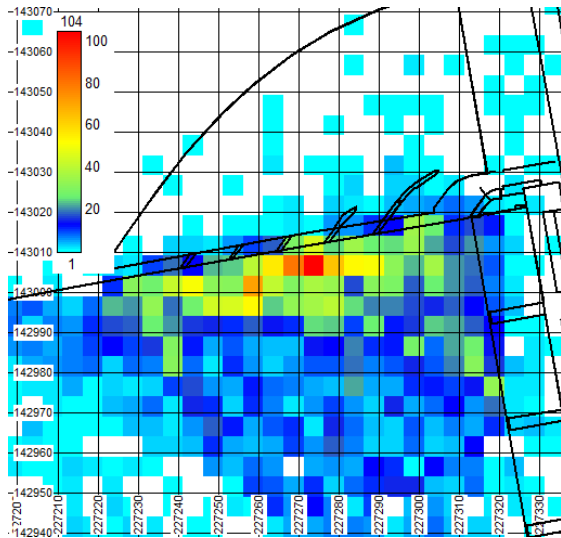


Figure II-6: Density maps at Ivoz-Ramet during the lock operation with a mesh resolution of 5 m and a threshold absolute velocity of 1 m/s.

## II.2.2 Hydraulic variables during monitoring period

### II.2.2.1 Free surface levels at the upstream reach of the mobile dams

During the monitoring of the smolts, the average free surface levels at the upstream reach of the mobile dams are respectively of 78.50 m and 63.65 m at the sites of Grands-Malades and Ivoz-Ramet. As shown in Figure II-7, the time fluctuation of the free surface levels during the monitoring period is low with values of the standard deviation around 2 cm and 5 cm at the two sites.

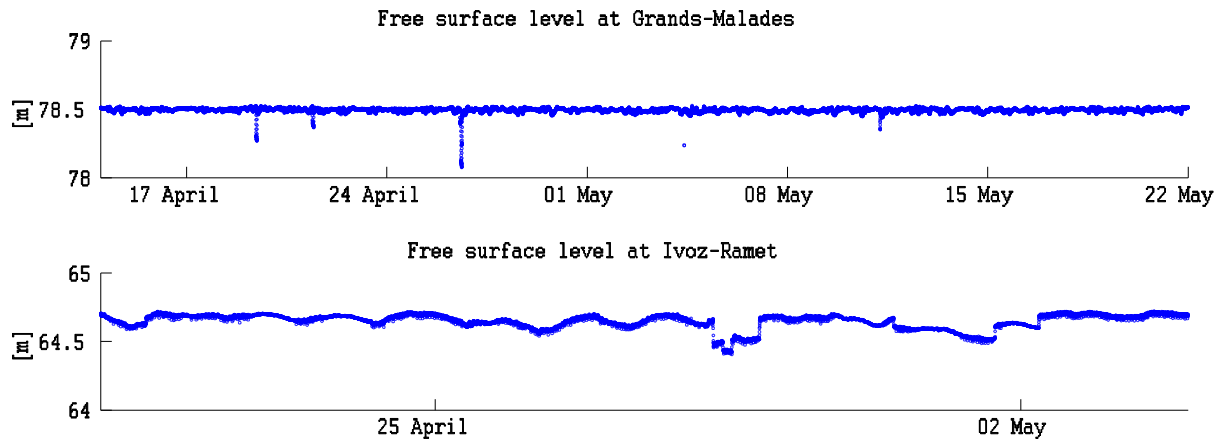


Figure II-7 : Evolution of the free surface levels at Grands-Malades and Ivoz-Ramet during the monitoring of the smolts.

### II.2.2.2 Discharges of the Meuse river

The discharge of the Meuse river is measured at the gauging station of Amay, located between the sites of Grands-Malades and Ivoz-Ramet (Figure II-8). In Figure II-9, the Meuse discharge varies within the range 22 – 125 m<sup>3</sup>/s with an average discharge of 70 m<sup>3</sup>/s. For the Walloon part of the Meuse river, such discharges are representative of a low-flow period since the average Meuse discharge is around 300 m<sup>3</sup>/s.



Figure II-8 : Localisation of the gauging station of Amay.

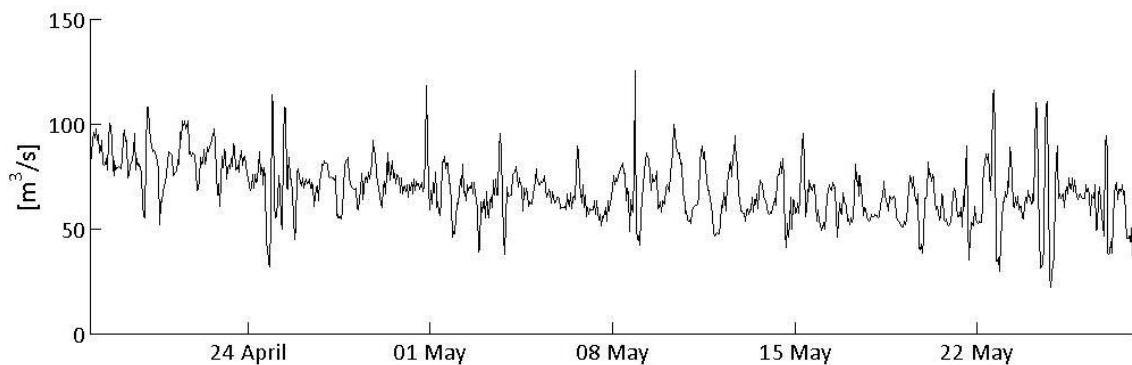


Figure II-9 : Discharge of the Meuse river at Amay during the monitoring period of the smolts.

### II.2.2.3 Operation of the facilities

The discharges at the mobile dams and at the hydropower plants are shown in Figure II-10 for the monitoring period of the smolts. The grey areas represent the time periods for which smolts are detected. The discharge at the hydropower plants fluctuates generally in-between 70 m<sup>3</sup>/s and 90 m<sup>3</sup>/s at Grands-Malades and in-between 50 m<sup>3</sup>/s and 80 m<sup>3</sup>/s at Ivoz-Ramet. Equipment discharge of the 2 power plants is respectively 161 and 285 m<sup>3</sup>/s. Discharges observed through the powerplant during fish migration are thus very low. There is generally no discharge passing through the mobile dams, consistently with the low-flow period of the Meuse river.

The number of cycles of lock operation during the monitoring period is shown in Figure II-11. The number of cycles at Ivoz-Ramet (296 per week) is around 10 times higher than at Grands-Malades (26 per week) with lock operation occurring during the detection of smolts.

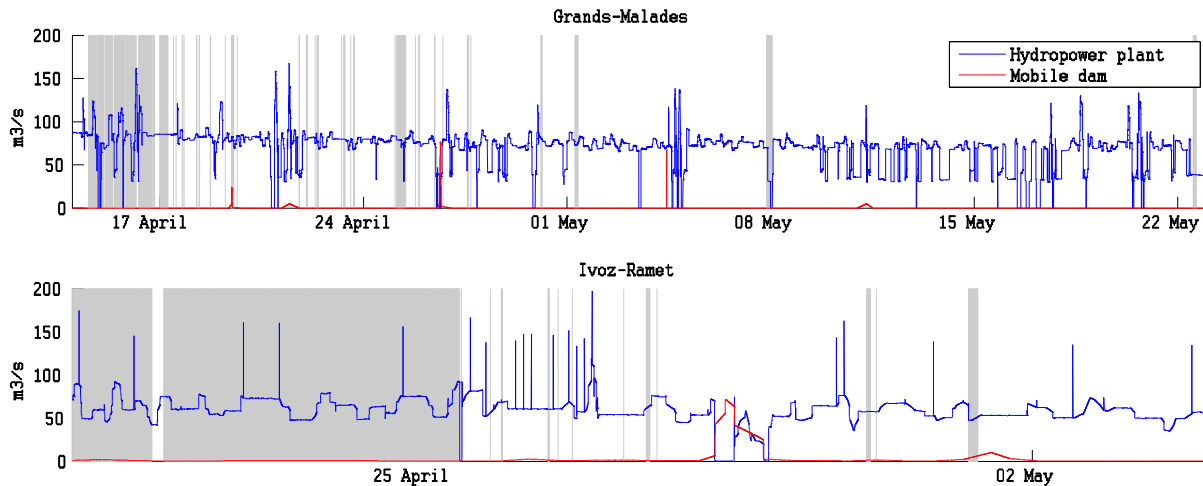


Figure II-10 : Discharge at the mobile dams and hydropower plants. The grey areas represent the time periods for which smolts are detected.

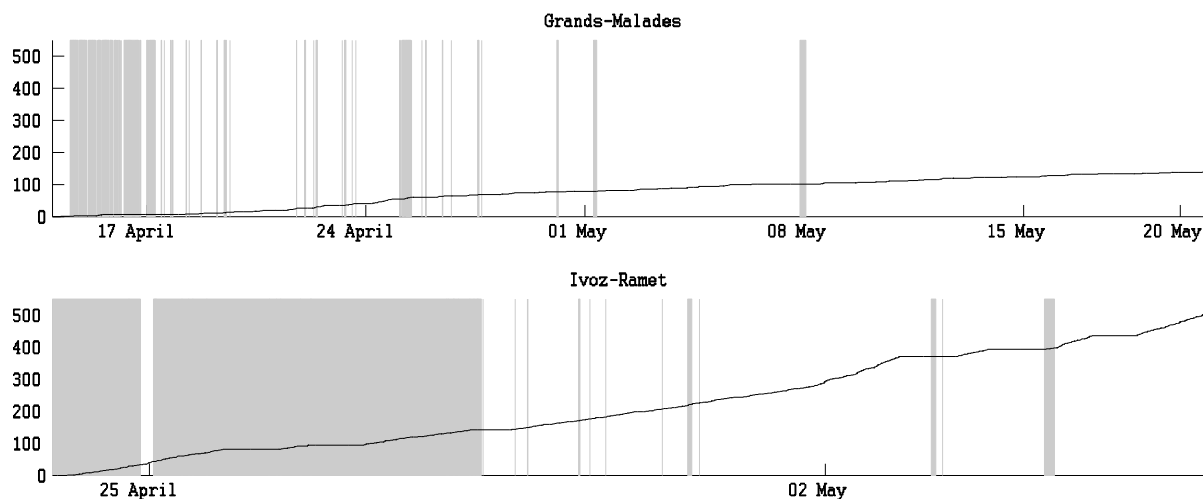


Figure II-11: Cumulative number of lock operation cycles. The grey areas represent the time periods for which smolts are detected.

### II.2.3 Guidelines for the prescription of the hydrodynamic conditions

As a reminder, a monitoring of downstream migrating smolts was performed during 5 weeks at the site of Grands-Malades and 2 weeks at the site of Ivoz-Ramet. During this monitoring period of the smolts, most of the smolt detections occur during the 3 first days of tracking. Based on an analysis of the characteristics of the Meuse river during this period, the following points should be considered in the numerical modelling of the Meuse river:

- Low variability of the free surface level at the two sites;
- Low-flow period of the Meuse river with an average discharge around 70 m<sup>3</sup>/s at Amay;
- The mobile dams are generally not used and the Meuse discharge is conveyed through the hydropower plants and the locks:
  - At Grands-Malades, most of the smolt monitoring data are measured outside lock operation periods.



- At Ivoz-Ramet, the valves of the locks are located at over 500 m of distance to the entrance of the water intake where the fishes are observed. The impact of the discharge through the locks on the hydrodynamic fields at the zone of interest is therefore expected to be non-significant. Density maps of fish presence confirm the very limited influence of lock operation on smolt location upstream of the Ivoz Ramet power plant.

## II.3 Eels

### II.3.1 Monitoring data

#### II.3.1.1 Temporal analysis

Eels were observed by Profish at the pilot sites of Grands Malades and Ivoz-Ramet respectively from October 10<sup>th</sup> to November 29<sup>th</sup> 2017 (56 days) and from October 12<sup>th</sup> 2017 to February 1<sup>st</sup> 2018 (113 days) (Table 3). The total raw number of eels observed during the monitoring period, before the filtering process (in grey in Table 3) indicates that the 2D coordinates after the filtering process remain representative of most of the eels. Among the eels considered, only a little fraction (resp. 20% and 30% at Grands Malades and Ivoz-Ramet) crosses the hydropower plant through the turbines.

The temporal distribution of the number of eels observed at the two sites is shown in Figure II-12. The results show that most observations of eels are done between October 10 and November 12 in Grands Malades and October 12 and November 16 in Ivoz-Ramet. These periods of detections are significantly longer than for the smolts (around 3 days). While the period of detections of the eels passing through the turbines may extend over several days (in average around 3 days), the eels passing through the dams spend in average around 1 minute at the hydropower sites. Finally, the period of detections of eels passing through the turbines (resp. from October 10 to November 12 and from October 12 to November 16 at Grands-Malades and Ivoz-Ramet) generally do not match with the ones of eels passing through the dams, which suggests a significant influence of the hydraulic characteristics on the type of fish passage.

	Grands Malades	Ivoz-Ramet
<b>Number of eels</b>	20 (20)	47 (60)
<b>Eels passing through the turbines</b>	4	14
<b>Eels passing through the dam</b>	6	20
<b>Eels passing through through the lock</b>	10	13
<b>Start of the detection</b>	October 10 <sup>th</sup> 2017	October 12 <sup>th</sup> 2017
<b>End of the detection</b>	November 29 <sup>th</sup> 2017	February 1 <sup>st</sup> 2018

Table 3 : Tracking of eels at the sites of Grands Malades and Ivoz-Ramet.



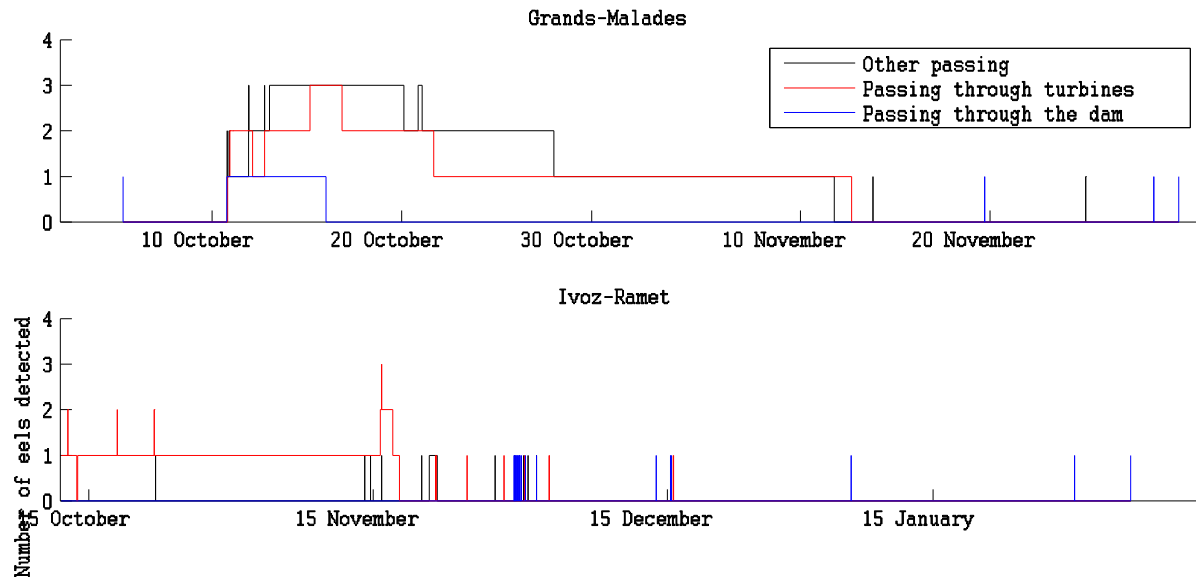


Figure II-12 : Number of eels detected at Grands-Malades and Ivoz-Ramet over the entire period of tracking.

### II.3.1.2 Spatial analysis

#### Total data

As done in section II.2.1.2 for the smolts, density maps are shown in Figure II-13 for the eels at the site of Grands Malades and Ivoz-Ramet. While the range of variation of the density values for the smolts is around  $0-10^3$  (section II.2.1.2), the range of density values for the eels is considerably lower ( $0-32$ ), consequently to the lower number of detections for the eels than for the smolts. The zones of detection of the eels at the two pilot sites are spread over a larger zone than for the smolts. At Grands Malades, the eels are slightly more located on the left side of the water intake and, at Ivoz-Ramet, they are spread over the upstream of the surface beam at the entrance of the water intake.

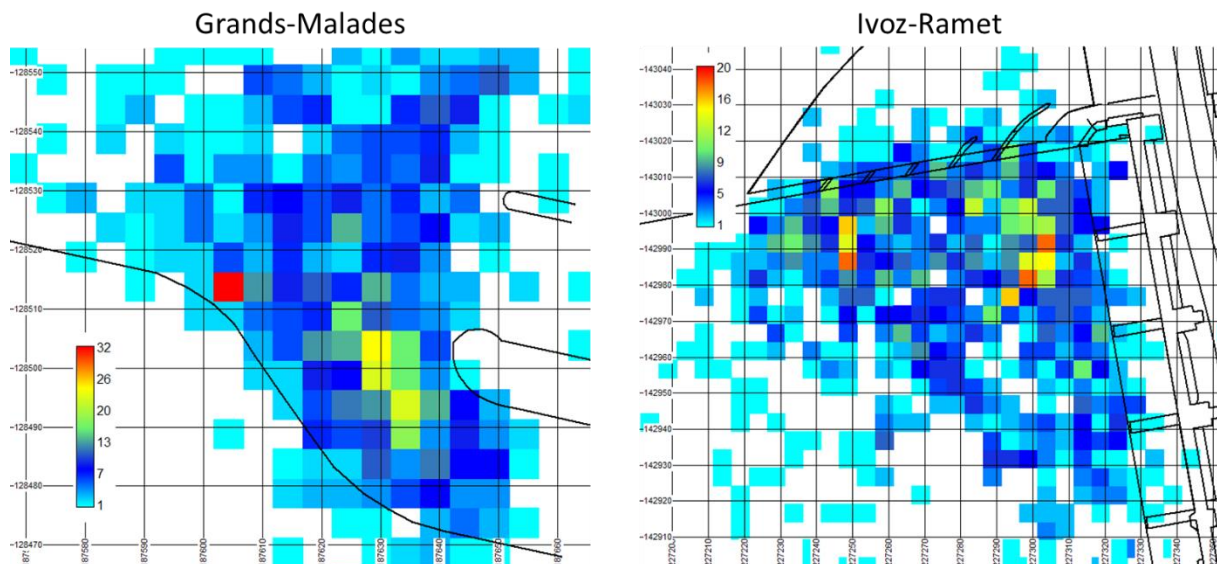


Figure II-13: Density maps at Grands-Malades and Ivoz-Ramet with a mesh resolution of 5 m.

## Distinction of the eels depending on their passage way

Using the distinction done by Profish between the eels passing through the turbines and the ones passing through the dams, the resulting density maps are shown in Figure II-14 (resp. 190 and 1,257 detection points at Grands Malades and Ivoz-Ramet for the passing through the turbines) and Figure II-15 (resp. 212 and 114 detection points at Grands Malades and Ivoz-Ramet for the passing through the dams). The density maps, built with a low amount of detection points, do not show particular zone of presence of eels except that eels are poorly present in the water intakes for the situations with a passage through the dams. For the situation with a passage through the turbines at Ivoz-Ramet, eels do not show a preferential zone of attraction at the upstream of the water intake, on contrary of the observation for the smolts.

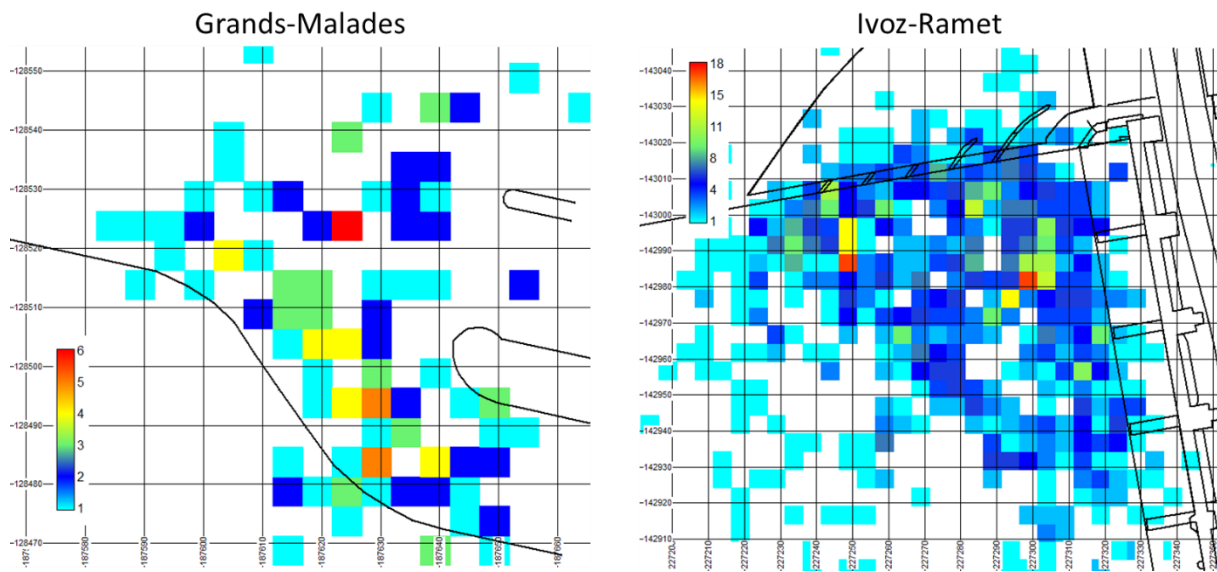


Figure II-14: Density maps at Grands-Malades and Ivoz-Ramet for the eels passing through the turbines.

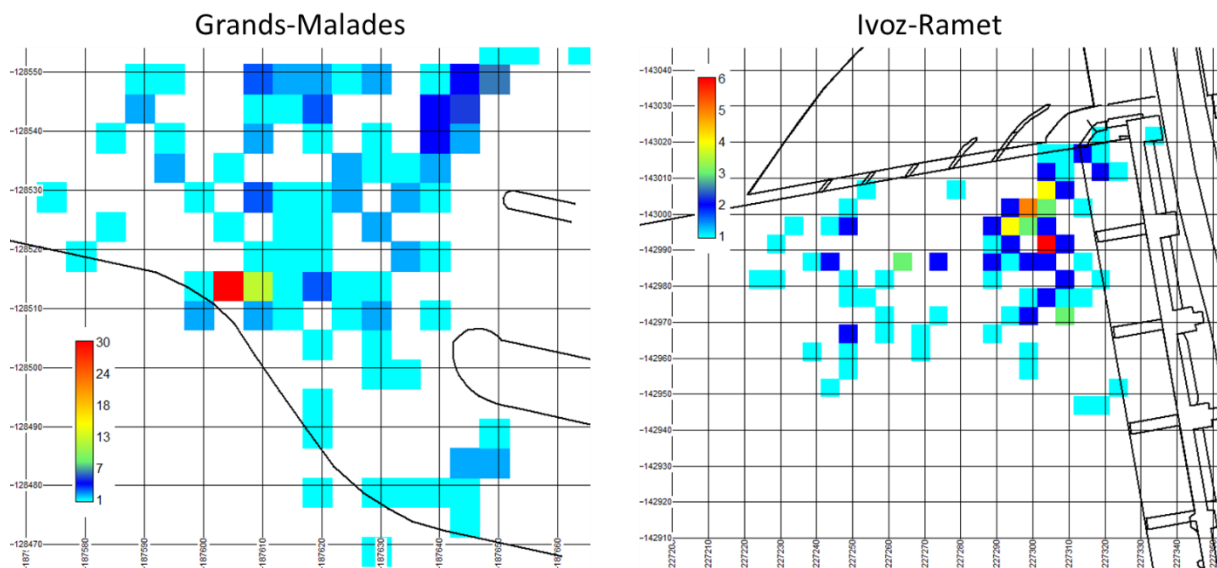


Figure II-15: Density maps at Grands-Malades and Ivoz-Ramet for the eels passing through the dams.

## II.3.2 Hydraulic variables during monitoring period

### II.3.2.1 Free surface levels at the upstream reach of the mobile dams

The free surface levels at the upstream of the mobile dam of Grands-Malades have a low range of variation during the period of monitoring and remain around a level of 64.6 m (Figure II-16). At Ivoz-Ramet, the free surface level remains close to a value of 78.5 m up to the beginning of December, which corresponds to the period of observation with a large amount of data and eels passing through the turbines (section II.3.1.1).

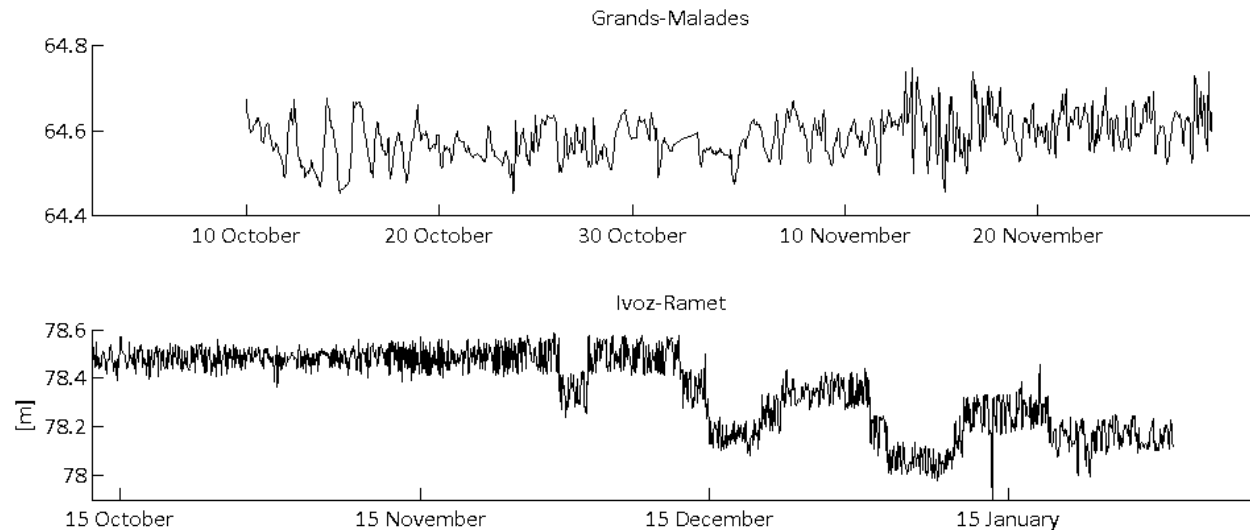


Figure II-16 : Evolution of the free surface levels at Grands-Malades and Ivoz-Ramet during the monitoring of the eels.

### II.3.2.2 Discharges of the Meuse river

Figure II-17 shows the discharges of the Meuse river at the upstream of the pilot site of Grands-Malades and at the gauging station of Amay (see section II.2.2.2 for the location) during the monitoring period. During the period representative of eels passages through the turbines, the Meuse discharge is generally lower than 150 m<sup>3</sup>/s (Figure II-18) while the Meuse discharge is significantly higher when eels go through the dams (after mid-November). Discharge of respectively 50 m<sup>3</sup>/s and 65 m<sup>3</sup>/s can be considered as representative of the discharge at the upstream of Grands-Malades and at Amay during the passage eels through the turbines. As highlighted for the smolts, such a discharge is representative of a low-flow discharge for the Walloon part of the Meuse river.

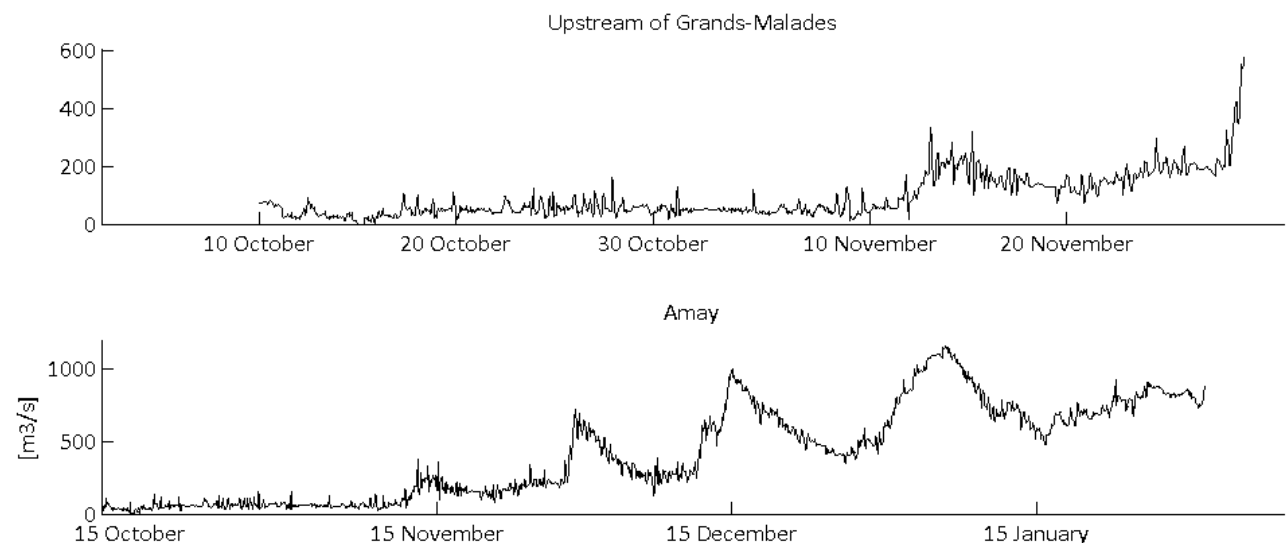


Figure II-17 : Discharge of the Meuse river at the upstream of Grands-Malades and Amay during the monitoring period of the eels.

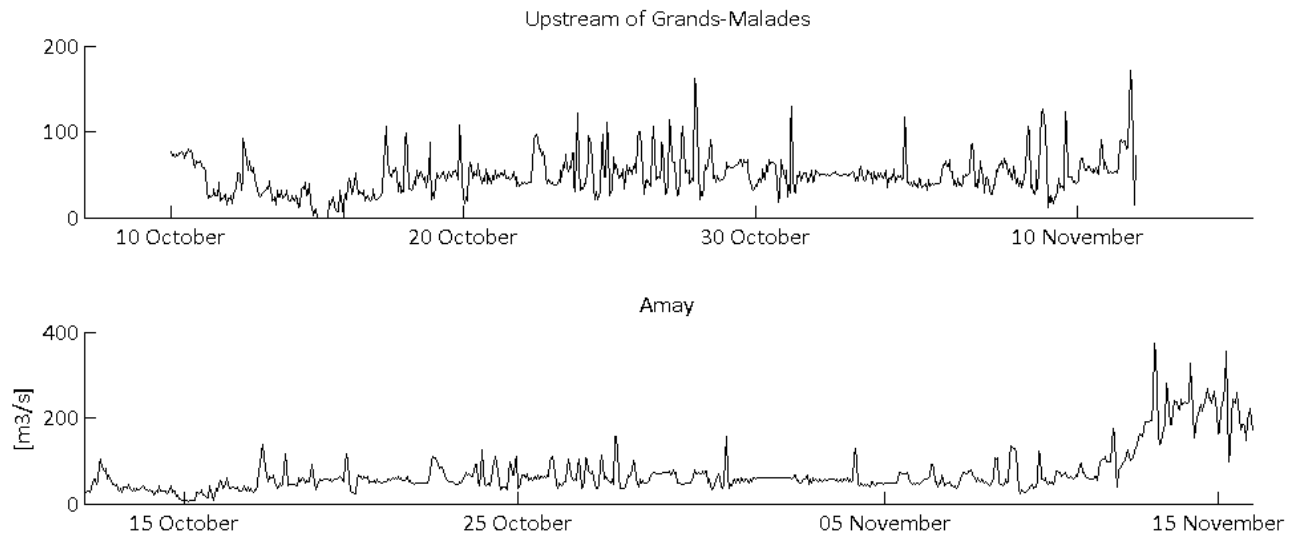


Figure II-18 : Discharge of the Meuse river at the upstream of Grands-Malades and Amay during the period of observation of eels going through the turbines.

### II.3.2.3 Operation of the facilities

Figure II-19 shows the discharges at the mobile dams during the period of observation of eels and the period of time during which eels are passing through the turbines and/or dams. When eels are passing through the turbines (red colour), no discharge is generally measured at the dams. On contrary, for the periods of time with a discharge at the dams, eels are generally passing directly through the dams (section II.3.1.1).

The discharges at the hydropower plants during the detection period are shown in Figure II-20. During the periods with eels passing through the turbines, the average discharges are 36 m<sup>3</sup>/s and 54 m<sup>3</sup>/s with 1 or 2 turbines opened at Grands-Malades and a single one opened at Ivoz-Ramet (Figure II-21).

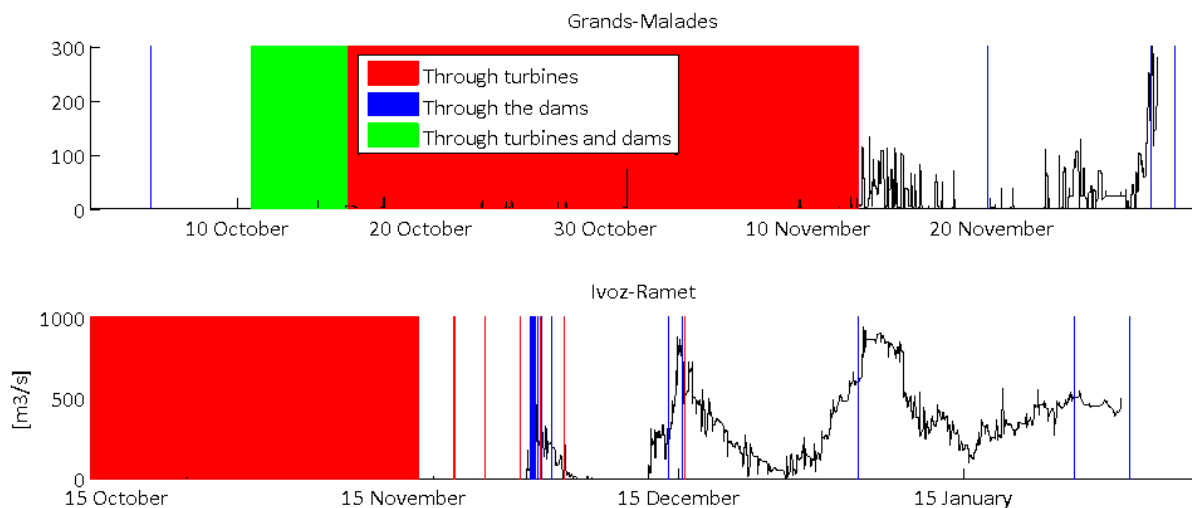


Figure II-19 : Discharge at the mobile dams during the total period of observation of eels and identification of the ways of passage of the eels.

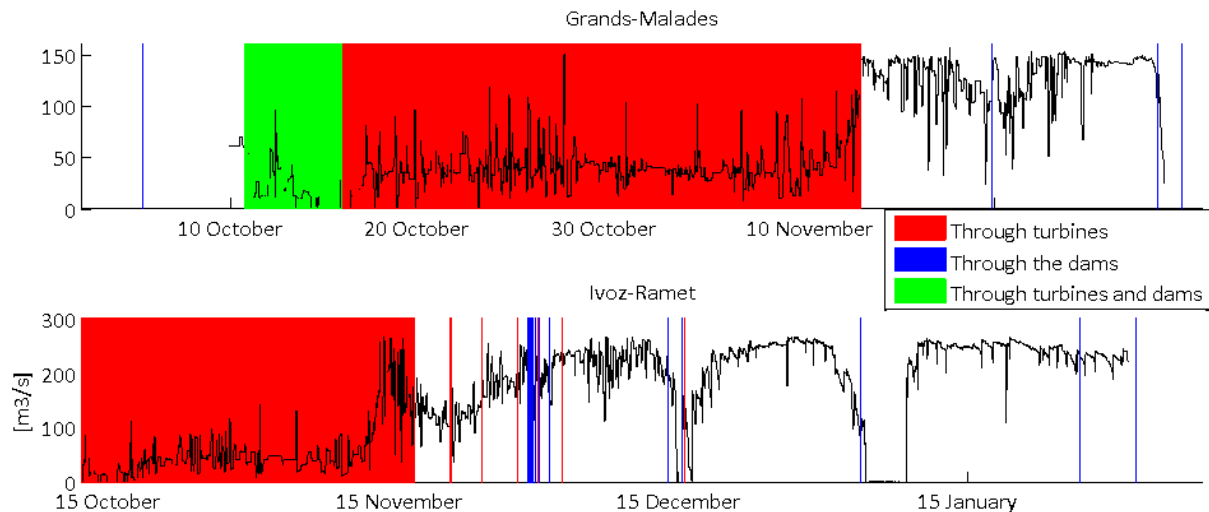


Figure II-20 : Discharge at the hydropower plants during the total period of observation of eels and identification of the ways of passage of the eels.

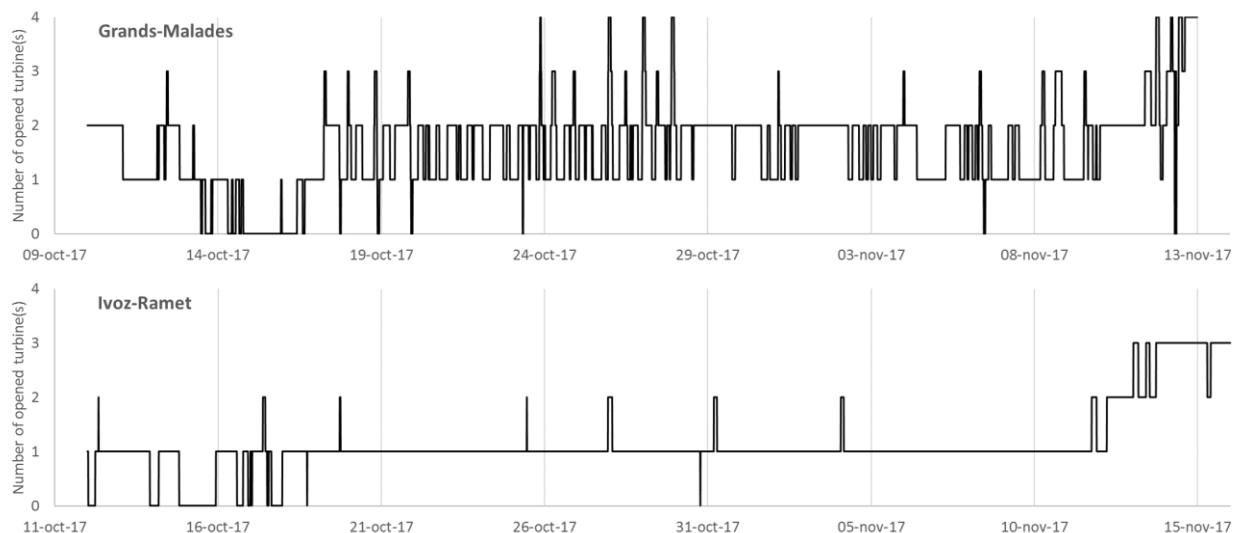


Figure II-21 : Number of opened turbines during the period of observation of eels passing through the turbines.

### II.3.3 Discharge distribution at the passage of eels

In addition to the 2D locations of eels, Profish has provided data giving, for each eel detected at Grands-Malades and Ivoz-Ramet:

- the time corresponding to the last detection of the eel,
- the passage way of the eel,
- a confirmation if the eel was detected at the downstream of the site.

Based on these data, Figure II-22 shows the range of variation of the discharges measured in the Meuse, at the dams and at the turbines, at the time corresponding to the last detection of the eels passing through the turbines or through the dams. Only the eels with a confirmation of the downstream passage are considered. At Grands-Malades (Ivoz-Ramet), respectively 5 (22) and 22 (55) eels moved across the site through the turbines and through the dams. The results indicate that:

- Generally, passages through the turbines occur for low values of the discharge in the Meuse river and at the dams, while the discharge at the turbines as a poor influence.
- Passages through the turbines at Grands-Malades occur for very low discharges at the dams, with a mean value around 10 m<sup>3</sup>/s.

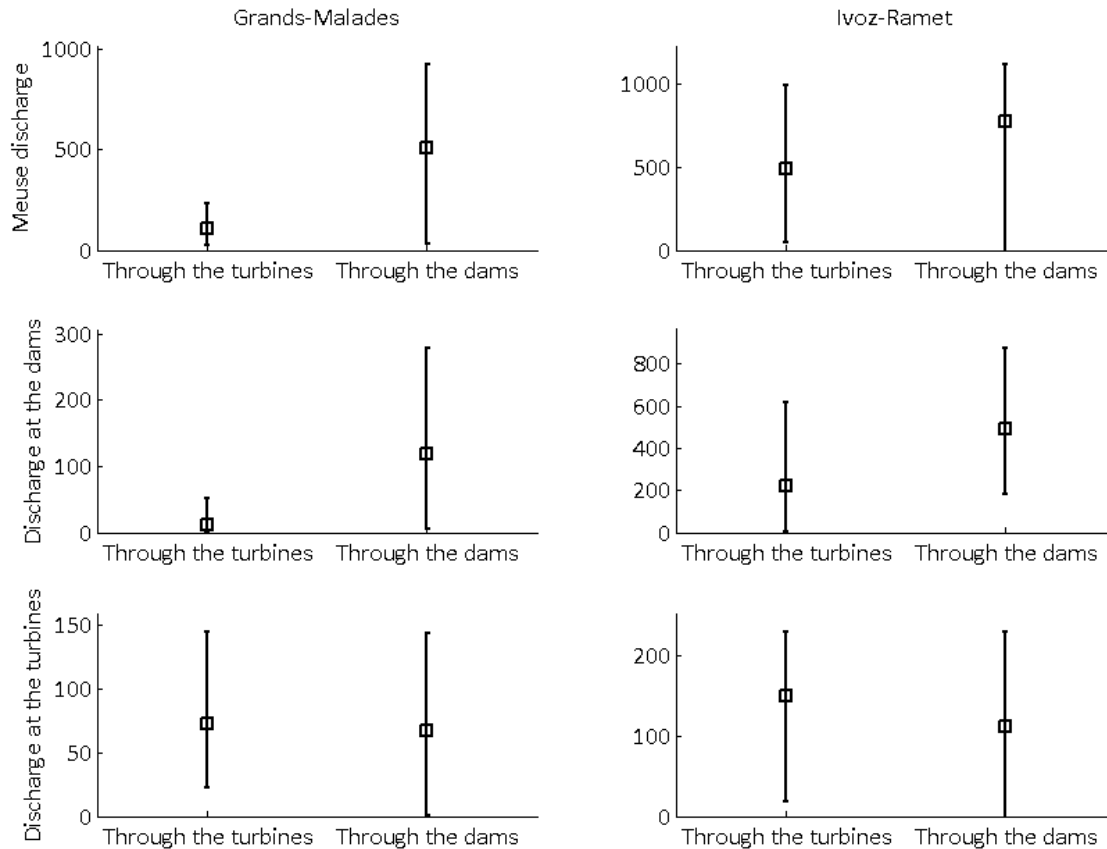


Figure II-22 : Discharge in the Meuse river, at the dams and at the turbines at the last detection time of eels passing through the turbines and the dams. The square represents the mean discharge while the extreme values represent the maximum range of variation (minimum and maximum values).

Figure II-23 confirms that passages through the turbines mainly occur in the absence of discharge at the mobile dam at Grands-Malades. Only a single passage through the turbines is observed with a significant discharge at the dam (around 50 m<sup>3</sup>/s). However, the discharge at the turbines at this time is high (125 m<sup>3</sup>/s) and around twice higher than at the dam.

At Ivoz-Ramet, several passages of eels through the turbines are observed with significant discharges at the dams. While most eels are passing through the dam once the dam discharge becomes higher than 400 m<sup>3</sup>/s, five passages of eels through the turbines are observed.

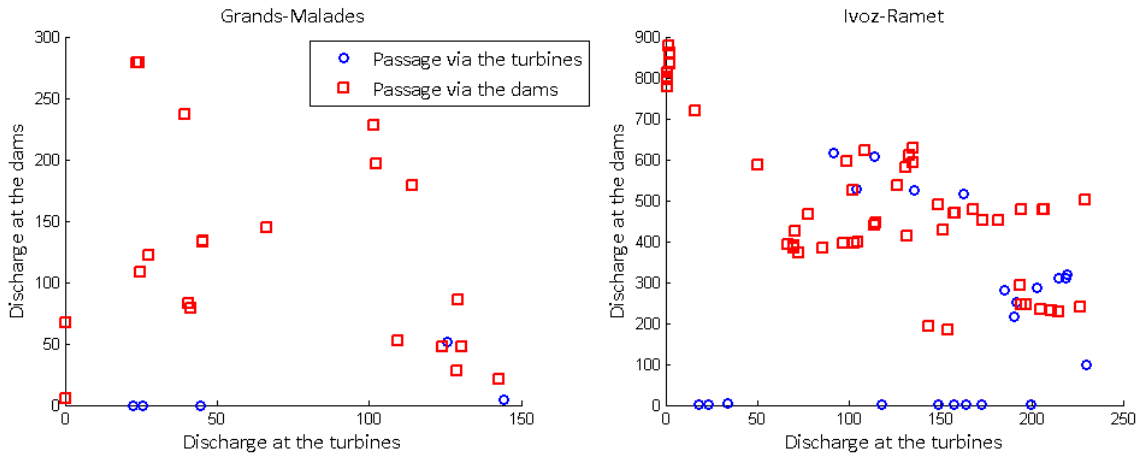


Figure II-23 : Relations between the discharges at the dams and at the turbines at the last detection time of eels passing through the turbines and the dams.

The impact of the discharge at the dam on the flow field at the entrance of the water intake of the turbines is expected to depend on the localization of the dam openings which are used to convey the flow. Indeed, a given discharge at the dam is expected to have a higher influence of the flow field at the entrance of the water intake if it is conveyed through the dam opening just next to the water intake than if it is conveyed through a further gate. To evaluate the sensitivity of the distribution of the dam discharge in-between the dam openings, a *dam opening coefficient* is used to represent, for a given discharge, the distribution of the dam openings used to convey the flow. Considering  $n$  dam openings with a same width, numbered 1 to  $n$  where number 1 refers to the dam opening closest to the water intake of the turbines, the *dam opening coefficient* is computed by:

$$\frac{\sum_{i=1}^n (i-1) Q_i}{\frac{n-1}{2} \sum_{i=1}^n Q_i}.$$

Therefore, a dam opening coefficient equal to 0 indicates that the total dam discharge is passing through the first dam opening while a value of 2 refers to a total dam discharge passing through the last dam opening. A value of 1 for the dam opening coefficient is representative of a dam discharge passing through the central dam opening.

At the site of Ivoz-Ramet, the dam opening coefficients are shown in Figure II-24 for discharges at dams higher than 50 m<sup>3</sup>/s at the last detection time of eels. Although the coefficients are lower than 1 for the four passing through turbines with the highest discharges at the turbines, which is representative of a dam discharge conveyed preferentially nearby the water intake of the hydropower plan, the values of the dam opening coefficient remain mostly close to unity. Hence, the dam discharge can generally be considered as fairly distributed at each side of the central dam opening.



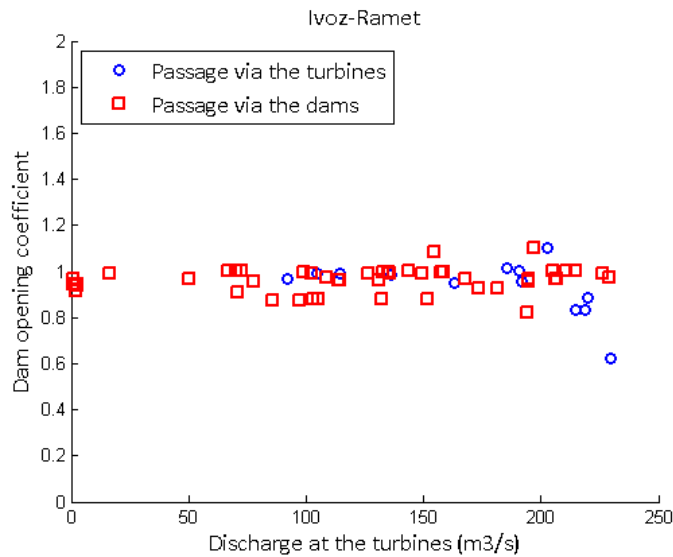


Figure II-24 : Relations between the dam opening coefficient and the discharge at the turbines at the last detection time of eels passing through the turbines and the dams.

#### II.4 Guidelines for the prescription of the hydrodynamic conditions

Eels passages **through the turbines** were observed from October 10 (resp. October 12) to November 12 (resp. November 16) at the site of Grands-Malades (resp. Ivoz-Ramet). Only a few number of 2-D locations of eels were measured: populations of respectively 4 and 14 individuals at Grands-Malades and Ivoz-Ramet. The characteristics of the hydrodynamic conditions during this period are the following:

- Constant upstream levels of 64.6 m and 78.5 m at Grands-Malades and Ivoz-Ramet.
- At Grands-Malades, low-flow discharges of the Meuse river are observed. Most of eel passages occur without any discharge at the dam. A single passage through the turbines is observed with a non-zero discharge at the dam in a situation in which the turbine discharge is more significant.
- At Ivoz-Ramet, wide range of discharges of the Meuse river are observed. On contrary to Grands-Malades, several passages of eels through the turbines occur in situations in which the discharge at the dams is higher than at the turbines.
- At Ivoz-Ramet, the discharge is generally fairly distributed along the dam openings.

From mid-November to the end of November at Grands-Malades and to the beginning of February at Ivoz-Ramet, passages of eels were observed through the dams. During this period, the hydrodynamic conditions were the following:

- Constant upstream levels of 64.6 m at Grands-Malades and variations in-between 78.0 m and 78.5 m at Ivoz-Ramet.
- High variations of the discharge of the Meuse river with values ranging from 100 m<sup>3</sup>/s to 1,000 m<sup>3</sup>/s.
- At Grands-Malades, eels were passing through the dam as soon as the discharge at the dam becomes higher than 50 m<sup>3</sup>/s.
- At Ivoz-Ramet, eels were generally passing through the dam as long as the discharge at the dams is higher than 400 m<sup>3</sup>/s.



### III. Setup of the Numerical modelling

The 2D numerical modelling of the Meuse River was performed with the free surface flow solver WOLF2D, presented in section III.1. The 2D numerical modelling of the sites of Grands-Malades and Ivoz-Ramet requires the design of the topographic modelling (river bathymetry and location of the facilities) in section III.2 and the prescription of the hydraulic conditions in section III.3.

At both site, the 2D numerical modelling extends from the mobile dam at the downstream end to around 1.5 km at the upstream end. This extension is chosen sufficiently long so that the prescription of the discharge distribution at the upstream end has no impact on the hydrodynamic variables at the zone of interest (area of fish tracking close to the water intakes of the powerplants).

#### III.1 Flow solver WOLF2D

The numerical studies of the flows in the Meuse River have been carried out with the 2D free surface flow solver WOLF2D using a square meshes grid. This numerical tool, part of the WOLF package for free surface flow modelling, solves by a finite volume method the conservative form of the depth-integrated Navier Stokes equations, able to represent all the flow specificities in the Meuse River.

##### III.1.1 The WOLF package

The flow software package WOLF has been completely developed for more than 15 years by the Research Unit HECE of the University of Liege. Its reliability and efficiency have been tested on a high number of theoretical, experimental as well as real case studies.

WOLF is a set of free surface or pressurized flow solvers where coexist, in the same development environment, tools for the resolution of the 1D and 2D Navier-Stokes equations with additional turbulence effects, or sediment, pollutant as well as air transport considerations. A physically based and spatially distributed hydrological model, a parameter optimization tool and a powerful graphical pre- and post-processing interface complete the package.

##### III.1.2 The solver WOLF2D

WOLF2D solves the conservative form of the depth integrated Navier-Stokes equations, i.e. three equations (one for mass conservation and two for momentum conservation), in order to compute in each point of a 2D grid the water height  $h$  and the unit discharges  $uh$  and  $vh$  and to deduce the mean flow velocity components  $u$  and  $v$  along respectively  $x$  and  $y$  axes:

$$\frac{\partial h}{\partial t} + \frac{\partial uh}{\partial x} + \frac{\partial vh}{\partial y} = 0$$

$$\frac{\partial uh}{\partial t} + \frac{\partial u^2 h}{\partial x} + \frac{\partial uvh}{\partial y} + \frac{g \cos \theta_z}{2} \frac{\partial h^2}{\partial x} = -gh \cos \theta_z \frac{\partial z_b}{\partial x} + g \cos \theta_z h J_x + gh \sin \theta_x$$

$$\frac{\partial vh}{\partial t} + \frac{\partial v^2 h}{\partial y} + \frac{\partial uvh}{\partial x} + \frac{g \cos \theta_z}{2} \frac{\partial h^2}{\partial y} = -gh \cos \theta_z \frac{\partial z_b}{\partial y} + g \cos \theta_z h J_y + gh \sin \theta_y$$

where  $\theta_x$  and  $\theta_y$  are the angles between the horizontal and  $x$  and  $y$  axis respectively,  $z_b$  is the bottom elevation,  $g$  is the gravity acceleration and  $J_{x,y}$  represent the components of the friction slope.

The only assumption needed for the depth integration of the equations is that the velocities perpendicular to the main flow direction remain small in comparison with the velocities in this main flow direction, in order that their product or the square of their ratio be negligible. This is weakly restrictive in most of the river engineering applications.

WOLF2D solves the equations by a finite volume method using an original flux-vector splitting technique adapted to free surface flow. Special care has been done for consistent bottom slope and

friction effects evaluation in case of real topography. Friction side edges are for example taken into account where a boundary between dry and wet cells is detected.

The algorithm is designed to deal automatically with any moving boundary. It incorporates an original method to handle covered and uncovered (wet and dry) cells. In addition, an adaptive grid extension technique achieves a drastic reduction in computation time, by restricting the simulation domain to the wet cells (and a surrounding narrow strip).

Thanks to an efficient iterative resolution of the continuity equation at each time step, based on a correction of the discharge fluxes before any evaluation of momentum balances, the conservation of the hydrodynamic properties is ensured in the whole simulation, even when the layout evolves along time (floods, dam break wave propagation...).

Turbulence modelling can be performed using various mathematical models in agreement with the depth integrated form of the equations, from algebraic models up to two additional equations  $k$ - $\varepsilon$  type ones.

The different features of the software WOLF2D can be summarized as follows:

- transient computations of the depth-integrated Navier-Stokes equations, by a finite volumes method,
- integrated and automated management of the topographical and morphological characteristics,
- explicit computation of the turbulent features,
- original technique of covered-uncovered cells,
- possibility of dealing with different types of boundary conditions (water depth, discharge, solid wall, control section), steady or transient,
- interactive user-interface, with high performance pre- and post-processing,
- results plots: speed or discharge vectors, water depth, free surface level, Froude, with possibility of three-dimensional representation and videos.

Thanks to these different characteristics, the software is able to model, among others:

- the two-dimensional free surface unsteady flows,
- the floods and low water stages for natural and artificial rivers, navigable or not (sub or super critical flow conditions),
- transient flooding phenomena,
- reservoirs and water fall crossing structures design,
- control hydraulic structures,
- stiff or gradual waves propagation, including the ones resulting from a high dam breaking.

### III.1.3 Reproduction of the bottom friction

The bottom friction is computed by an explicit Manning-Strickler formulation with uniformly distributed values of the Strickler coefficient equal to respectively  $0.025 \text{ sm}^{-1/3}$  and  $0.023 \text{ sm}^{-1/3}$  for the reach at the upstream of the pilot sites of Grands Malades and Ivoz-Ramet. These values were chosen consistently with the calibration done by the HECE research group in the context of the AMICE project.

## III.2 Topographic modelling

Raw bathymetric data are available from SPW surveys with a high spatial resolution of 50 cm and an elevation accuracy of 10 cm. The raw bathymetry required some topographic treatments to improve the accuracy or to complete some missing data.

### III.2.1 Grands-Malades

An overview of the topographic modelling at the upstream of the site of Grands-Malades is shown in Figure III-1. The  $50 \times 50 \text{ cm}^2$  Cartesian grid contains 670,000 cells. The reproduction of the

bathymetry of the water intake of the hydropower plant, located on the right side of the mobile dam, is shown in Figure III-2. A local depression can be observed at the upstream of the water intake with a topographic drop around 80 cm.

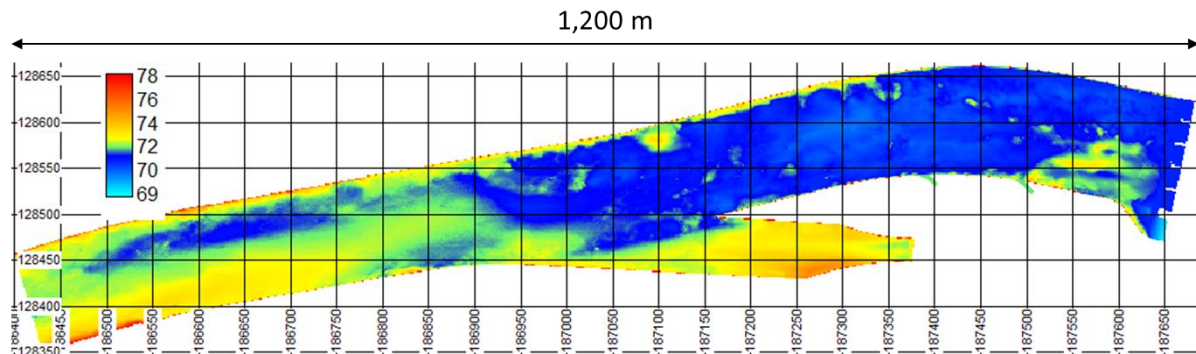


Figure III-1: Topographic modelling of the upstream of the site of Grands-Malades.

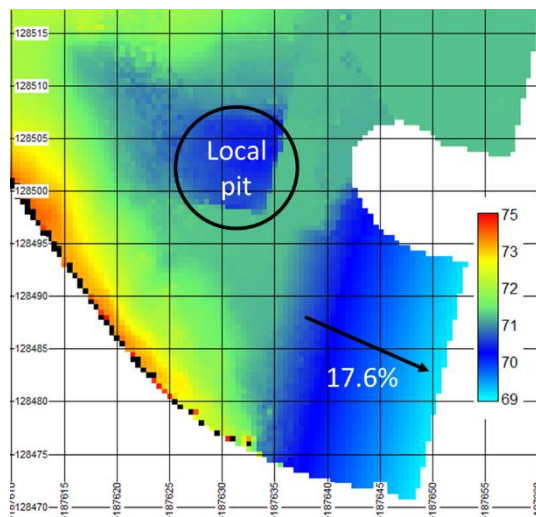


Figure III-2: Topographic modelling of the water intake of the hydropower plant at Grands-Malades.

### III.2.2 Ivoz-Ramet

The topographic modelling at the upstream of the site of Ivoz-Ramet contains 910,000 cells at a resolution of  $50 \times 50 \text{ cm}^2$  (Figure III-3). At the entrance of the water intake of the hydropower plant (on the left side of the downstream end), there is a topographic step around 1 m high and a surface beam forcing a pressurized flow under the level 63.5 m (Figure III-4).

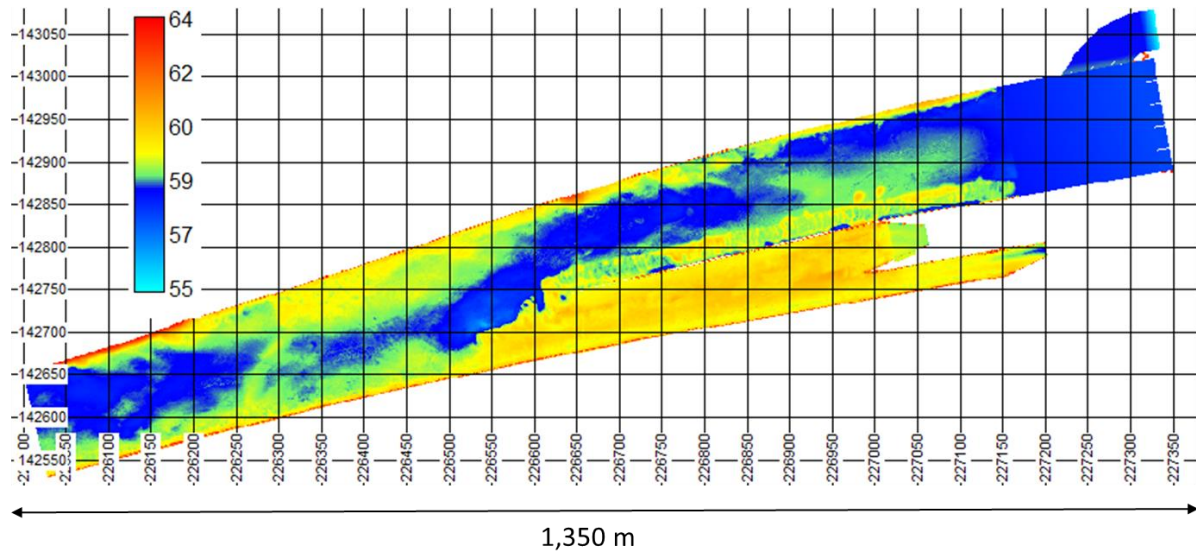


Figure III-3: Topographic modelling of the upstream of the site of Ivoz-Ramet.

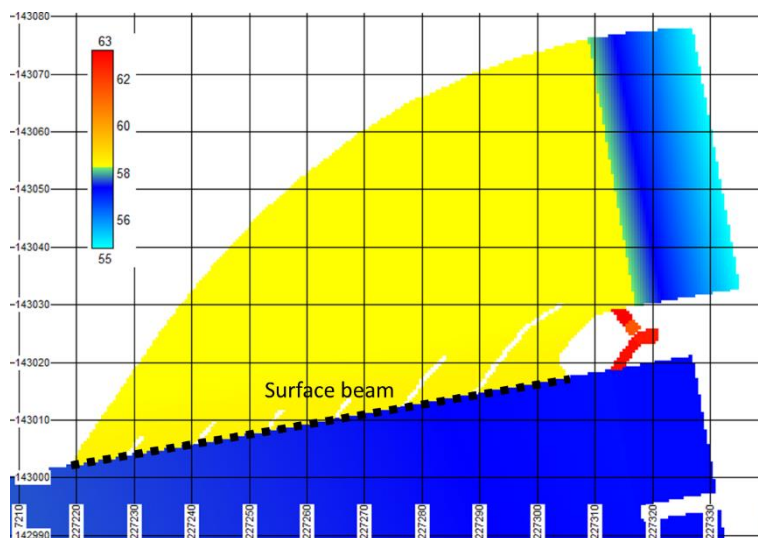


Figure III-4: Topographic modelling of the water intake of the hydropower plant at Ivoz-Ramet.

### III.3 Hydraulic conditions

#### III.3.1 Boundary conditions

The inflow river discharge is prescribed uniformly along the upstream end of the numerical model. At the hydropower plants, the outflow discharge is prescribed as a function of the free surface level in the water intake, consistently with the regulation rules used by the operators of the hydropower facilities. The sites of Grands-Malades and Ivoz-Ramet are respectively equipped by 4 and 3 turbines.

#### III.3.2 Influence of the reproduction of the surface beam

At Ivoz-Ramet, a sensitivity analysis was conducted to evaluate the influence of the reproduction of the pressurized flow under the surface beam in the numerical modelling. We analyse its influence on the velocity distribution at the entrance of the water intake where the smolts are mostly located (section II.2.1.2).

Two steady simulations are conducted with a Meuse discharge of  $69 \text{ m}^3/\text{s}$ , completely released through the right side turbine, and without any turbulence effects. For the two simulations, with and without the reproduction of the surface beam, we compare the absolute velocity profile just at the upstream of the beam (AA' in Figure III-5).

While the reproduction of the surface beam has a local impact of the velocity values, the 2D time-average absolute velocity profiles represented in Figure III-6 are very close to each other at the upstream of the surface beam, which indicates a poor impact of the beam on the velocity distribution at the upstream of the water intake. Consistently, the beam will no more be represented in the numerical modelling.

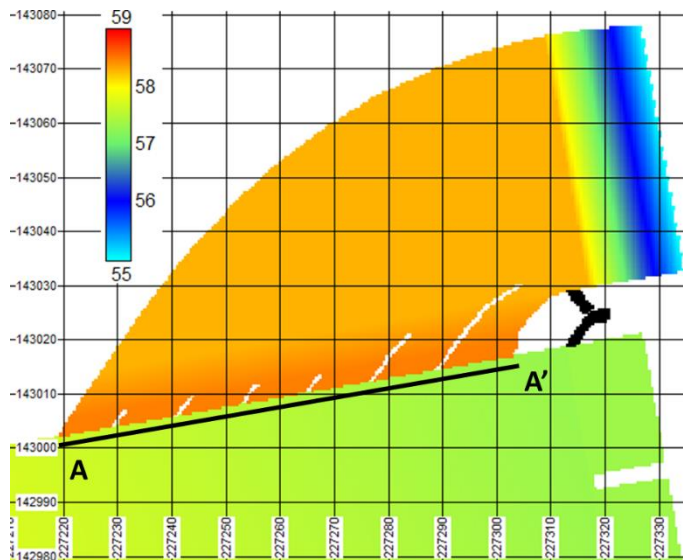


Figure III-5: Profile AA' for the extraction of the absolute velocities.

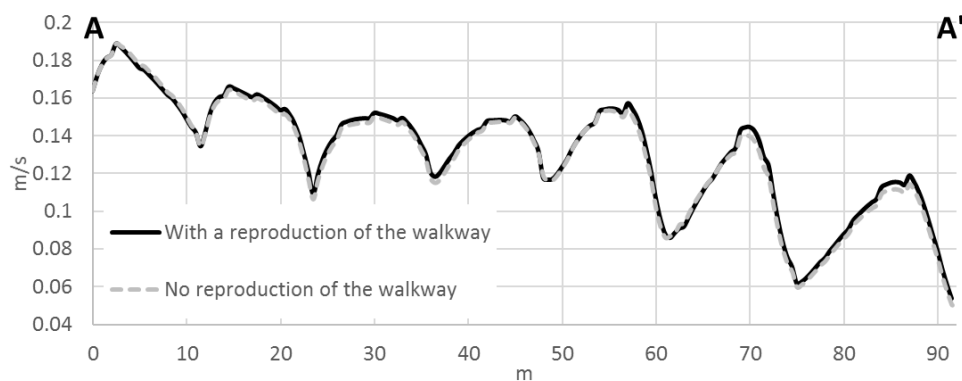


Figure III-6: Absolute velocity distribution along the profile AA' of Figure III-5.



## IV. Influence of the mesh resolution and turbulence activation

The setup of the numerical modelling was introduced in section III with a mesh resolution of 50 cm. In this section, the influence of the resolution of the mesh is assessed (section IV.2), as well as the influence of the consideration of turbulence effects in the modelling (section IV.1).

### IV.1 Influence of the turbulence activation

The influence of considering the turbulence effects in the numerical modelling is assessed for the sites of Grands-Malades and Ivoz-Ramet. A comparison is done between the numerical results obtained with a resolution of 50 cm and without a turbulence model and the ones resulting from a same resolution but using a  $k-\epsilon$  turbulence model.

At Grands-Malades, we consider a Meuse discharge of  $78.5 \text{ m}^3/\text{s}$  and the use of the two turbines located at the sides to maximize the turbulence effects. The distributions of the absolute unit discharges are compared in Figure IV-1 nearby the hydropower plant and indicators of the differences between the two distributions are given in Table 4. The correlation  $C$  and error  $E$  coefficients between two matrices  $X$  and  $Y$  are computed by the following equations:

$$C = \frac{\sum_i \sum_j (X_{ij} - \bar{X})(Y_{ij} - \bar{Y})}{\sqrt{\left( \sum_i \sum_j (X_{ij} - \bar{X})^2 \right) \left( \sum_i \sum_j (Y_{ij} - \bar{Y})^2 \right)}}$$

$$E = \frac{\sum_i \sum_j |X_{ij} - Y_{ij}|}{\sum_i \sum_j \bar{X}}$$

where  $\bar{X}$  represents the mean value of  $X$ .

A comparison of the two pictures of Figure IV-1 and the values of the correlation coefficients show a non-significant influence of the turbulence model on the unit discharge distribution. The values of the error coefficients (8% and 5%) remain low.

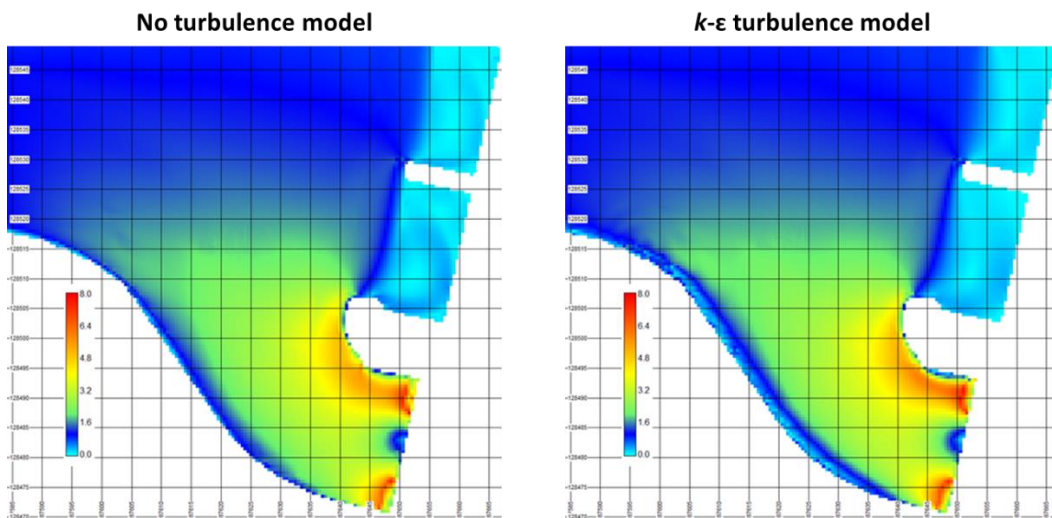


Figure IV-1: Distribution of the absolute unit discharge ( $\text{m}^2/\text{s}$ ) nearby the hydropower plants of Grands-Malades without (left) and with (right) a turbulence model.

$C_{qx}$	$C_{qy}$	$E_{qx}$	$E_{qy}$
0.990	0.995	8%	5%

Table 4: Correlation  $C$  and error  $E$  coefficients between the distributions of unit discharges  $q$  in the  $x$ - and  $y$ - directions computed with or without a turbulence model at Grands-Malades.

At the site of Ivoz-Ramet, the units discharge distributions are computed for a Meuse discharge of  $69 \text{ m}^3/\text{s}$  and the use of a single turbine on the right side of the hydropower plan. As depicted in Figure IV-2, the distributions of unit discharges in the water intake and along its entrance are significantly impacted by the use of a  $k-\epsilon$  turbulence model, comparing to the results computed without any turbulence model. For the zone represented in red in Figure IV-2, the correlation and error coefficients are computed for the distributions of unit discharges in the  $x$ - and  $y$ - direction with or without a turbulence model. The errors in Table 5 are significantly higher than at Grands-Malades and confirm the necessity of using a turbulence model in the numerical computation.

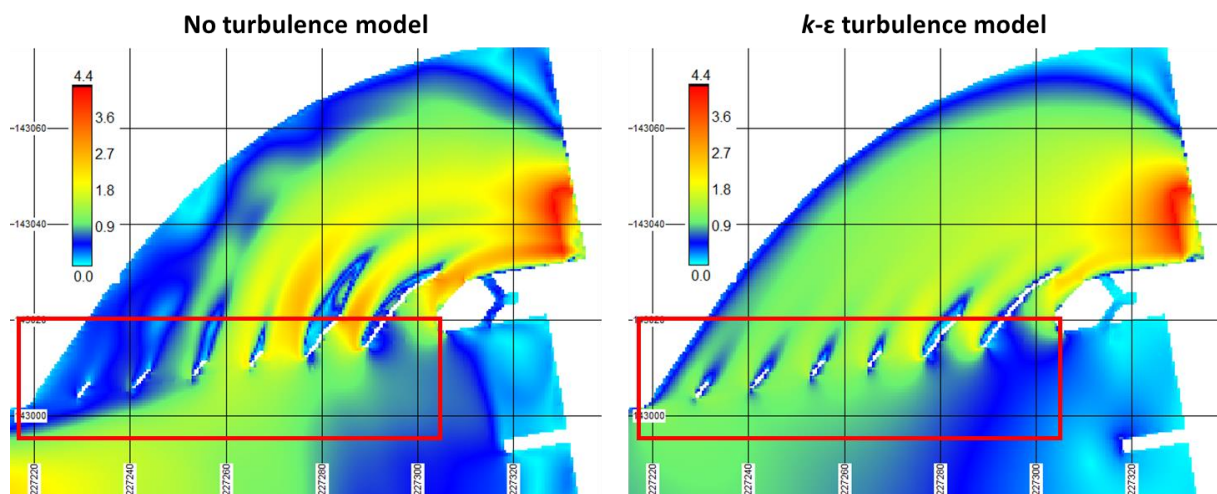


Figure IV-2: Distribution of the absolute unit discharge ( $\text{m}^2/\text{s}$ ) nearby the hydropower plants of Ivoz-Ramet without (left) and with (right) a turbulence model.

$C_{qx}$	$C_{qy}$	$E_{qx}$	$E_{qy}$
0.754	0.884	29%	13%

Table 4: Correlation  $C$  and error  $E$  coefficients between the distributions of unit discharges  $q$  in the  $x$ - and  $y$ - directions computed with or without a turbulence model at Ivoz-Ramet.

The values of the Strickler roughness coefficients were not modified depending on the activation of turbulence as the overall head loss remains very limited due to the low discharges which are considered in this study.

## IV.2 Influence of the mesh resolution

The impact of the mesh resolution on the unit discharge distribution is analysed for the site of Grands-Malades. Grands-Malades is considered more likely for a mesh coarsening than the site of Ivoz-Ramet where local topographic variations would not be accurately reproduced at the coarse scale

(piers at the entrance of the water intake, topographic step, perforated piers, etc.). Therefore, as shown here below, the degradation of the results should be exacerbated for the site of Ivoz-Ramet.

Simulations are performed with a Meuse discharge of  $78.5 \text{ m}^3/\text{s}$  and using a  $k-\epsilon$  turbulence model. Three mesh resolutions are compared: 50 cm, 2 m and 4 m (Figure IV-3). Correlation and error coefficients are given in Table 5 and the profiles of normal unit discharges in the water intake are compared in Figure IV-4.

The results indicate a significant downgrading of the unit discharge distribution consequently to a coarsening of the mesh resolution. For instance, the preferential flow observed on the left side of the water intake with a mesh resolution of 50 cm is poorly reproduced with the coarser resolutions.

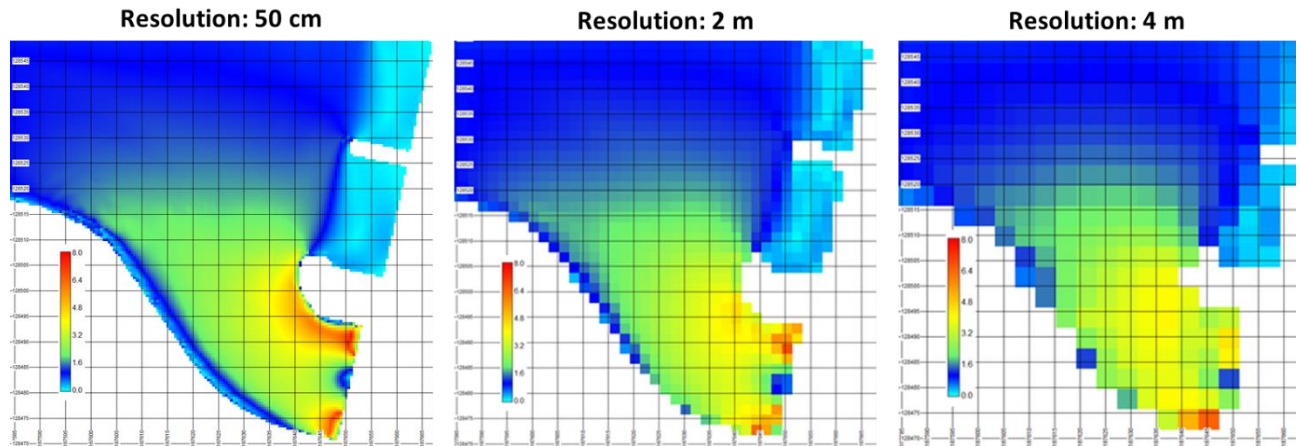


Figure IV-3: Distribution of the absolute unit discharge ( $\text{m}^2/\text{s}$ ) nearby the hydropower plants of Grands-Malades at different mesh resolutions.

	$C_{qx}$	$C_{qy}$	$E_{qx}$	$E_{qy}$
2 m	0.936	0.949	16%	12%
4 m	0.875	0.909	24%	19%

Table 5: Correlation  $C$  and error  $E$  coefficients between the distributions of unit discharges  $q$  in the  $x$ - and  $y$ - directions computed with a mesh resolution of 50 cm and with mesh resolutions of 2 m and 4 m.

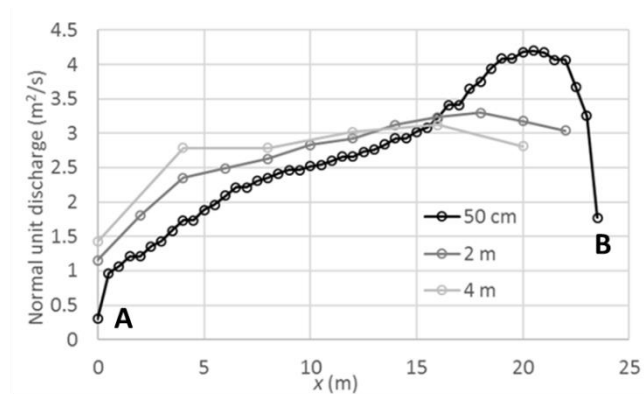
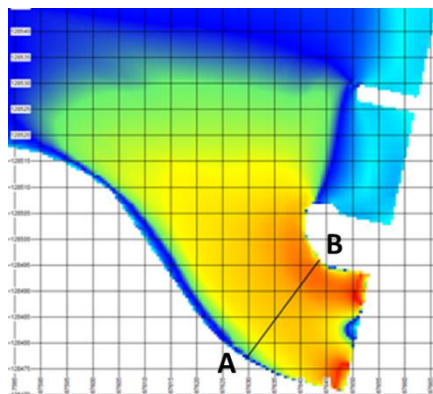


Figure IV-4: Normal unit discharge in the water intake with different mesh resolutions.



### IV.3 Conclusion

The results of the sensitivity analysis of the activation of the turbulence and of the mesh resolution indicate that:

- The use of a turbulence model does not impact significantly the unit discharge distribution in the water intake at Grands-Malades but impact significantly the hydrodynamic results at the entrance of the water intake at Ivoz-Ramet. In the following of the report, the turbulence effects were included in the numerical modelling at both pilot sites.
- The unit discharge distribution in the water intake of Grands-Malades, computed with a mesh resolution of 50 cm, is significantly downgraded with a coarser mesh resolution. At Ivoz-Ramet, the downgrading is expected to be aggravated due to the more complex topography.

In conclusion, numerical simulations of the hydrodynamic variables will be performed using a 50 cm grid (fine grid) with a  $k-\epsilon$  turbulence model for the both sites.

## V. Correlations between the hydraulic parameters and smolt monitoring data

In this section, the fish monitoring data (section II.2.1) are compared with the numerical hydrodynamic fields to look for correlations which will serve for the design of an effective downstream migration system. The 2D coordinates of fish are filtered using a threshold absolute velocity of 1 m/s as detailed in section II.1.

Consistently with the conclusions of the analysis of the hydrodynamic parameters during the period of observation of smolts at the sites of Grands-Malades and Ivoz-Ramet (section **Erreur ! Source du renvoi introuvable.**), the numerical hydrodynamic fields are computed for a steady Meuse discharge and without lock and dam operation.

The correlation with the fish monitoring data is analyzed for the following hydrodynamic parameters: absolute velocity, absolute unit discharge, two-dimensional turbulent viscosity and gradient of absolute velocity. Two method of analysis are used:

- Based on a **qualitative** comparison between density maps, showing the spatial distribution of fishes, and maps representing the hydrodynamic parameters.
- Based on an original **quantitative** analysis of the distribution of the hydrodynamic parameters in the presence of fishes.

The quantitative methodology is illustrated in Figure V-1 for a simple 3 x 3 grid giving the spatial distribution of the values of a given hydrodynamic parameter (left side grid) and the number of 2D fish coordinates detected in each cell (right side grid). The first step of the quantitative analysis consists in the computation of the density distribution of the hydrodynamic variables over the grid ① (4 values in [0 - 10[, 2 values in [10 - 20[ and 3 values in [20 - 30]). In the second step, a *combined* density distribution is computed by counting how many fishes are detected in cells for which the value of the hydrodynamic parameter lies in each interval of hydrodynamic values ② (17 fishes in [0 - 10[, 24 fishes in [10 - 20[ and 57 fishes in [20 - 30]). Finally, the difference between the two probability density function shows the attractiveness or repulsion effect of the values of the hydrodynamic parameters ③. In this configuration, the results indicate an attractiveness for the highest values of the hydrodynamic parameter and a repulsion for the lowest ones.

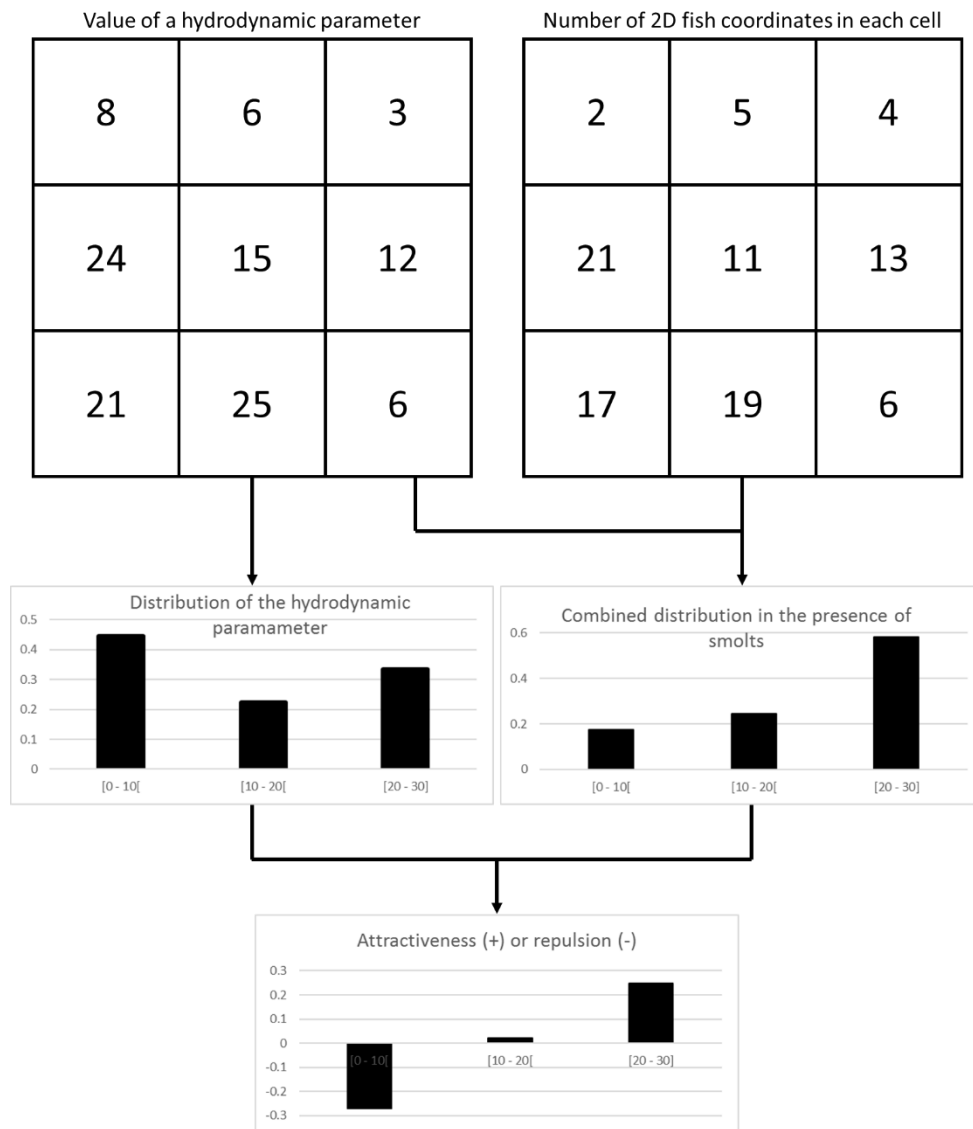


Figure V-1: Illustration of the quantitative analysis of the distribution of the hydrodynamic parameters in the presence of fishes.

## V.1 Smolts at Grands-Malades

### V.1.1 Hydrodynamic scenarios representative of the period of observation

At the site of Grands-Malades, the monitoring zone is the water intake of the hydropower plant where smolts locations were measured from 14 April 2017 to 10 May 2017. The temporal distribution of the 2D coordinates in Figure V-2 shows that around 3/4 of them are measured during the three first days of monitoring (consistently with section II.2.1.1).

For each detection of a smolt by the 2D monitoring system, the discharge at the turbines of the hydropower plant are reported in Figure V-3. Group 1 corresponds to the turbine on the left side on the hydropower plant while Group 4 stands for the turbine on the right side. The extreme and mean values of the discharge at each turbine is reported in Table 6, as well as the fraction of 2D coordinates corresponding to the different combinations of turbine openings. The discharge at each turbine is around 40 m<sup>3</sup>/s in average with low variations. The mean Meuse discharge over the period of monitoring is around 73 m<sup>3</sup>/s, corresponding therefore to an operation of two groups. The flow variables resulting from the combinations representing more than 5% of the total 2D coordinates G-

34, G-23, G-24 and G-0 are representative of 83% of the total measurements. As indicated in Table 7, the number of smolts observed for each combination is higher than 10.

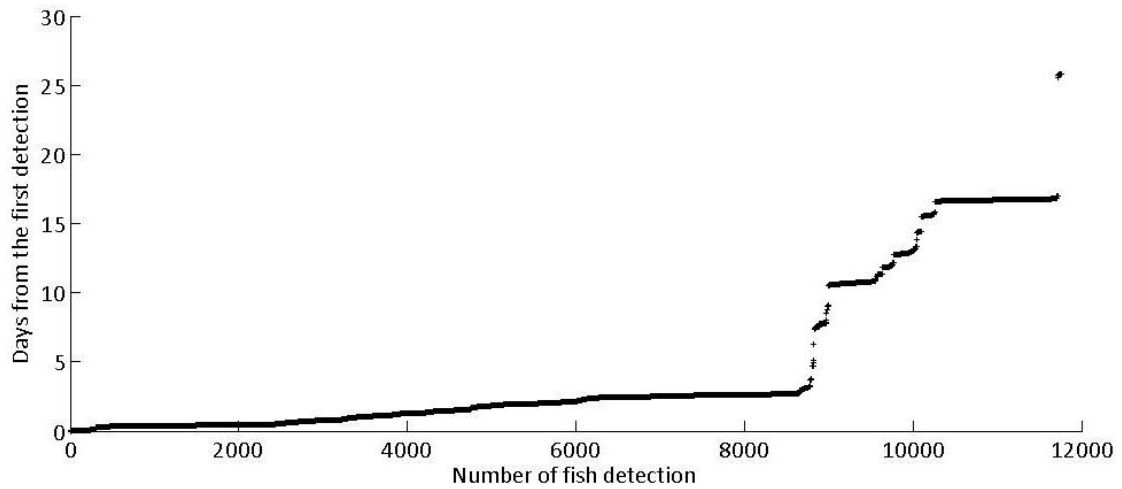


Figure V-2: Temporal distribution of 2D detections of smolts at Grands-Malades.

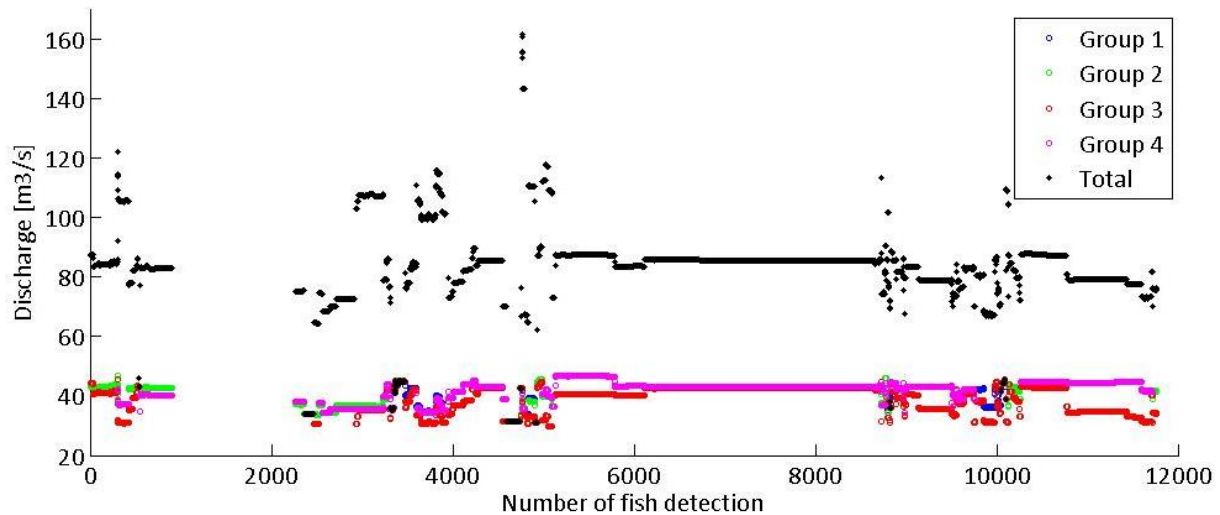


Figure V-3: Discharge at the turbines of the hydropower plant at Grands-Malades during the fish tracking.

	Group 1	Group 2	Group 3	Group 4	
$Q_{\min}$	34 m <sup>3</sup> /s	31 m <sup>3</sup> /s	30 m <sup>3</sup> /s	34 m <sup>3</sup> /s	
$Q_{\max}$	44 m <sup>3</sup> /s	47 m <sup>3</sup> /s	46 m <sup>3</sup> /s	47 m <sup>3</sup> /s	
$Q_{\text{mean}}$	38 m <sup>3</sup> /s	39 m <sup>3</sup> /s	39 m <sup>3</sup> /s	42 m <sup>3</sup> /s	
Combination	Group 1	Group 2	Group 3	Group 4	Distribution of measured 2D coordinates
G-34	☒	☒	☑	☑	57%
G-24	☒	☑	☒	☑	8%
G-23	☒	☑	☑	☒	6%
G-0	☒	☒	☒	☒	12%
	Total				83%
G-13	☑	☒	☑	☒	4%
G-134	☑	☒	☑	☑	3%
G-234	☒	☑	☑	☑	5%
G-123	☑	☑	☑	☒	1%
	Total				96%

Table 6 : Discharge at the turbines of the hydropower plant at Grands-Malades during the fish tracking and fraction of fish coordinates corresponding to different combinations of turbine operation.

Combination	Number of fishes observed
G-34	18
G-24	17
G-23	29
G-0	11

Table 7 : Number of smolts observed for the different combinations of turbine operation.

### V.1.2 Density maps and maps of hydrodynamic parameters

Figure V-4 shows the density maps at Grands-Malades for the combinations of turbine operation identified in the previous section. The square in a black thick line represents the domain for which fields of absolute velocities, absolute discharges, turbulent viscosity and velocity gradient are shown in Figure V-5 to Figure V-8. The previous figures result from a steady computation of a Meuse discharge of 78.5 m<sup>3</sup>/s fully released by the turbines at the downstream end (always 2 turbines in operation).

In Figure V-4, the smolts are evenly distributed over the section of the water intake for the configuration without any turbine operation (G-0), consistently with no hydrodynamic parameters variation (no flow in the water intake). For this configuration, the upstream discharge is either released by the lock or dam operation or (and) is (partially) stored at the upstream reach through an increase of the free surface level. For the combinations of two turbine openings (G-34, G-23 and G-24), the smolts are generally more present on the left side of the water intake where the absolute velocities (Figure V-5) and unit discharges (Figure V-6) are considerably higher. The density map for configurations G-24 suggests an attraction of some smolts on the right side of the water intake consequently to the operation of the turbine located on this side.

Concerning the distributions of absolute velocity and unit discharge in Figure V-5 and Figure V-6, the values are the highest on the left side of the water intake for all the simulations. Then, the absolute velocities are higher when the turbines in operation are located on the left side of the water intake ( $V_{\max,G-23} > V_{\max,G-24} > V_{\max,G-34}$ ). The turbulent viscosity is the lowest in the central part of the water intake and increases to both sides (Figure V-7). The results indicate a low impact of the combination of turbines in operation on the spatial distribution of the turbulent viscosity. Similarly, the distributions of the velocity gradient in Figure V-8 are lowly modified by the combination of the turbines used.



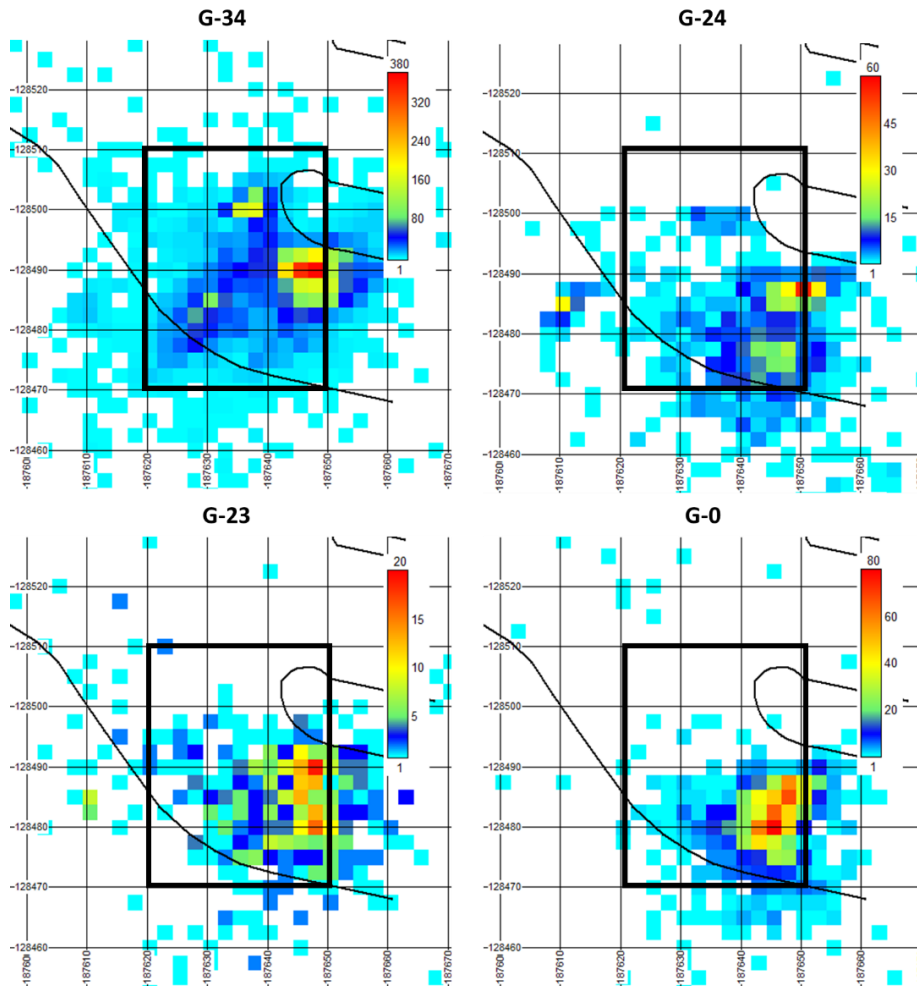


Figure V-4: Density maps at Grands-Malades for the different combinations of turbine openings.

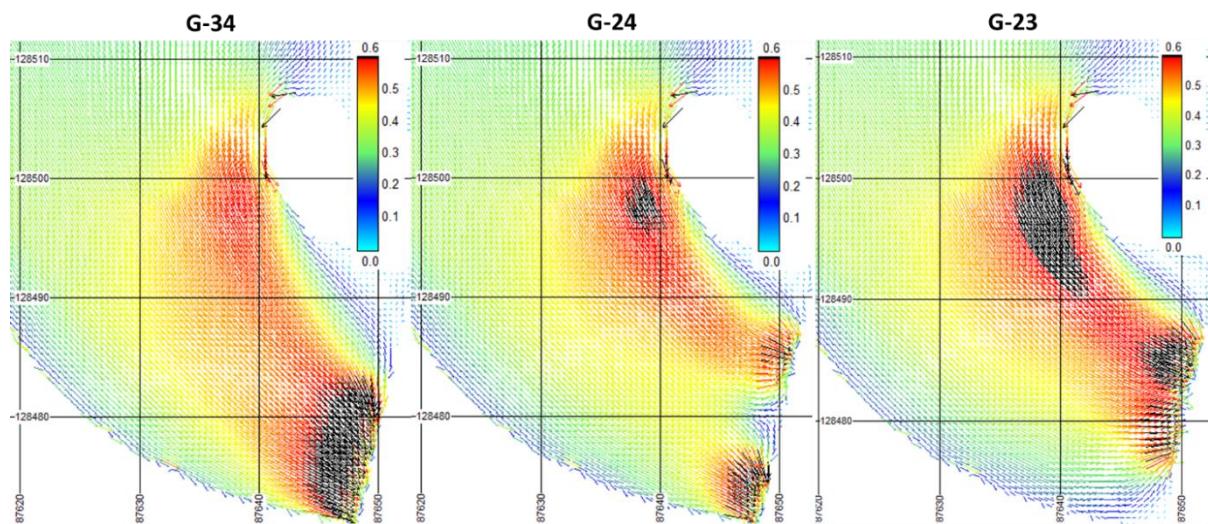


Figure V-5: Absolute velocity distributions at Grands-Malades for the different combinations of turbine openings.

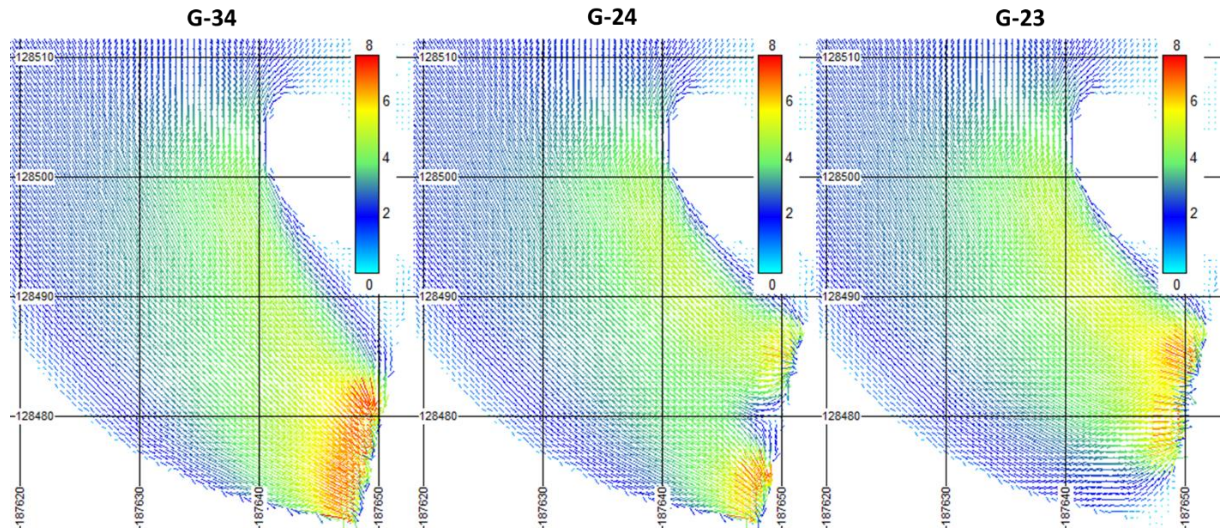


Figure V-6: Absolute unit discharge distributions at Grands-Malades for the different combinations of turbine openings.

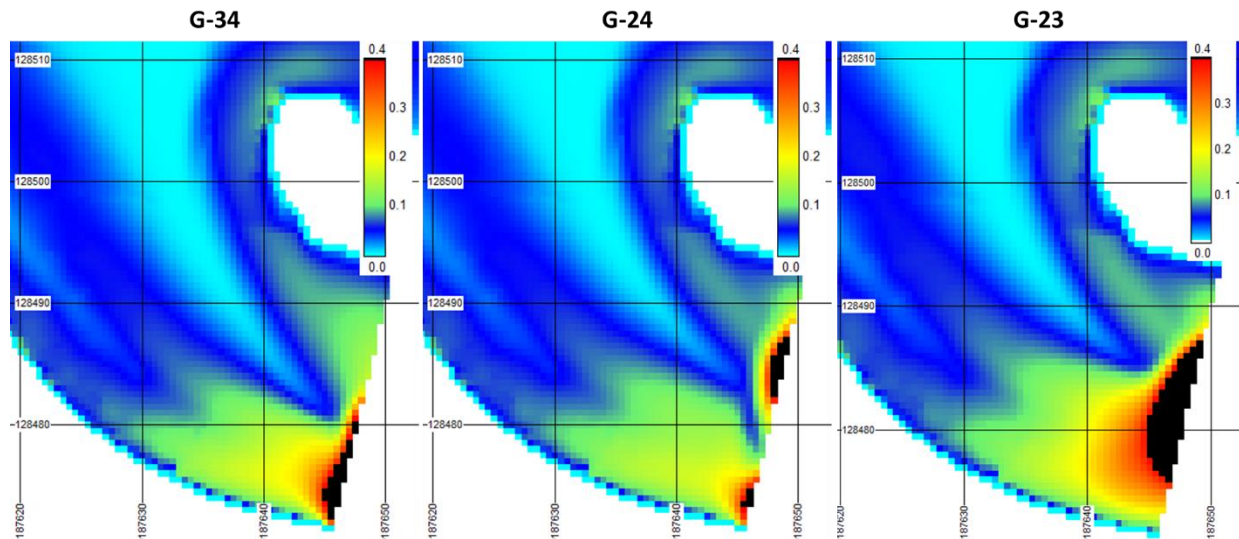


Figure V-7: Turbulent viscosity distributions at Grands-Malades for the different combinations of turbine openings.

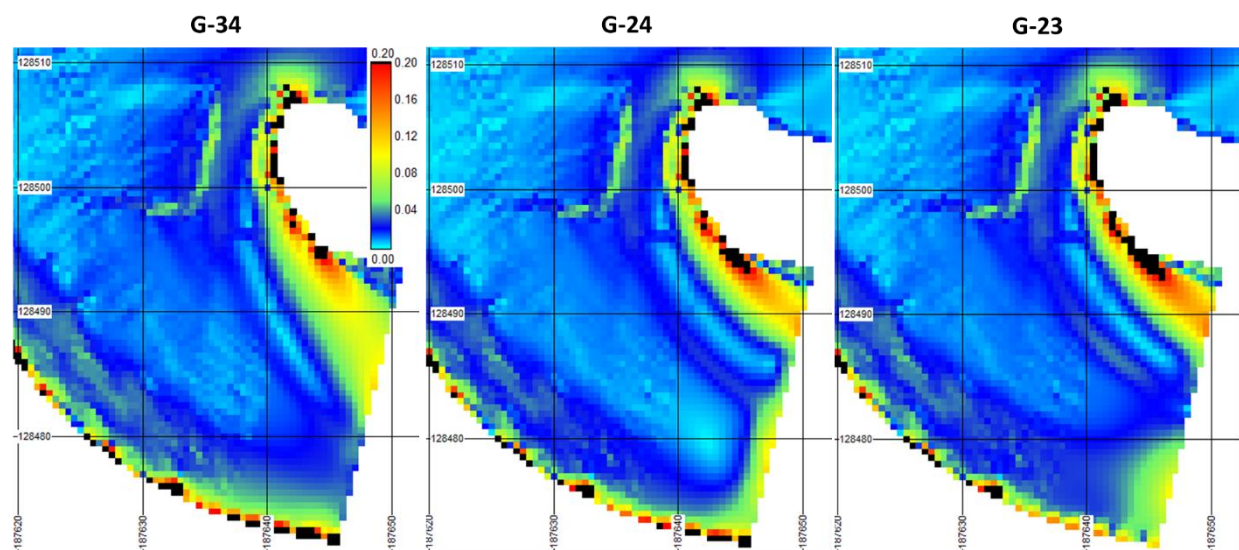


Figure V-8: Velocity gradient distributions at Grands-Malades for the different combinations of turbine openings.



### V.1.3 Probability density functions

The zone of interest for the computation of the correlations between the hydrodynamic parameters and the smolt coordinates was selected to ensure that the zone is completely covered by the 2D monitoring system (Figure V-9).

Consistently with the observations of section V.1.2, the results of Figure V-10 show that:

- Smolts are attracted by high values of absolute velocities and absolute discharges. The distinction between attractiveness and repulsion appears for an absolute velocity of 0.35 m/s.
- Smolts are repulsed by the low values of 2D turbulent viscosity and velocity gradient.

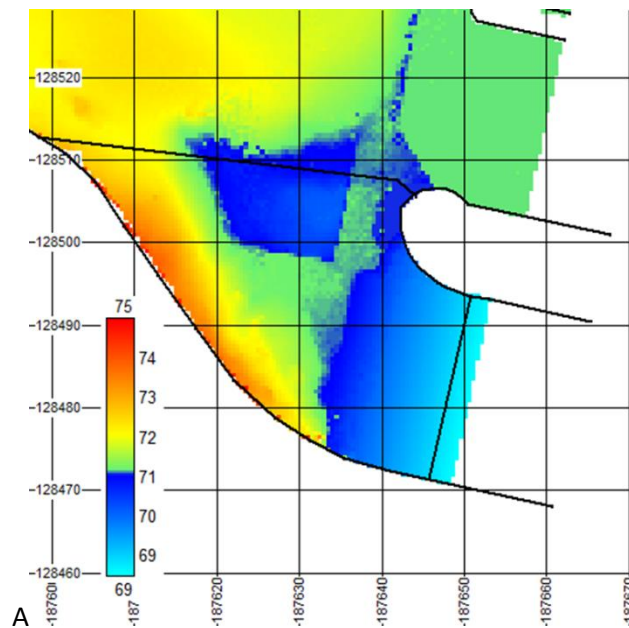


Figure V-9: Topography of the zone of interest for the computation of the correlations between the fish locations and the hydrodynamic parameters at Grands-Malades.

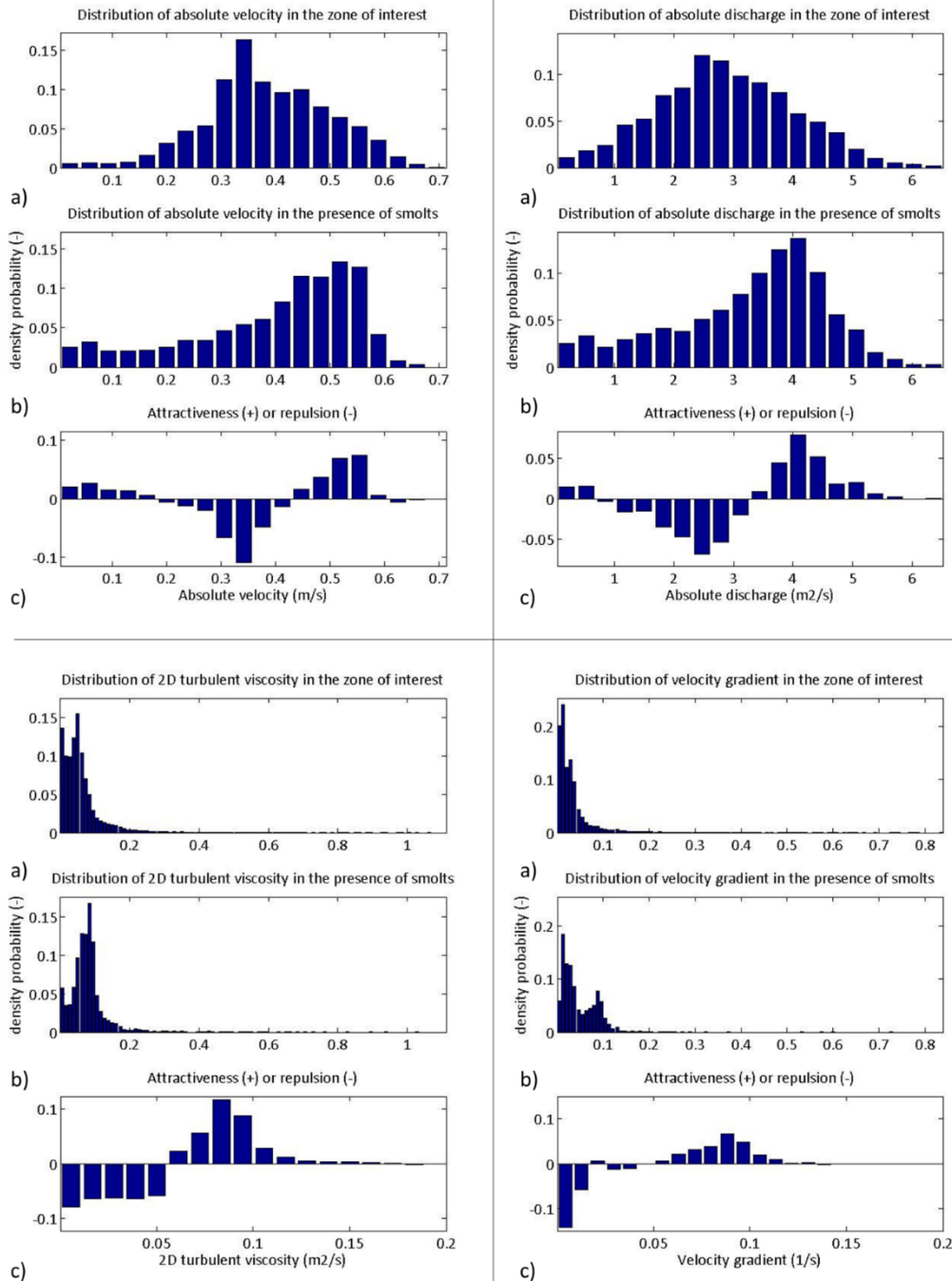


Figure V-10: Probability density distributions (a) in the zone of interest, (b) in the presence of smolts and (c) attractiveness of absolute velocity, absolute discharge, 2D turbulent viscosity and velocity gradient for the smolts at Grands-Malades

## V.2 Smolts at Ivoz-Ramet

### V.2.1 Hydrodynamic scenarios representative of the period of observation

Based on the turbine regulation rules, the Meuse discharge representative of the period of observation (section II.2.2.2) is evacuated through a single turbine of the hydropower plant. However, for the site of Ivoz-Ramet, data describing the turbine operation during the period of observation of smolts were not available. For this reason, we considered two extreme hydrodynamic scenarios consisting in operating a single turbine on the left side or on the right side. Then a sensitivity analysis of the impact of the scenario on the results is performed.

### V.2.2 Density maps and maps of hydrodynamic parameters

The density maps for the site of Ivoz-Ramet were shown in Figure II-5. To facilitate the reading, this figure is reproduced in Figure V-11. The distributions of absolute velocities, absolute discharges and velocity gradients are shown in Figure V-12 to Figure V-14 for the two scenarios. The 2D turbulent viscosity distribution is not represented since the values in the zone of interest remain very weak (lower than  $10^{-3} \text{m}^2/\text{s}$ ).

The smolt density is mainly influenced by the blockage effect of the surface beam at the entrance of the water intake. However, the smolt density is the highest in the central part of the entrance of the fish passage where the velocities are important (Figure V-12). The discharge and gradient velocity do not show any clear relation with the locations of the smolts.

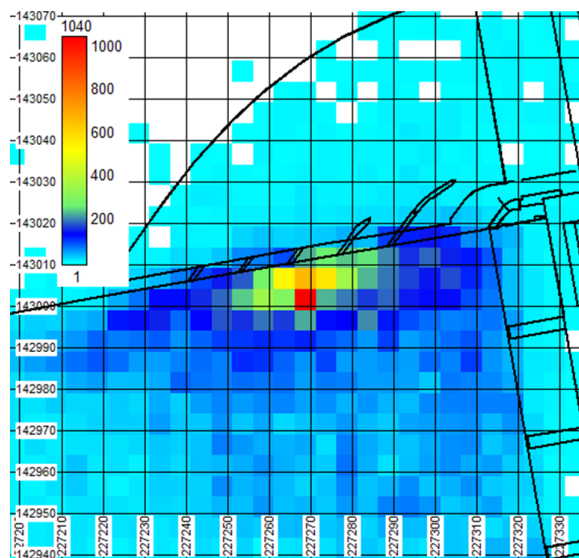


Figure V-11: Density maps at Ivoz-Ramet with a mesh resolution of 5 m.



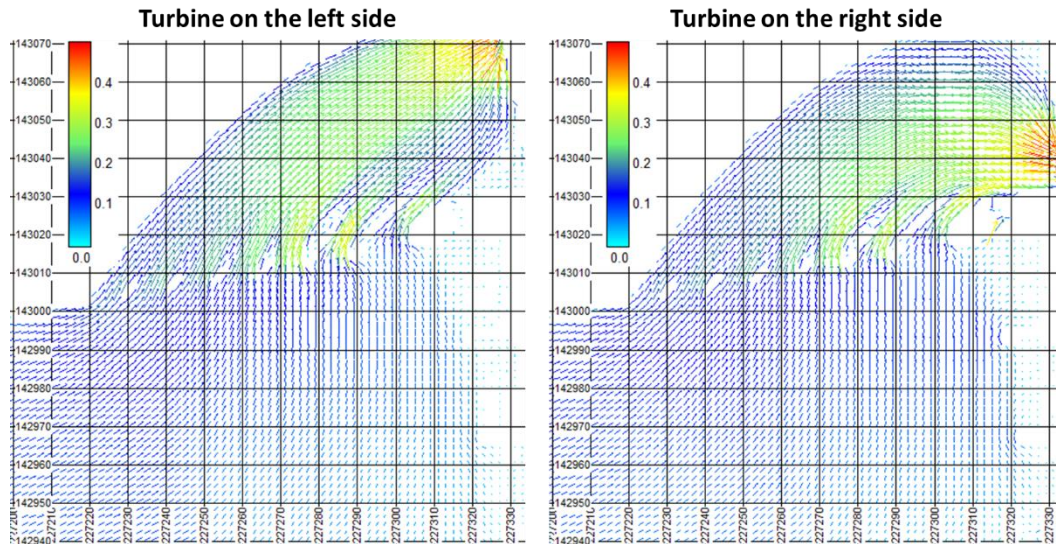


Figure V-12: Absolute velocity distributions at Ivoz-Ramet

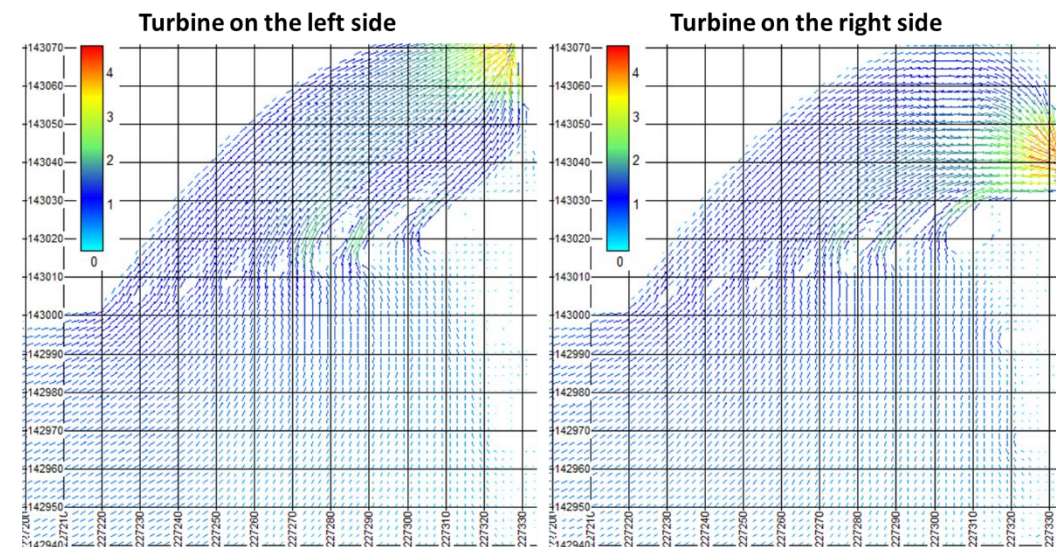


Figure V-13: Absolute discharge distributions at Ivoz-Ramet

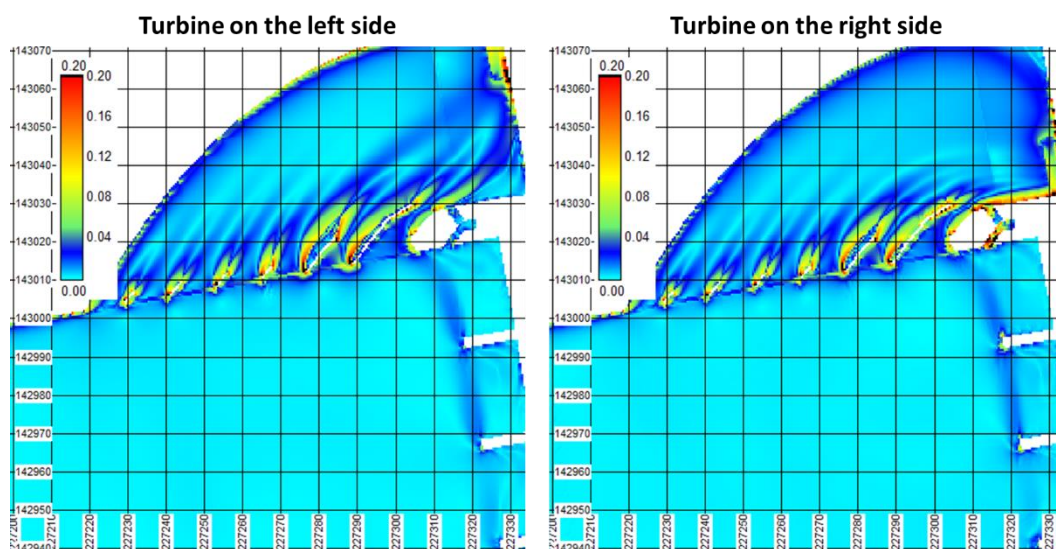


Figure V-14: Velocity gradient distributions at Ivoz-Ramet



### V.2.3 Probability density functions

Probability density functions are computed for a zone of interest stretching from the mobile dam and the hydropower plant to a distance of 190 m at the upstream. The probability density functions of the absolute velocity, absolute discharge and velocity gradient are shown in Figure V-15 and Figure V-16 for the two scenarios of turbine operation. For each scenario, the results indicate:

- An attractiveness of smolts to areas with mid range absolute velocities and absolute discharges.
- No clear correlation for the velocity gradient.

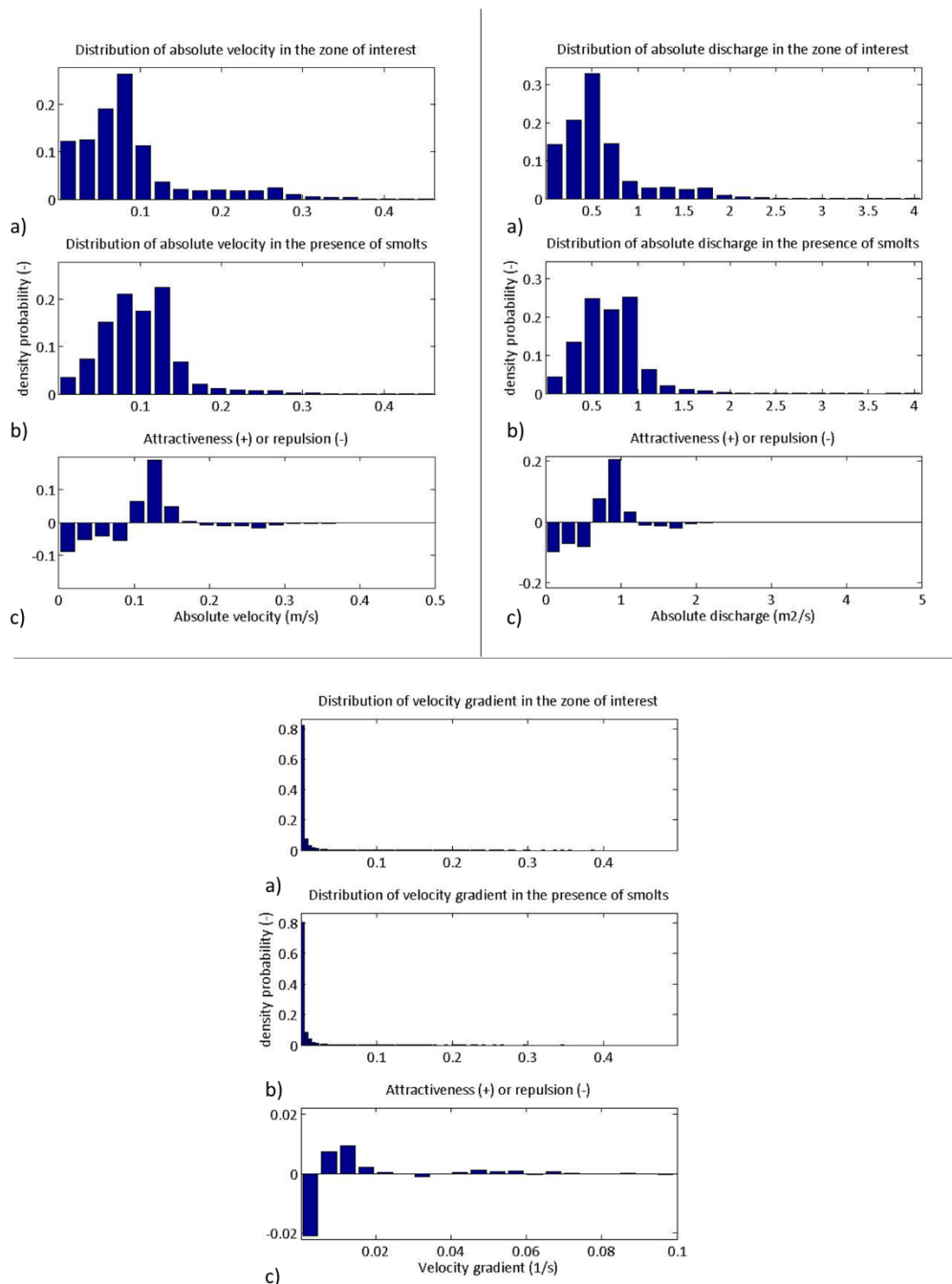


Figure V-15: Probability density distributions (a) in the zone of interest, (b) in the presence of smolts and (c) attractiveness of absolute velocity, absolute discharge and velocity gradient for the smolts at Ivoz-Ramet for the scenario with a turbine opening on the **left** side.

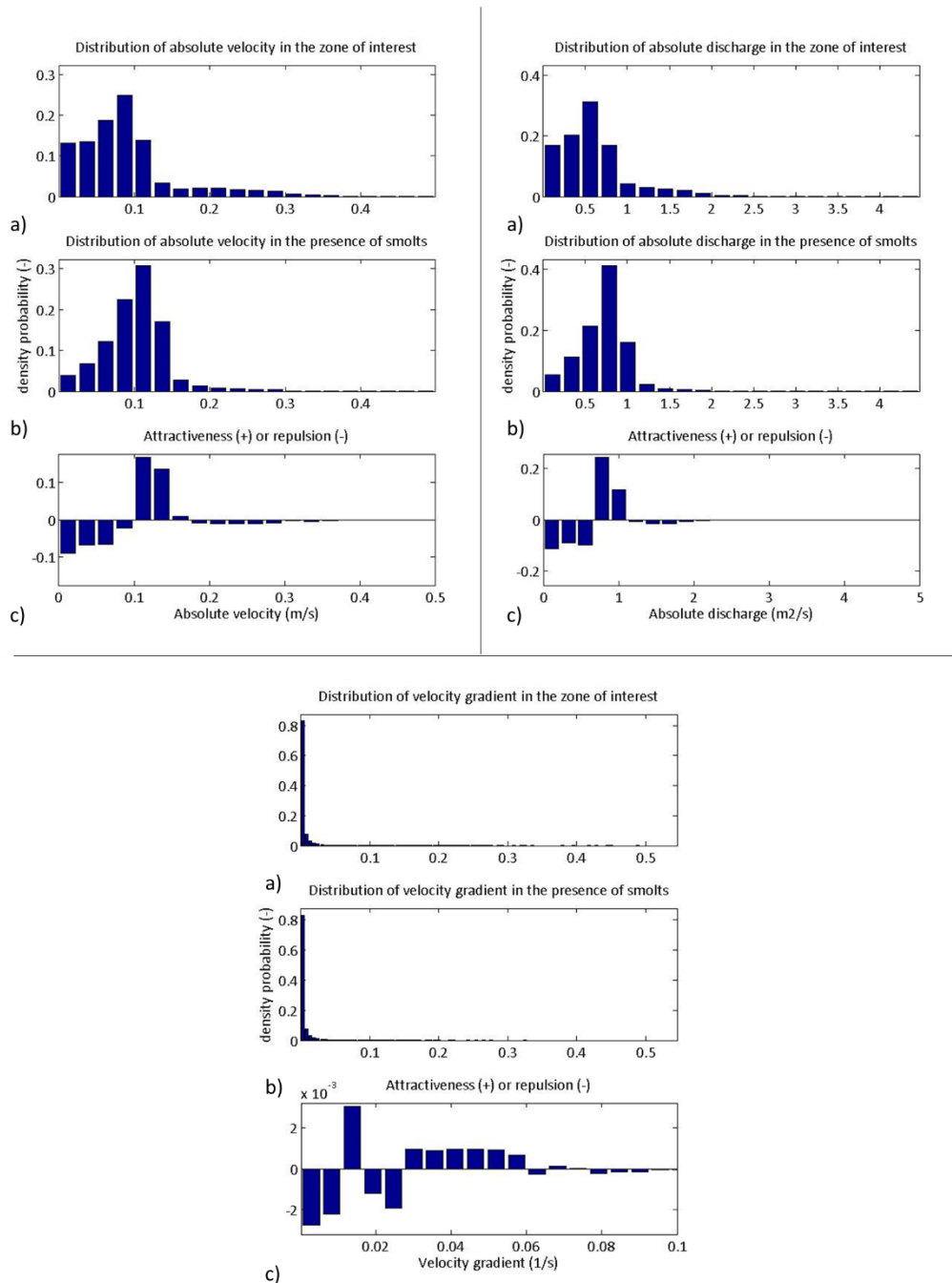


Figure V-16: Probability density distributions (a) in the zone of interest, (b) in the presence of smolts and (c) attractiveness of absolute velocity, absolute discharge and velocity gradient for the smolts at Ivoz-Ramet for the scenario with a turbine opening on the **right** side.

### V.3 Conclusion

This section analyses correlations between the 2D locations of the smolts at the sites of Grands-Malades and Ivoz-Ramet and the hydrodynamic variables computed with a 2D numerical model.

At Grands-Malades, a set of three scenarios of turbine operation, representative of the hydraulic conditions for around 83% of the monitoring data has been selected for the computation of the hydrodynamic variables. At Ivoz-Ramet, the absence of data concerning the turbine operation during the monitoring period leads us to consider two extreme scenarios of turbine operation to assess the sensitivity of the turbine operation on the results.

In both cases, as the Meuse discharge was very low, no flow was released on the dam and the powerplant was running far below its full capacity. This situation is said to be rare for the Meuse river during smolts migration period. In addition, data tend to show that locks operation has a very limited influence on fishes behavior close to the power plant intakes, at least for the discharge conditions in the Meuse considered here.

A qualitative analysis of the correlations has been done through the comparison of maps representing the density of smolts and maps showing hydrodynamic variables such as the absolute velocity, absolute unit discharge, 2D turbulent viscosity and velocity gradient. More importantly, an original methodology for a quantitative analysis of the correlations between hydrodynamic variables and smolt locations has been introduced, which could be applied in future research.

At Grands-Malades, the results of the quantitative analysis indicate that the attractiveness of smolts is higher where the velocity is the highest. Additionally, a repulsion of smolts is observed in areas with the lowest values of the 2D turbulent viscosity and velocity gradient.

At Ivoz-Ramet, the combination of the topographic step and the surface beam at the entrance of the water intake was already shown to have a strong blockage effect on the smolts at this location. However the analysis shows again a positive correlation (attractiveness) between the location of smolts and higher absolute velocities.

Besides these specific conclusions, an original methodology has been developed during the first months of the project to analyze quantitatively the possible links between observed fish behavior on site and hydrodynamic conditions at the same place. This methodology is now available for further applications, in particular during the next stages of the Life4Fish project.

## VI. Velocity fields corresponding to eels passing through the turbines

While particular zones of presence of smolts were observed in the density maps generated in section II.2.1.2, the density maps corresponding to eels (section II.3.1.2) do not show particular zones of presence of eels. Additionally, the analysis of the hydraulic variables during the monitoring period (section II.3.2) indicates that eels:

- are strongly attracted by the discharge at the dam of Grands-Malades even for configurations in which the discharge at the turbines is higher than the discharge at the dam,
- may cross the site of Ivoz-Ramet through the turbines for configurations in which the discharge at the turbines is lower than at the dam.

Based on these observations, the following numerical computations are computed:

- At Grands-Malades, a discharge of  $130 \text{ m}^3/\text{s}$  at the turbines and respectively  $25 \text{ m}^3/\text{s}$ ,  $50 \text{ m}^3/\text{s}$  and  $100 \text{ m}^3/\text{s}$  at the dam opening next to the water intake of the hydropower plant. The goal of these computations is to identify the impact of the dam discharge on the velocity field in configurations in which eels are preferentially attracted by the dam opening.
- At Ivoz-Ramet, discharges at the turbines of respectively  $95 \text{ m}^3/\text{s}$  and  $190 \text{ m}^3/\text{s}$  at the turbines with discharges of  $300 \text{ m}^3/\text{s}$  and  $600 \text{ m}^3/\text{s}$  at the dams. These configurations are representative of hydraulic variables for which eels are either through the turbines or through the dam.

### VI.1 Impact of discharges at the dam on the attraction of the eels at Grands-Malades

Without any information concerning the dam openings used to convey the discharge at the dam, we consider the most favourable configuration for the passage of eels through the dam, i.e. the total discharge is conveyed through the dam opening on the right side of the site, the closest to the water intake.

Figure VI-1 shows that the velocity fields are highly oriented to the water intake for discharges at the dams of  $25 \text{ m}^3/\text{s}$  and  $50 \text{ m}^3/\text{s}$ . Only the velocity components located just at the upstream of the dam opening are oriented to the dam opening. For a discharge at the dam of  $100 \text{ m}^3/\text{s}$ , a more significant part of the velocity components is oriented to the dam opening. These numerical results, computed for the most favourable configuration for the passages of eels through the dams, highlight that eels are (1) poorly attracted to the hydropower plant and are (2) lowly impacted by the velocity field. Indeed, while a low discharge at the dam has a limited impact on the velocity field, the passage way of the eels generally switches from a passage through the turbines to a passage to the dam.

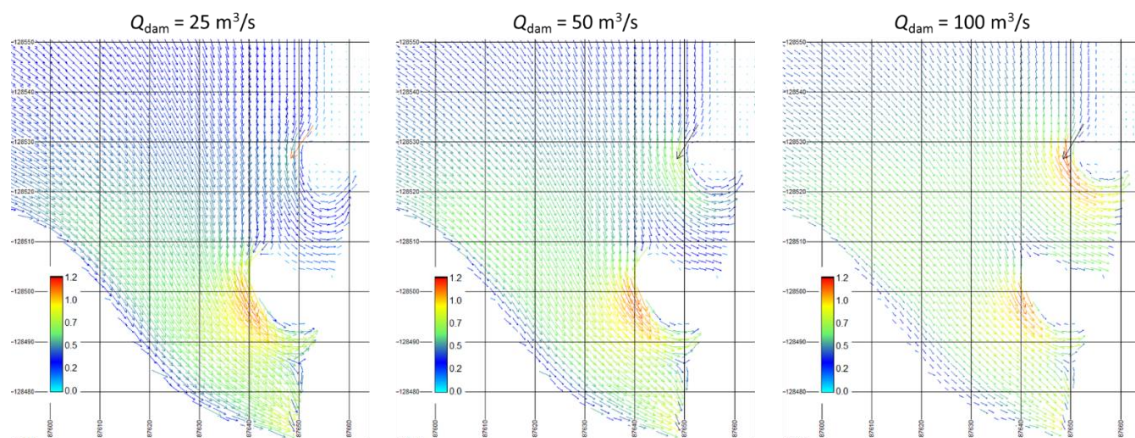


Figure VI-1: Velocity fields at Grands-Malades for a discharge of  $130 \text{ m}^3/\text{s}$  at the turbines and different values of the discharge at the single dam opening on the right side.



## VI.2 Configuration with eel passages either through the turbines or through the dam at Ivoz-Ramet

The analysis of the discharge distribution at the passage of eels in section II.3.3 has shown that several eels were passing through the turbines in situation in which the discharge at the dam is high (from 200 m<sup>3</sup>/s to 600 m<sup>3</sup>/s) and higher than the discharge at the turbines. The flow field in such configurations is investigated in this section through two discharge scenarios (resp. 95 m<sup>3</sup>/s and 190 m<sup>3</sup>/s at the turbines and 600 m<sup>3</sup>/s to 300 m<sup>3</sup>/s at the dam) combined with two scenarios of discharge distribution at the turbines. The discharge at the dam is fairly distributed between the different dam openings, consistently with the results of Figure II-24.

For a dam discharge of 600 m<sup>3</sup>/s with a turbine discharge of 95 m<sup>3</sup>/s (Figure VI-2), the flow is mainly oriented to the dam while the only velocity components oriented to the turbines are located along the surface beam. As shown in section VI.1 for the site of Grands-Malades, this indicates that eels can be attracted by a discharge even if this discharge has a poor impact on the flow distribution.

For a dam discharge of 300 m<sup>3</sup>/s with a turbine discharge of 195 m<sup>3</sup>/s (Figure VI-3), a significant fraction of the river at the upstream of the site is oriented to the turbines since the higher dam discharge is fairly distributed over the 5 gates of the dam while the lower turbine discharge is conveyed through the lower section at the surface beam.

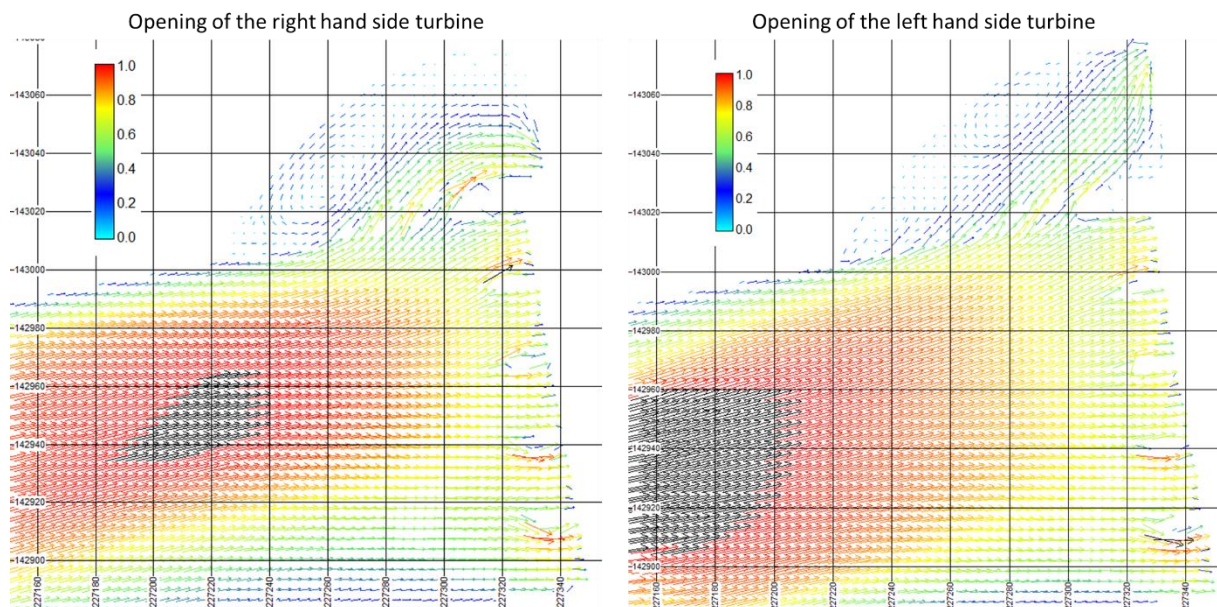


Figure VI-2: Velocity fields at Ivoz-Ramet for a discharge of 95 m<sup>3</sup>/s at the turbines and a discharge of 600 m<sup>3</sup>/s at the dam.

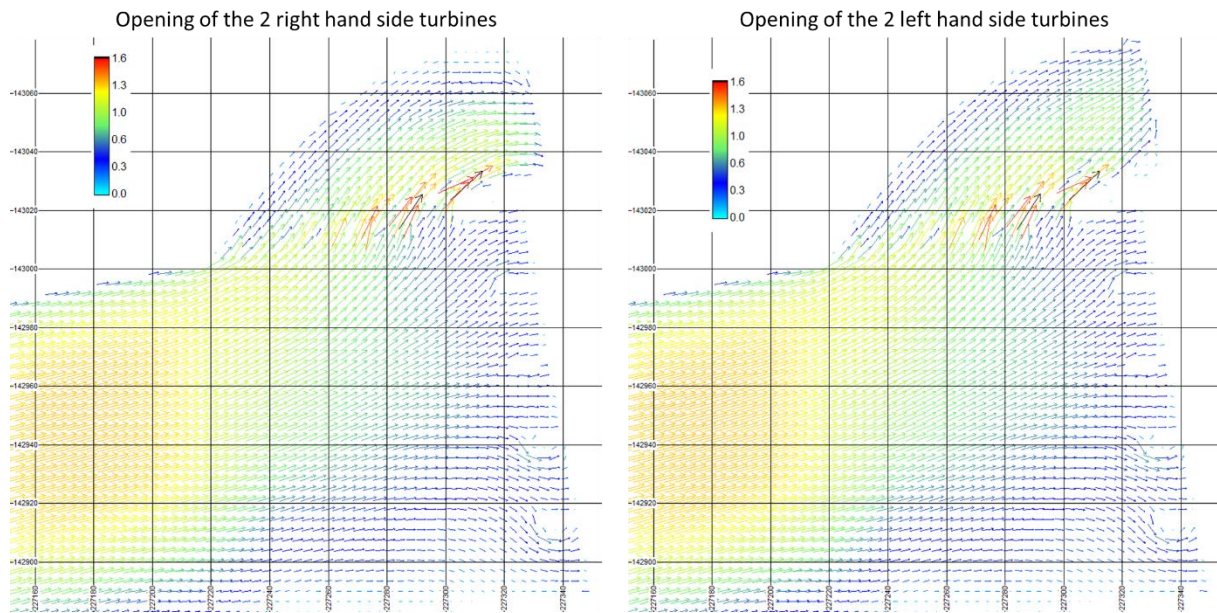


Figure VI-3: Velocity fields at Ivoz-Ramet for a discharge of  $190 \text{ m}^3/\text{s}$  at the turbines and a discharge of  $300 \text{ m}^3/\text{s}$  at the dam.

### VI.3 Conclusion

Based on numerical computations of flow fields in specific configurations of eel passages, the following statements can be highlighted concerning the eel passage:

- At Grands-Malades, eels are strongly attracted by the discharge at the dam, even if the flow field is mainly oriented to the water intake of the turbines.
- At Ivoz-Ramet, eels are mainly attracted by the discharge at the dam although a passage through the turbines may occur even if the flow field is mainly oriented to the dams.

These results indicate that the behaviour of eels also responds to other factors than the hydraulic characteristics.



## VII. Numerical design of the fish passages

The objective of the numerical design of different configurations of fish passages is the evaluation of the efficiency of a fish passage location to attract fishes arriving close to or in the water intake of the turbines.

### VII.1 Design assumptions

Following discussions with the project partners, the numerical design of the fish passages has been done considering the worst-case hydraulic scenario, i.e. using all the turbines of the hydropower plant without any release of water at the mobile dams. Indeed, this operation of the facilities is expected to maximize the attraction of the fishes to the turbines. Hence, the design Meuse discharges at Grands-Malades and Ivoz-Ramet are respectively 161 m<sup>3</sup>/s and 285 m<sup>3</sup>/s, corresponding to the equipment discharge of the turbines with a 90% opening.

According to the project guidelines, the discharges in the fish passages have been determined based on an annual loss of hydropower production of 2% and 5%. This represents discharges of 3.4 m<sup>3</sup>/s and 7.3 m<sup>3</sup>/s at Grands-Malades (respectively 2% and 4.5% of the discharge used by the turbines) and of 2.9 m<sup>3</sup>/s and 7.1 m<sup>3</sup>/s at Ivoz-Ramet (respectively 1% and 2.5% of the discharge used by the turbines).

Following the conclusions of the previous sections of this report, in agreement with the partners of the project, the fish passages are designed mainly for smolts. Indeed, eels downstream migration can be managed by dedicated stops of the powerplants during limited periods of time, with opening of a gate of the dams. On the contrary, smolts migration occur during long periods, with important discharge variations, and require thus a dedicated passage to downstream which remains effective when powerplants are in operation. The objective of the downstream passage intake is then to create attraction currents just below the free surface, in the upper part of the water column, where the smolts are expected to be.

### VII.2 Velocity distribution for the actual configuration

The velocity distributions for the actual configuration (without fish passages) and for the design hydrodynamic conditions prescribed in section VII.1 are shown in Figure VII-1 and Figure VII-2.

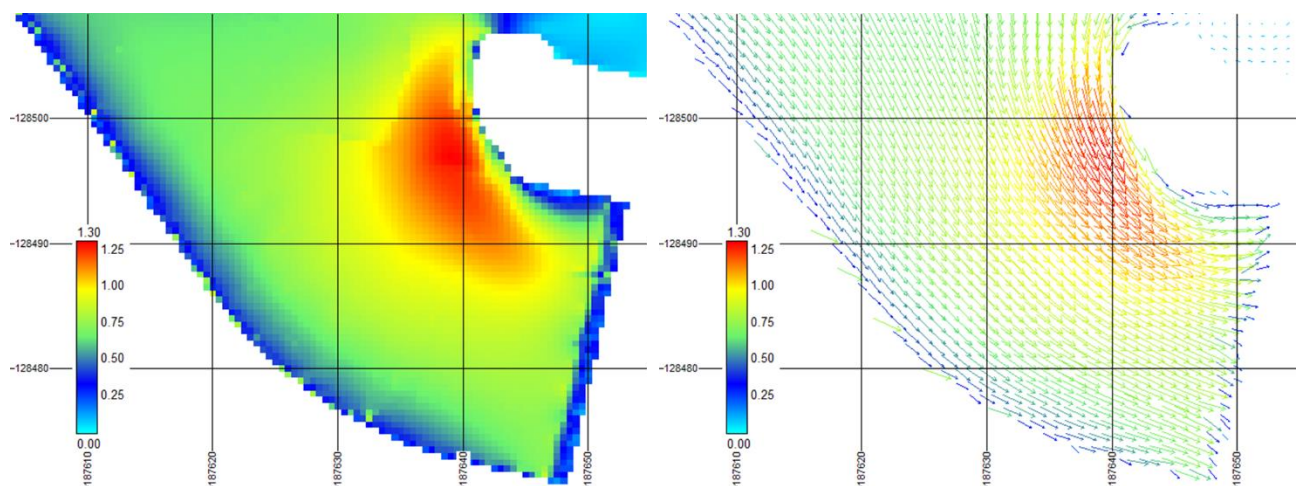


Figure VII-1: Velocity distribution at the site of Grands-Malades for the actual configuration and for the design hydrodynamic conditions.

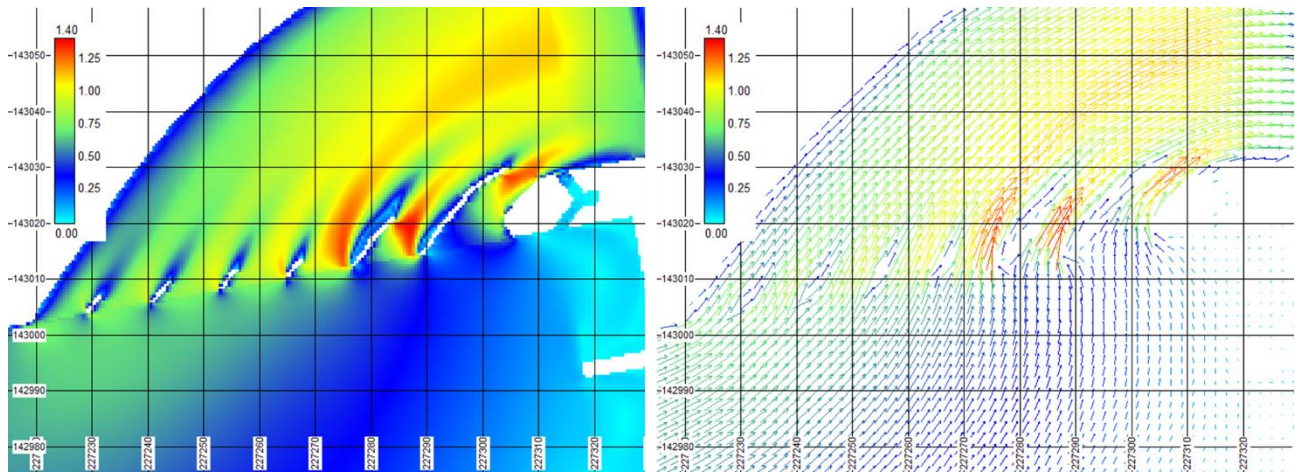


Figure VII-2: Velocity distribution at the site of Ivoz-Ramet for the actual configuration and for the design hydrodynamic conditions.

### VII.3 Numerical simulations of fish passage configurations

#### VII.3.1 Overview of the configurations

Considering the works layout, varied locations for fish passage positions have been tested at both pilot sites:

##### **Grands-Malades (Figure VII-3)**

- Fish passage on the gate of the mobile dam adjacent to the hydropower plant (full width of the gate) (G0);
- **1.5 m wide** fish passage at the **upstream** of the pier between the hydropower plant and the mobile dam (G1);
- **4.5 m wide** fish passage at the **upstream** of the pier between the hydropower plant and the mobile dam (G2);
- **1.5 m wide** fish passage at the **downstream** of the pier between the hydropower plant and the mobile dam (G3);

##### **Ivoz-Ramet (Figure VII-4)**

- Fish passage on the gate of the mobile dam adjacent to the hydropower plant (full width of the gate) (I0);
- **1.5 m wide** fish passage in the Meuse river side of the pier between the hydropower plant and the mobile dam (I1);
- **4.5 m wide** fish passage in the Meuse river side of the pier between the hydropower plant and the mobile dam (I2);

Based on the results gained with these first rough configurations, Arcadis designed with more details two configurations of fish passage for each site, taking into account the current situation as well as good practice hydraulic conditions for the passage of fishes (maximum drop, velocity, etc.). These configurations are:

##### **Grands-Malades**

- 2.4 m wide fish passage with an equipped discharge of 3.4 m<sup>3</sup>/s at the downstream of the pier between the hydropower plant and the mobile dam (G4);

- 5 m wide fish passage with an equipped discharge of 7.3 m<sup>3</sup>/s at the downstream of the pier between the hydropower plant and the mobile dam (G5).

#### Ivoz-Ramet

- 2.1 m wide fish passage with an equipped discharge of 2.9 m<sup>3</sup>/s in the Meuse river side of the pier between the hydropower plant and the mobile dam (I4);
- 6 m wide fish passage with an equipped discharge of 7.1 m<sup>3</sup>/s in the Meuse river side of pier between the hydropower plant and the mobile dam (I5).

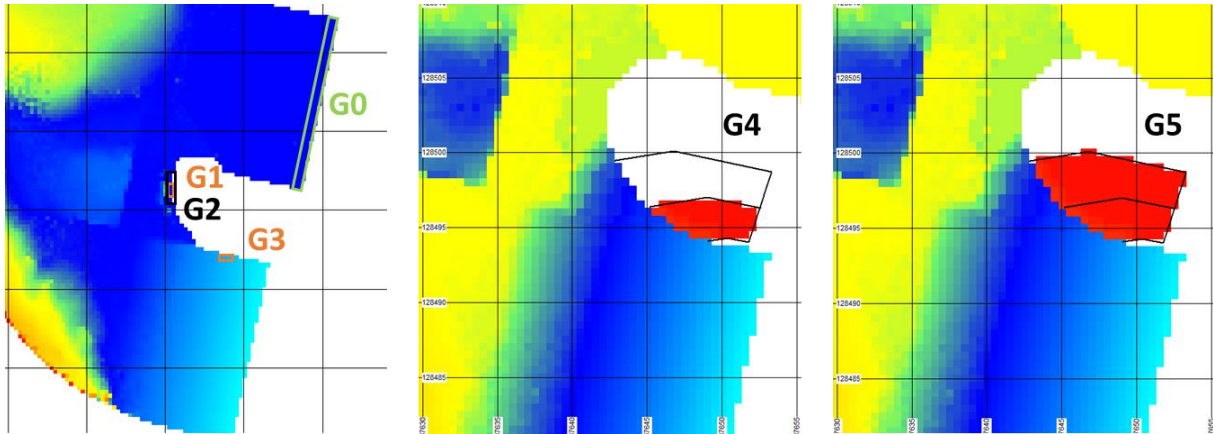


Figure VII-3: Configurations of fish passages at Grands-Malades.

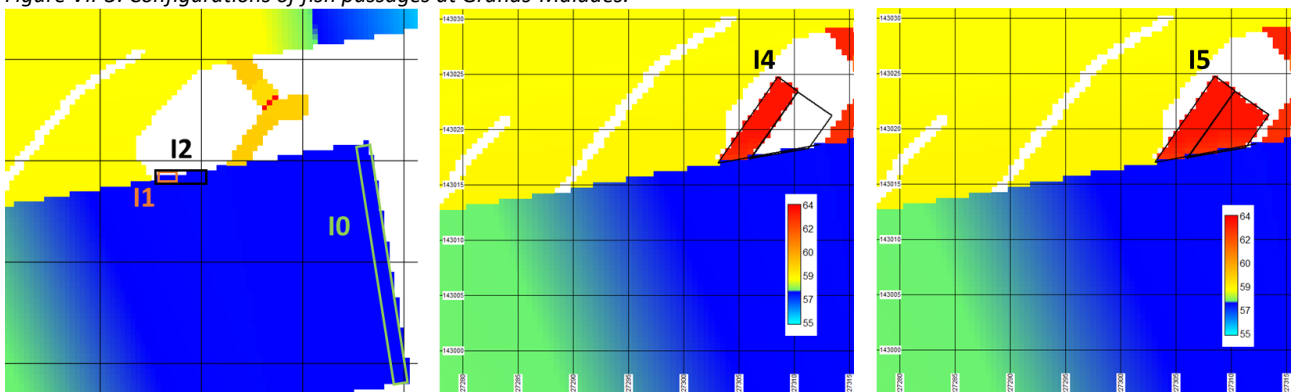


Figure VII-4: Configurations of fish passages at Ivoz-Ramet.

#### VII.3.2 Fish passage on a gate of the mobile dam (full width of the gate) (configurations G0 and I0)

This configuration consists in using the gate of the mobile dam adjacent to the hydropower plant in order to evacuate the fish passage attraction discharge. We consider the gate adjacent to the hydropower plant since our goal is to attract fishes going “naturally” to the hydropower plant.

At both sites, the velocity field is not significantly affected by the discharge on the dam gate and it remains mainly directed toward the hydropower plant (Figure VII-5). This is due to the large width of the valve (i.e. low velocities for a given discharge) and to the low fraction of the total discharge (4.5% and 2.5%) diverted to the fish passage. Hence, the changes of absolute velocity compared to the present configuration (lower than 0.1 m/s in Figure VII-6) are lower than 10% of the reference absolute velocities.

Based on these results, the efficiency of smolts passage on a gate of the mobile dam is expected to be very limited. Only fishes looking for a passage close to the gate could find their way to downstream.



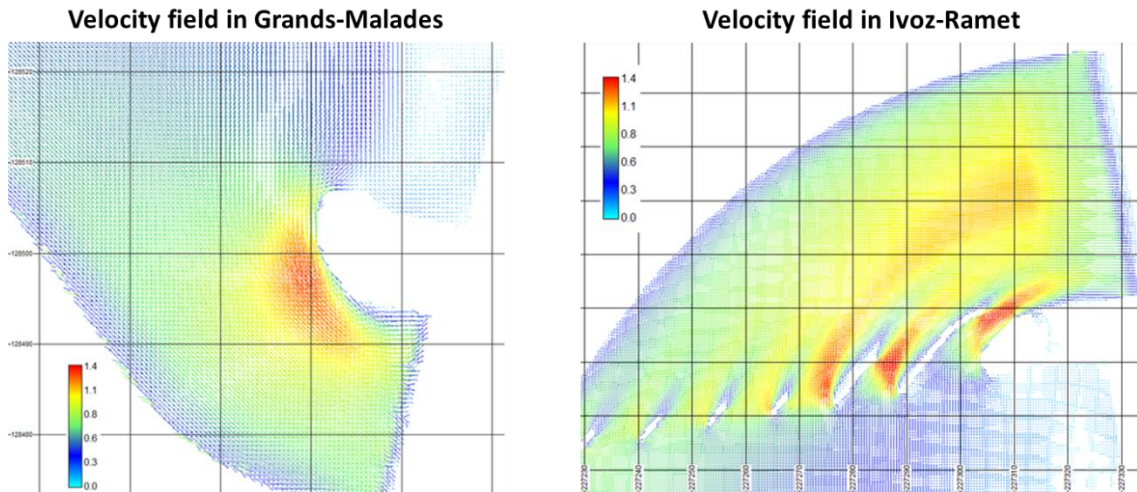


Figure VII-5: Velocity field for the configurations G0 and I0 with a fish passage through a valve of the mobile dam with the maximum equipped discharge (equipped discharge of 7.3 m<sup>3</sup>/s at Grands-Malades and 7.1 m<sup>3</sup>/s at Ivoz-Ramet).

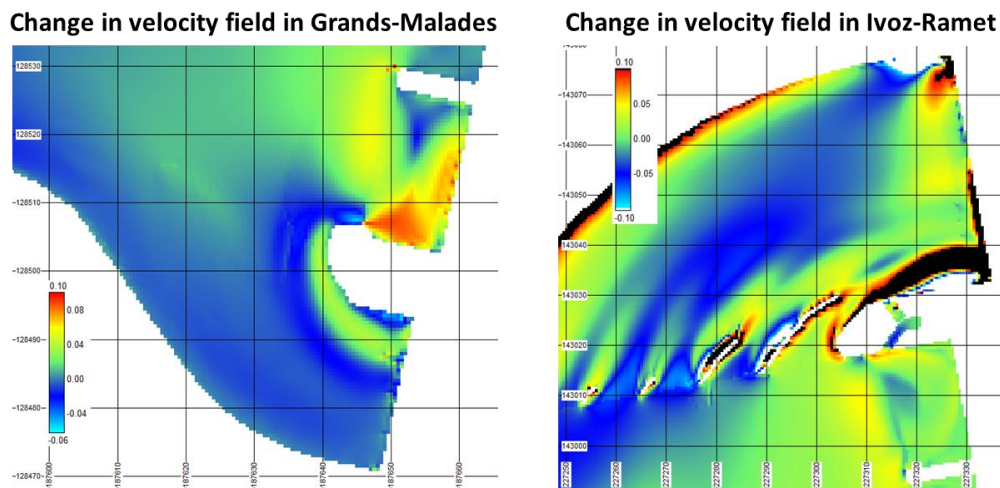


Figure VII-6: Field of change of absolute velocity for the configurations G0 and I0 with a fish passage through a valve of the mobile dam with the maximum equipped discharge (equipped discharge of 7.3 m<sup>3</sup>/s at Grands-Malades and 7.1 m<sup>3</sup>/s at Ivoz-Ramet).

### VII.3.3 Fish passage at the upstream of the pier between the hydropower plant and the mobile dam at Grands-Malades (G1 and G2)

In these configurations, the fish passage is located on the left side of the water intake, where the velocities are the highest. The fish passage is located at the upstream of the pier to attract the fishes before they arrive in the water intake.

The velocity fields are represented in Figure VII-7 for the most favourable configuration: higher attraction discharge (7.3 m<sup>3</sup>/s) and smaller width of the fish passage (G1), maximizing the velocity gradient nearby the fish passage. For the design Meuse discharge of 181 m<sup>3</sup>/s, the velocities are tangent to the entrance of the fish passage with high intensity values. These hydraulic conditions are not expected to be favourable for the attraction of fishes by the fish passage as no significant velocity component is directed towards the fish passage. Additional computations performed for lower Meuse discharges indicate that, even for a low Meuse discharge of 80 m<sup>3</sup>/s, the hydraulic conditions remain poorly favourable for fish attraction.

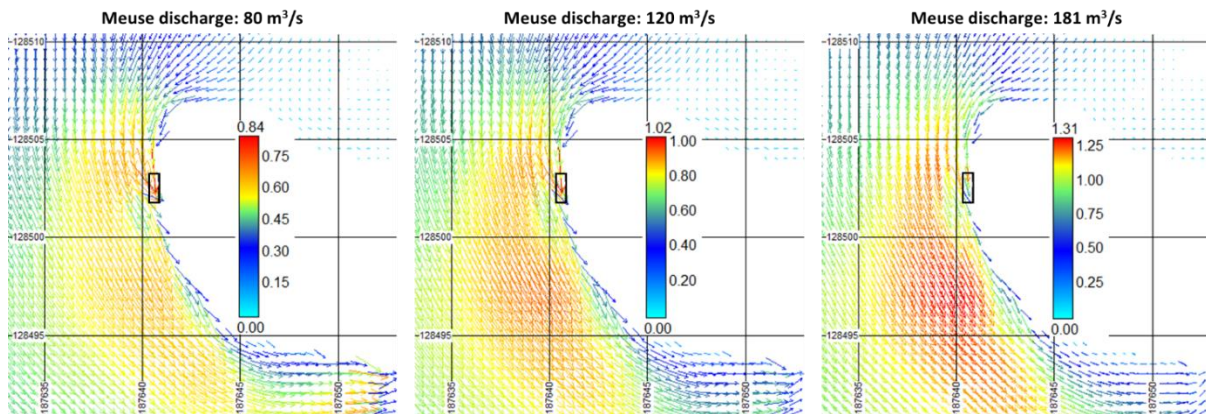


Figure VII-7: Velocity fields for the configuration G1 with a fish passage at the upstream of the pier between the hydropower plant and the mobile dam at Grands-Malades (discharge of 7.3 m<sup>3</sup>/s).

### VII.3.4 Fish passage in the Meuse river side of the pier between the hydropower plant and the mobile dam at Ivoz-Ramet (I1 and I2)

At Ivoz-Ramet, the fish monitoring (section II.2.1.2) indicates a high density of fishes along the entrance of the water intake where a topographic step combined with a pressurized flow induced by a surface beam obstructing the passage of fishes to the water intake. Following this observation, this configuration consists in the installation of the fish passage in the pier at the downstream side of the entrance of the fish passage.

As in section VII.3.3, the velocity distributions are shown in Figure VII-8 for the expected most favourable situation for the fish passage: higher attraction discharge (7.1 m<sup>3</sup>/s) and smaller width of the fish passage (I1). For the design Meuse discharge (285 m<sup>3</sup>/s), the velocity distribution is poorly oriented toward the fish passage as the attraction discharge represents only 2.5% of the total discharge. The reduction of the Meuse discharge (190 m<sup>3</sup>/s and 95 m<sup>3</sup>/s) increases the impact of the fish passage on the velocity directions although most of velocity components in front of the beam remain oriented toward the hydropower plant.

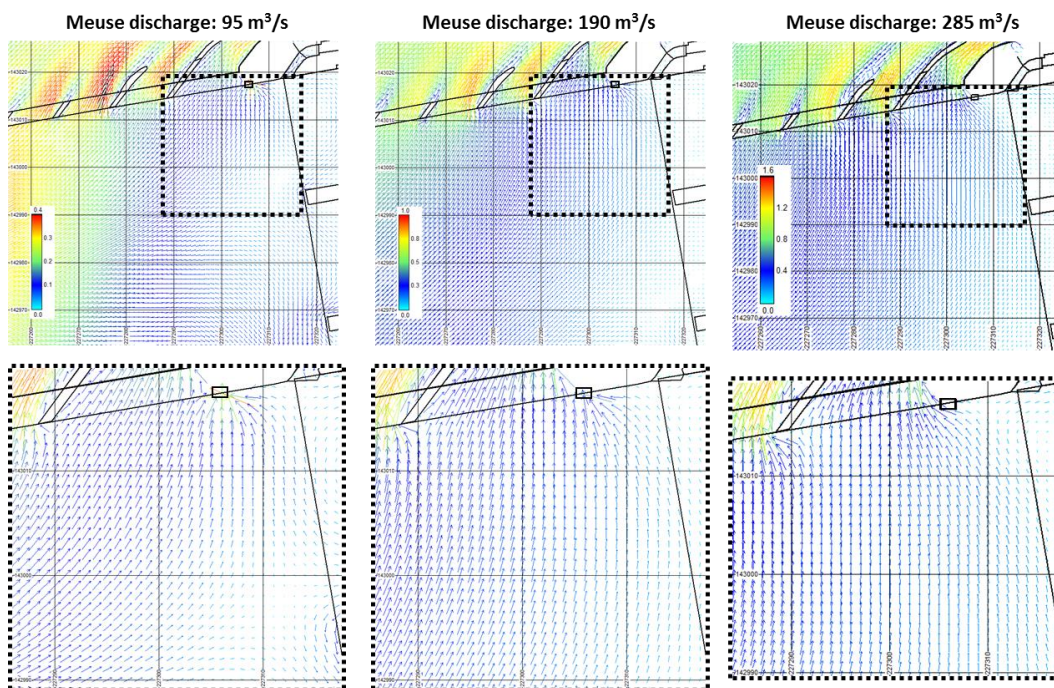


Figure VII-8: Velocity fields for the configuration I1 with a fish passage in the river Meuse side of the pier between the hydropower plant and the mobile dam at Ivoz-Ramet (discharge of 7.1 m<sup>3</sup>/s).



### VII.3.5 Fish passage at the downstream of the pier between the hydropower plant and the mobile dam at Grands-Malades (G3)

The fish passage designed in section VII.3.3 is considered unfavourable due to the high tangential component of the flow velocity. In this section, the fish passage is therefore located at the downstream of the pier, close to the turbines where the velocity intensities are lower.

Figure VII-9 shows the velocity distribution for the design Meuse discharge as well as for 80 m<sup>3</sup>/s and 120 m<sup>3</sup>/s. For the design discharge, some velocities are locally directed toward the fish passage. The reduction of the Meuse discharge promotes this effect since the fraction of discharge diverted to the fish passage increases accordingly. For the lowest Meuse discharge of 80 m<sup>3</sup>/s for which the turbine on the left side of the hydropower plant is not used, a significantly higher impact of the fish passage on the velocity directions is observed.

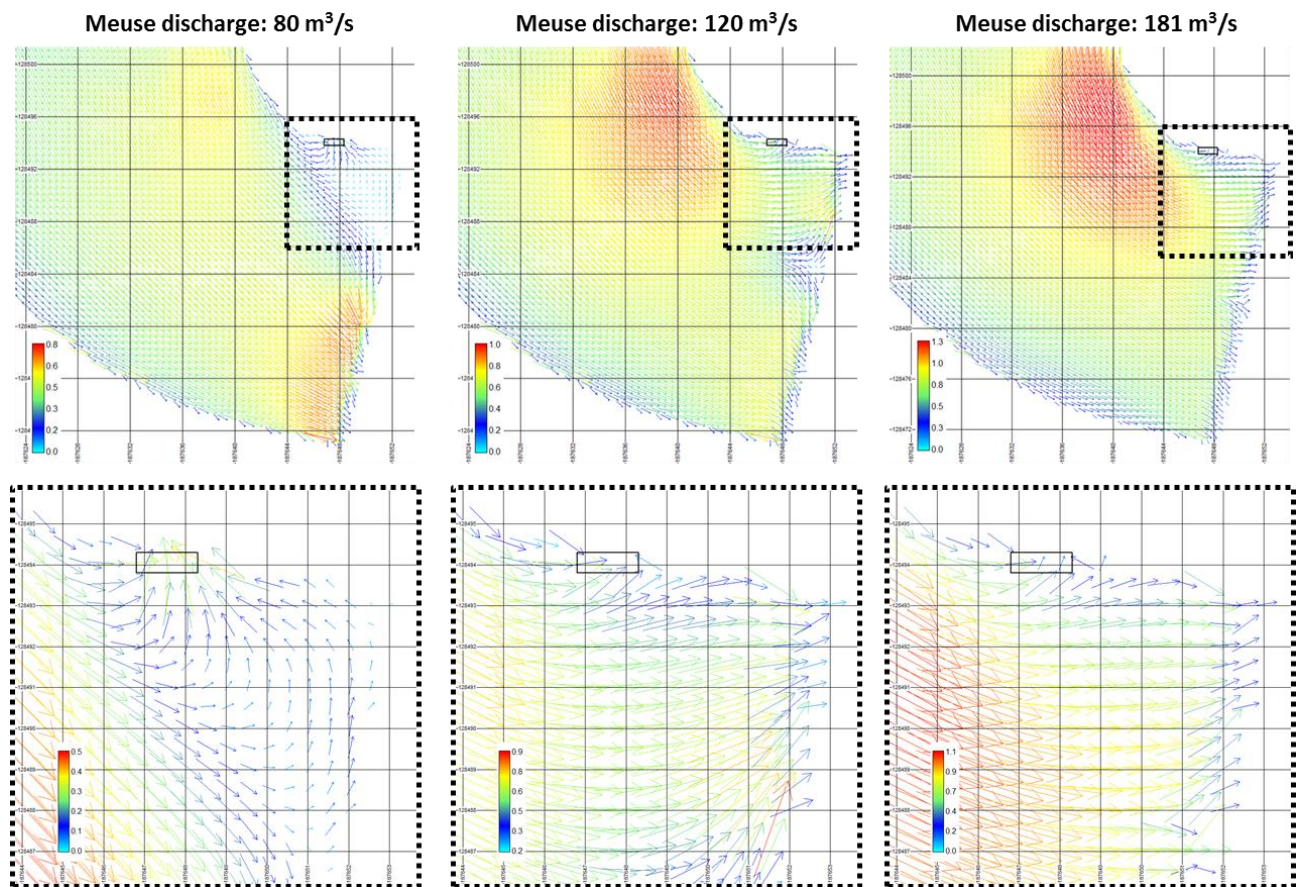


Figure VII-9: Velocity fields for the configuration G3 with a fish passage at the downstream of the pier between the hydropower plant and the mobile dam at Grands-Malades (discharge of 7.3 m<sup>3</sup>/s).

### VII.3.6 Detailed design at Grands-Malades (G4 and G5)

The velocity fields resulting from the computation of the two detailed designs provided by Arcadis for Grands-Malades are shown in Figure VII-10 for the design Meuse discharge. The velocity distribution at the entrance of the fish passage is mainly oriented toward the hydropower plant for both configurations. For the wider solution (G5), significant velocity components tangent to the fish passage entrance are created as a combination of the pier shape effect and the bottom elevation variation at the fish passage entrance. They do not induce adequate fish attraction conditions. On the contrary, with the smaller opening (Config G4), the velocity field transition to the fish passage is smoother. In both cases, the building of a fish passage requires the installation of a behavioural barrier to direct the fishes to the fish passage and thus increase the efficiency of the system.



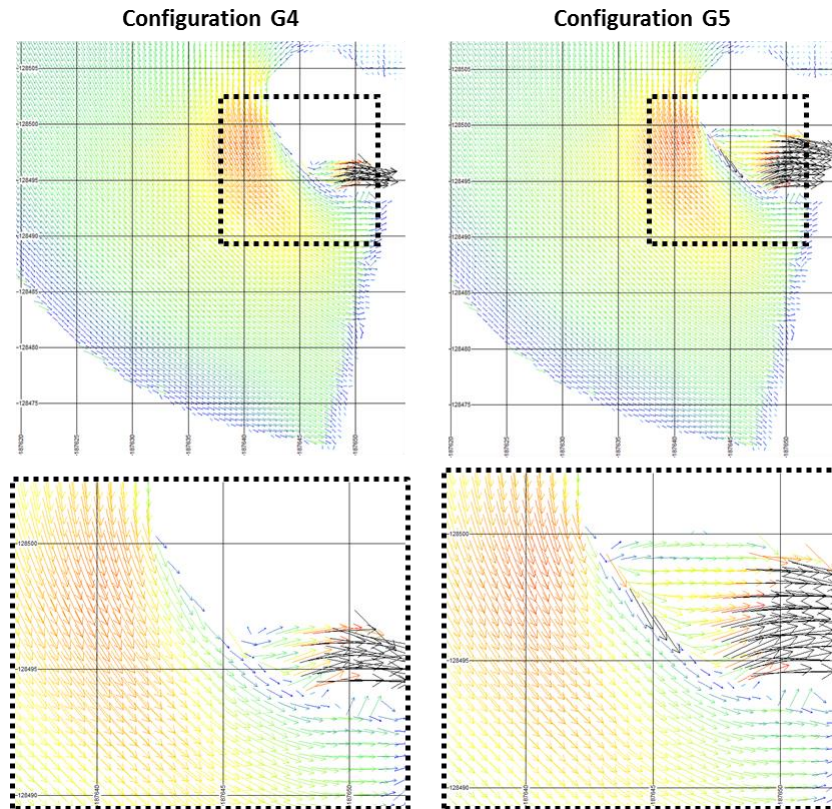


Figure VII-10: Velocity fields for the configurations G4 and G5 designed by Arcadis at Grands-Malades.

### VII.3.7 Detailed design at Ivoz-Ramet (I3 and I4)

For the two detailed configurations designed by Arcadis at Ivoz-Ramet, the velocity fields along the entrance of the water intake are oriented toward the water intake (Figure VII-11). In front of the fish passage, velocities are mostly oriented toward the fish passage for configuration I4, with a larger opening and higher discharge. For configuration I3, the attraction of the fish passage is lower than for configuration I4 even if some velocities are oriented toward the fish passage.

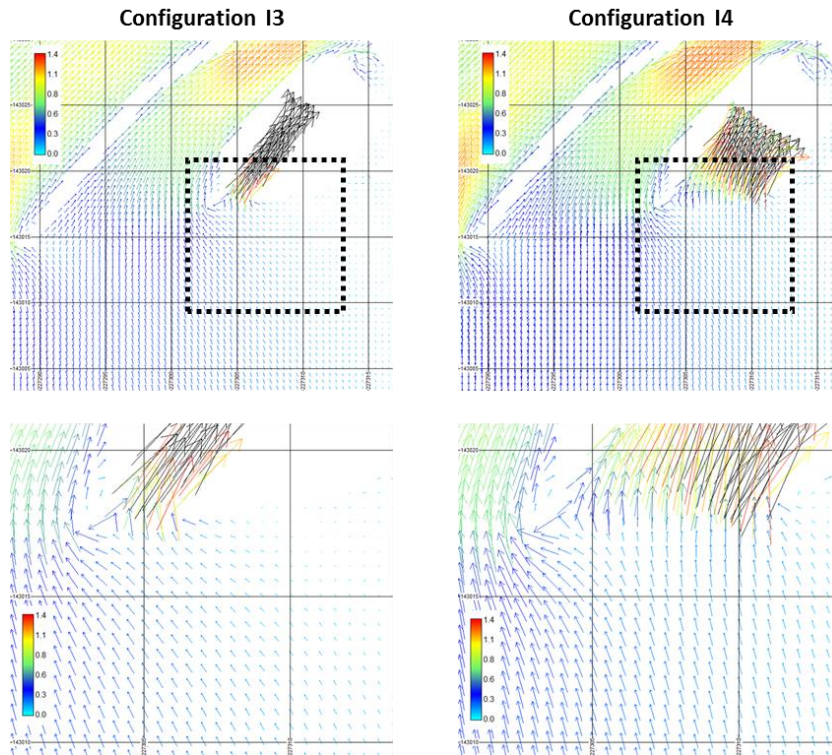


Figure VII-11: Velocity fields for the configurations I3 and I4 designed by Arcadis at Ivoz-Ramet.

## VII.4 Conclusion

Hydrodynamic variables were computed for a set of respectively 6 and 5 designs of fish passage at the sites of Grands-Malades and Ivoz-Ramet and for a Meuse discharge corresponding to the worst-case situation for fish diversion to the powerplant in which the discharge passing through the hydropower plant is maximum without any discharge over the mobile dam. These designs have been proposed considering limitations imposed by the existing works on the site. The numerical results indicate that:

- Considering the low fraction of the Meuse discharge assigned to the fish passage and the width of the gate of the mobile dams, the use of the gate closest to the plant as a fish passage leads to low attraction velocities and thus very poor efficiency in terms for fish attraction. This is true for both sites. An alternative would be to create a small opening in the upper part of the gate flap to concentrate the discharge and thus increase the attraction velocities, while providing a deeper water depth in the fish passage.
- At Grands-Malades, because of the specific effect on the flow velocity field of the pier between the dam and the power plant, a location of the fish passage at the downstream of the pier on the left side of the water intake is expected to be more effective than a location at the upstream of the pier.
- At Ivoz-Ramet, because of the blockage of the smolts upstream of the entrance of the water intake due to the combine effect of the topographic step and the surface beam, the fish passage is located outside of the water intake, on the right side. This position is favourable to local attractiveness conditions.

## VIII. Characteristics of the physical scale models

In order to complement the 2D numerical models results for designing the fish passages, 3D physical models of the pilot sites have been built at the Laboratory of Engineering Hydraulics of ULiège. These models have been used to optimize the geometry of the passages intake (Section IX) and to validate the solutions to be built on site.

### VIII.1 Model extent and upstream boundary condition

In order to maximize the scale factor, the physical models represent a limited area of the pilot sites (Figure VIII-1). The numerical models have then been used to define the best location and features of the physical models limits in order to reproduce similar flows close to the area of interest, i.e. around the water intakes of the HPP.

In each case, it has been decided to represent at least the two first bays of the mobile dam close to the HPP and the HPP intake channel in order to be able to reproduce operation conditions with one dam gate opened.

#### VIII.1.1 Configurations

For each pilot site, three geometries of the physical models upstream limits and water supply zone have been successively modeled numerically (Figure VIII-2 and Figure VIII-3). The resulting hydrodynamic fields have been compared in each case with the ones extracted from the full extend numerical models for design discharges corresponding to the equipment discharges of the 2 power plants (161 and 285 m<sup>3</sup>/s) and without any discharge evacuated through the mobile dams or the locks. For each design, the grey lines represent the water supply zone (Figure VIII-2 and Figure VIII-3). Considering uniform distributions of the inflow along the water supply zones in the laboratory models, the goal of this section is to identify the most appropriate design of the model and prescription of upstream boundary conditions for the reproduction of the discharge distribution at the zones of interest.

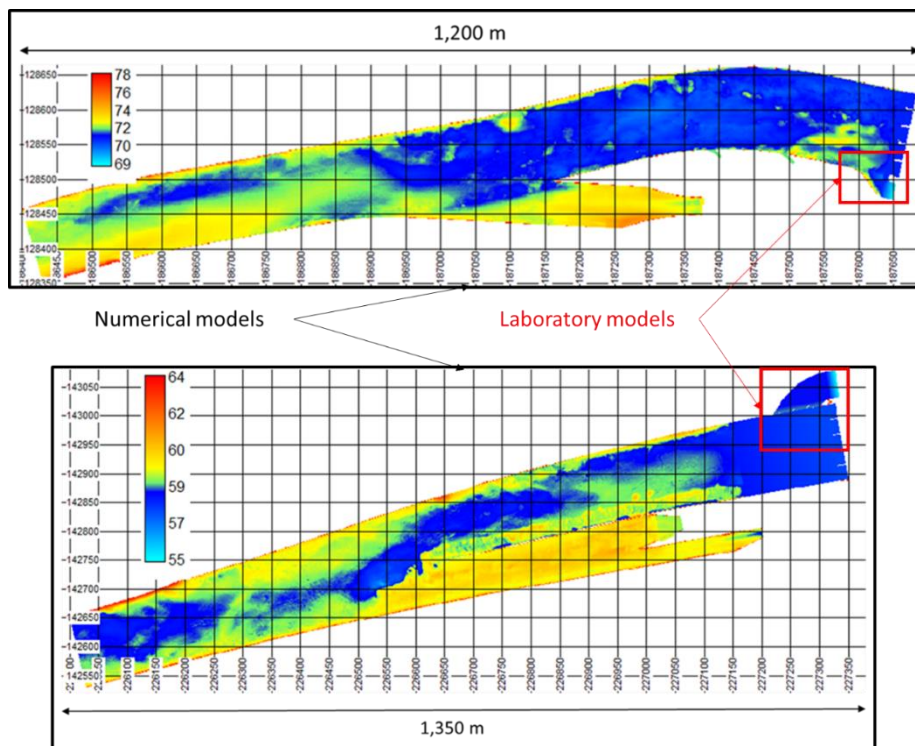


Figure VIII-1: Numerical and laboratory models at Grands-Malades and Ivoz-Ramet.



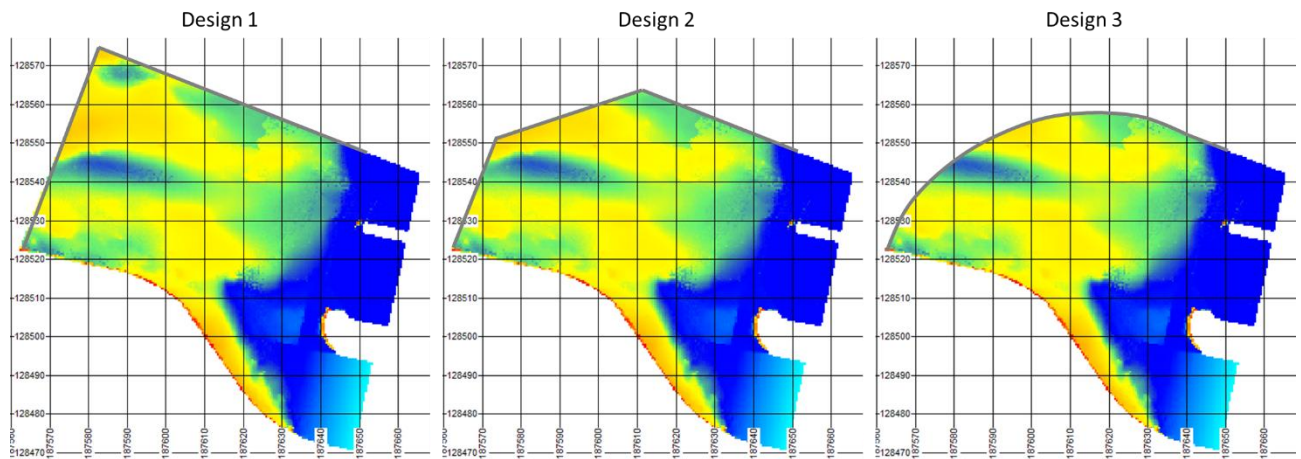


Figure VIII-2: Design of laboratory models at Grands-Malades. The grey lines represent the water supply zones.

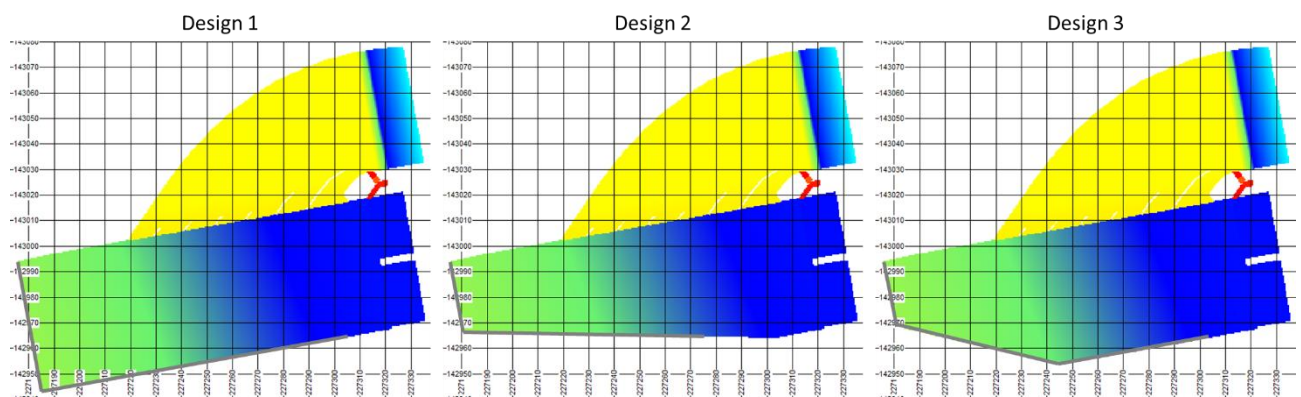


Figure VIII-3: Design of laboratory models at Ivoz-Ramet. The grey lines represent the water supply zones.

### VIII.1.2 Grands-Malades pilot site

The unit discharge distributions for the three layouts of the laboratory models are compared to the one computed for the full numerical model (reference) in Figure VIII-4. The maps indicate unintended concentrations of unit discharges arising from the corners of the infiltration zones of the designs 1 and 2 while, for the design 3, the curvature of the infiltration zone enables a more uniform distribution of the unit discharges at the upstream of the laboratory model.

The correlation  $C$  and error  $E$  coefficients (definition in section IV.1) resulting from the comparison of the unit discharge distribution computed with the numerical model to the ones computed for the designs of the laboratory model are given in Table 8. The absolute values of the unit discharge at the entrance of the water intake are compared in Figure VIII-5. The values of Table 8 and the profiles of Figure VIII-5 confirm that the unit discharge distribution is better reproduced with the third design of the laboratory model.

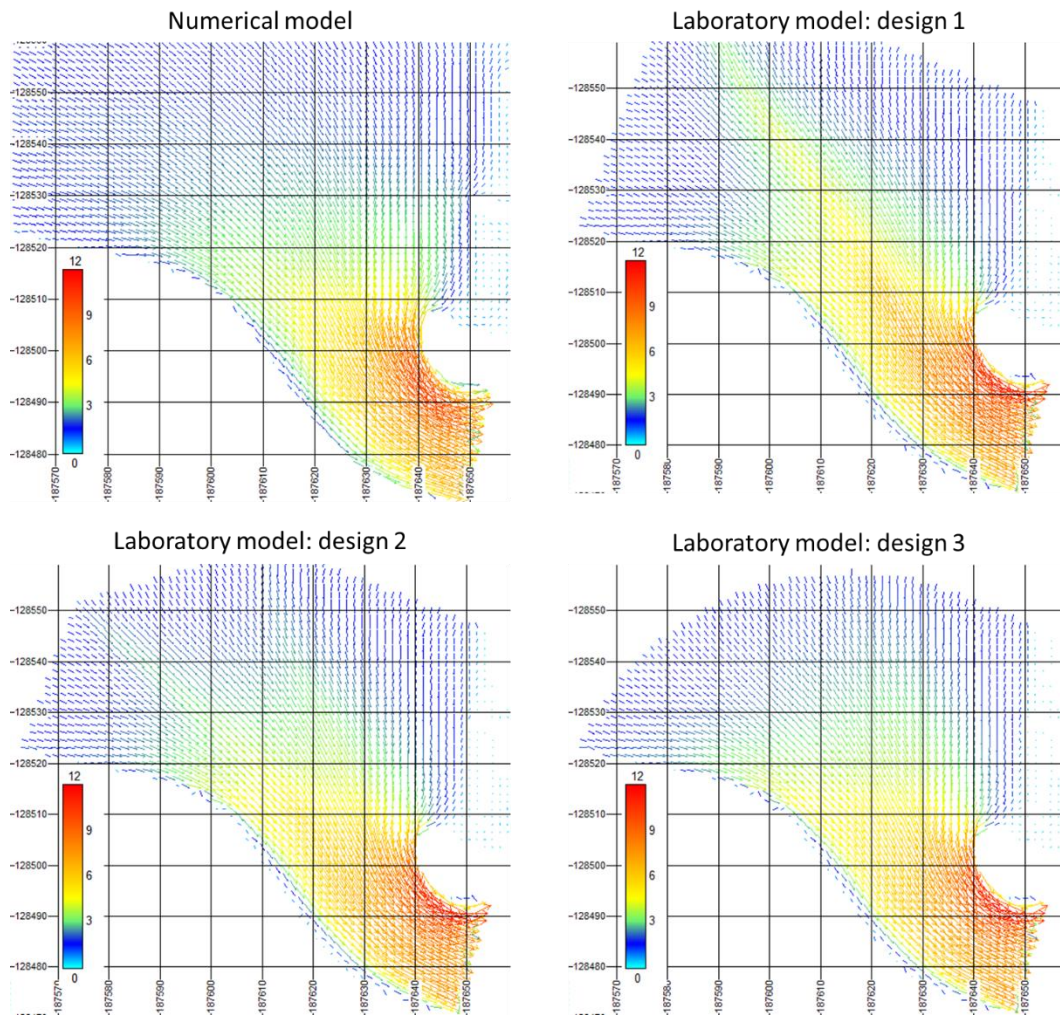


Figure VIII-4: Unit discharge distributions for the numerical and laboratory models at Grands-Malades.

	$C_{qx}$	$C_{qy}$	$E_{qx}$	$E_{qy}$
<b>Design 1</b>	0.9729	0.9621	19%	17%
<b>Design 2</b>	0.9756	0.9752	17%	14%
<b>Design 3</b>	0.9789	0.9795	14%	11%

Table 8 : Correlation and error coefficients for the unit discharge distribution resulting from the computation of the designs 1 to 3 of the laboratory model compared to the results obtained for the numerical model – Grands-Malades.



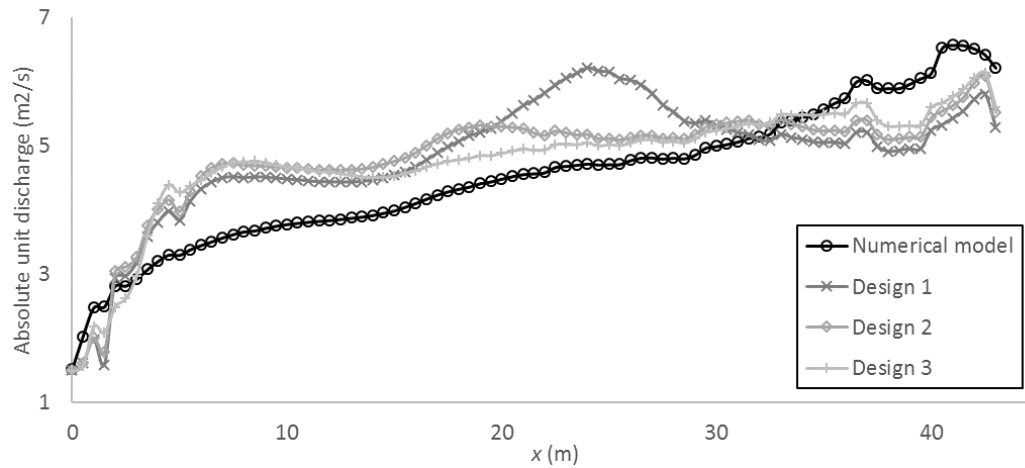


Figure VIII-5: Absolute values of the unit discharge at the entrance of the water intake of Grands-Malades (from the right side to the left side of the water intake).

### VIII.1.3 Ivoz-Ramet pilot site

Figure VIII-6 and Figure VIII-7 show a significant influence of the design of the laboratory model on the distribution of the unit discharges at the upstream of the surface beam at the entrance of the water intake. In agreement with the values of the correlation and error coefficients of Table 9, the second design of the laboratory model is identified as the most effective to reproduce the distribution of unit discharge computed with the full numerical model.

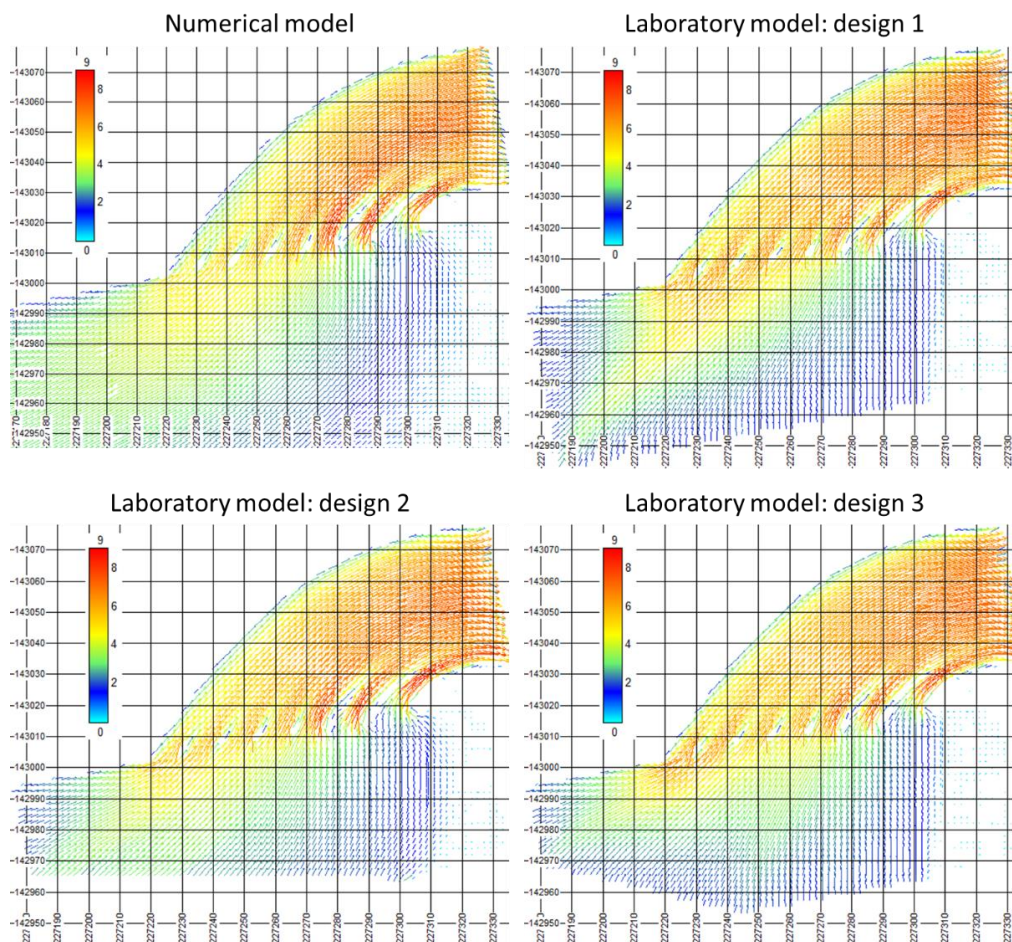


Figure VIII-6: Unit discharge distributions for the numerical and laboratory models at Ivoz-Ramet.



	$C_{qx}$	$C_{qy}$	$E_{qx}$	$E_{qy}$
Design 1	0.9707	0.9749	16%	13%
Design 2	0.9813	0.9906	11%	8%
Design 3	0.9669	0.9806	17%	12%

Table 9 : Correlation and error coefficients for the unit discharge distribution resulting from the computation of the designs 1 to 3 of the laboratory model compared to the results obtained for the numerical model – Ivoz-Ramet.

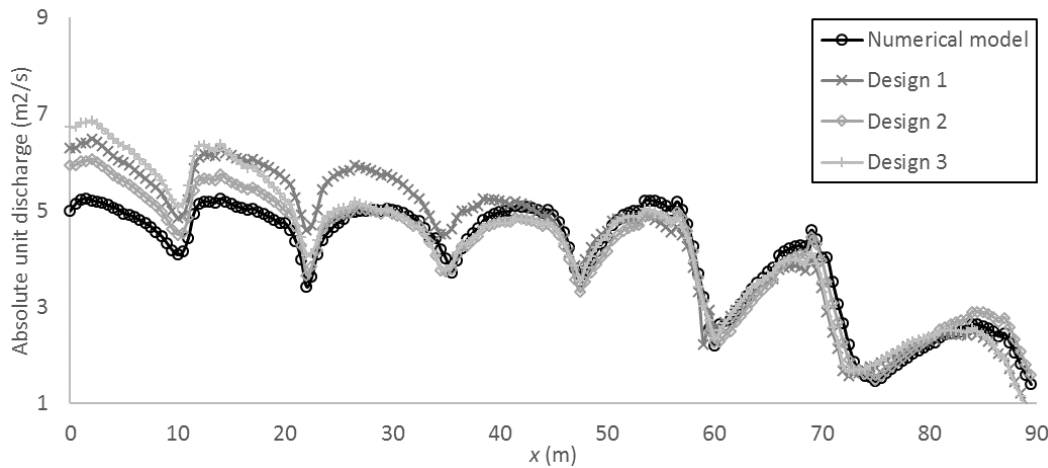


Figure VIII-7: Absolute values of the unit discharge at the entrance of the water intake of Ivoz-Ramet (from the right side to the left side of the water intake).

## VIII.2 Similitude

The flows to be studied are free surface ones, i.e. mainly controlled by gravity. Thus, the study on scale model is performed to keep constant the non-dimensional number of Froude between model and prototype (Froude similitude), i.e. considering the same ratio between inertia and gravity forces on the model as on the prototype.

The conservation of the Froude number  $Fr$  leads to the following relation that sets the velocity scale  $V^*$  when the geometric length scale  $L^*$  is chosen:

$$\frac{Fr_m}{Fr_p} = 1 \Rightarrow V^* = \frac{u_m}{u_p} = \sqrt{\frac{h_m}{h_p}} = \sqrt{L^*}$$

where

- $m$  indexes refer to scale model characteristics,
- $p$  indexes refer to the real model characteristics (prototype),
- $u$  is the flow velocity,
- $h$  is the water depth.

The only assumption made at this stage is the conservation of the gravity acceleration  $g$ . The discharge scale  $Q^*$  and the time scale  $T^*$  can be obtained from the relation above:

$$Q^* = V^* L^{*2} = L^{*5/2}$$

$$T^* = \frac{L^*}{V^*} = \sqrt{L^*}$$

### VIII.3 Scale factor

The choice of the length scale used to build the physical model has been made regarding the accuracy of the measurements, the elimination of disruptive scale effects that could make the similarity imperfect and the model extent defined in section VIII.1.

A scale factor of 1:25 has been selected for Grands Malades site. A scale factor of 1:35 has been selected for Ivoz Ramet site, which is larger than Grands Malades.

### VIII.4 Scale model layout

The scale models extent has been defined from numerical model results in section VIII.1. For Grands Malades site, it covers an area in the Meuse river 100 m long upstream of the mobile dam and 50 m wide from the right bank of the river. At Ivoz-Ramet site, the extent is 158 m long upstream of mobile dam and 53 m wide from left bank of the river. Layout of the models on real sites are shown on Figure VIII-8 and Figure VIII-9.

As already mentioned, both models represent the HPP, the HPP intake channel, the 2 first bays of the mobile dam along the HPP as well as a part of the Meuse river bed upstream of the dam. In addition, the intake of the forecasted downstream passage for fish has been represented.

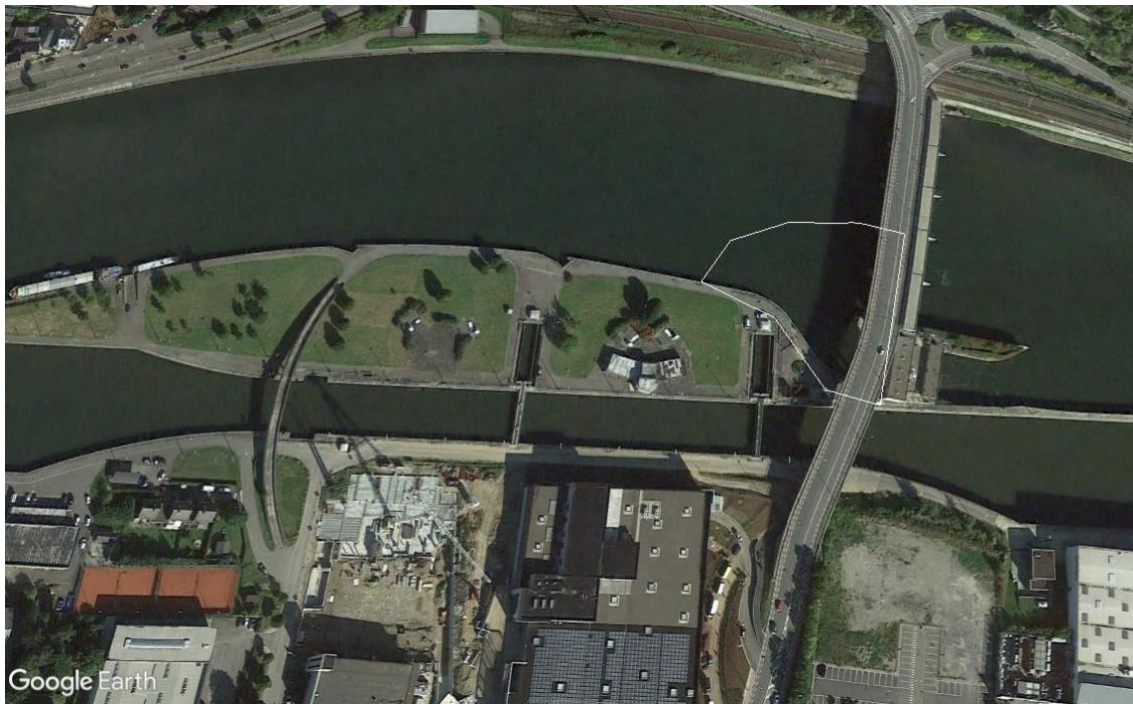


Figure VIII-8: Scale model layout on the real site for Grands Malades site



Figure VIII-9: Scale model layout on the real site for Ivoz Ramet site

Regarding the scale factors, the overall size of the scale models in the Laboratory, including the systems for water supply and recovery, is 11 m x 6 m. Both models use a common water supply reservoir with a mobile separation plate to disconnect one model from the other (Figure VIII-10).

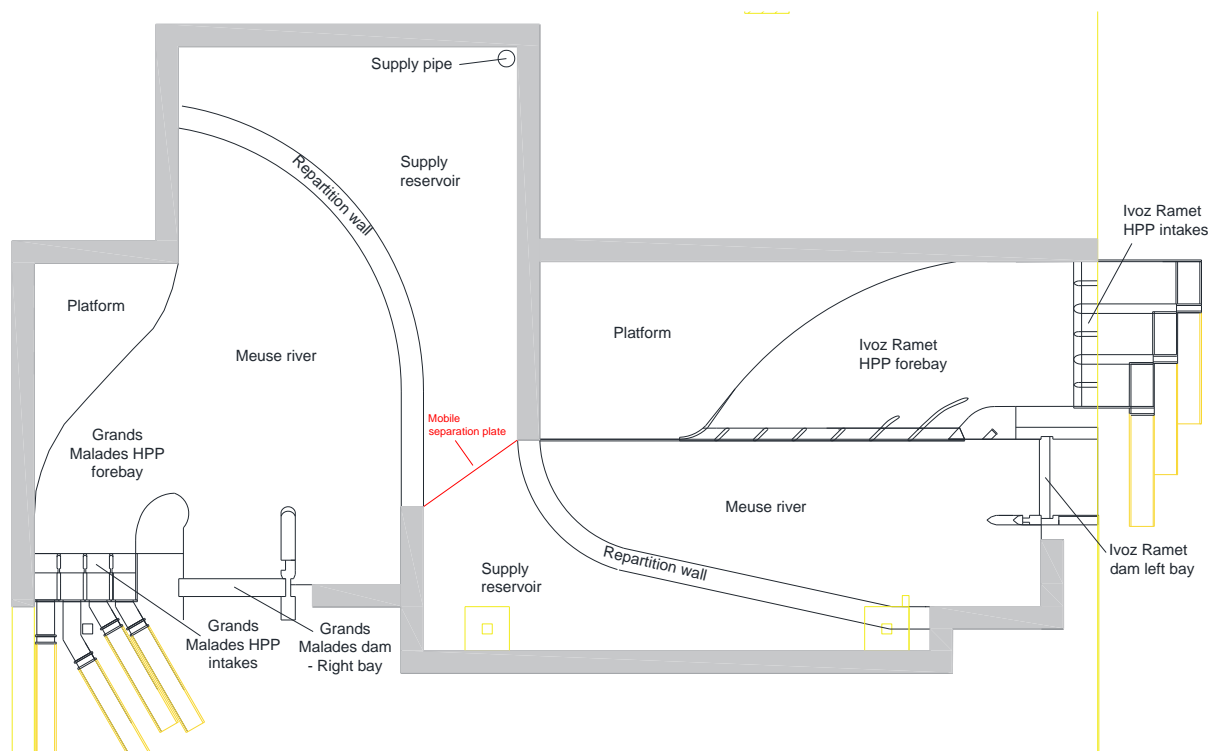


Figure VIII-10: plan view of the scale models

### VIII.5 Water supply system

The water supply system is a closed circuit: a regularized pump takes water from a storage tank and injects it in the model. The water enters the supply reservoir through a pipe and then a repartition wall made of perforated bricks (uniform velocity distribution along the reservoir upstream

limit, identical to the numerical model). Downstream of the model, a collecting channel brings the water back to the storage tank.

### VIII.6 Materials

The HPP and the mobile dams structures have been made of PVC, aluminium and 3D printed plastic parts. Meuse River and intake channels bathymetry has been made of concrete blocks covered by a layer of mortar. High-density foam has been used to model the area where fish passage intakes are located (Figure VIII-11). This makes easiest the adaptation and optimization of the geometry of these structures.



Figure VIII-11: Separation wall on Grands Malades model made using high-density foam (yellow material)

### VIII.7 Boundary conditions

The upstream boundary condition is the total discharge injected in the scale models.

Downstream, the discharge is controlled at the HPP by adjusting the opening of valves located downstream of each turbine and at the fish passage also by adjusting a valve. These adjustments are done in a way to get a target water level in the model, corresponding to the operating level of the navigable reach upstream of the dam (78.4 m at Grands Malades and 64.45 m at Ivoz Ramet).

### VIII.8 Measurement devices

Several measurement devices have been used during the scale model building and operation:

- A cathetometer Wild equipped with a vernier (accuracy of 0.2 mm) and a laser level to measure the elevations of the whole of the model elements during their construction;
- An electromagnetic discharge meter (accuracy of 1% at full span) positioned on the upstream water supply pipe to measure the discharges injected in the model;
- An Acoustic Doppler Velocymeter to measure 3D velocity components at selected locations;
- A camera Panasonic DMC-GH4 to take films and pictures of the tests.

### VIII.9 Drawings

In order to build the models, detailed drawings of the structures and topography have been made by the Laboratory at the model scale, from the project and building drawings provided by EDF Luminus and Service Public de Wallonie.



## VIII.10 Views of the scale models

The following pictures show general views of the scale models (Figure VIII-12 to Figure VIII-14).

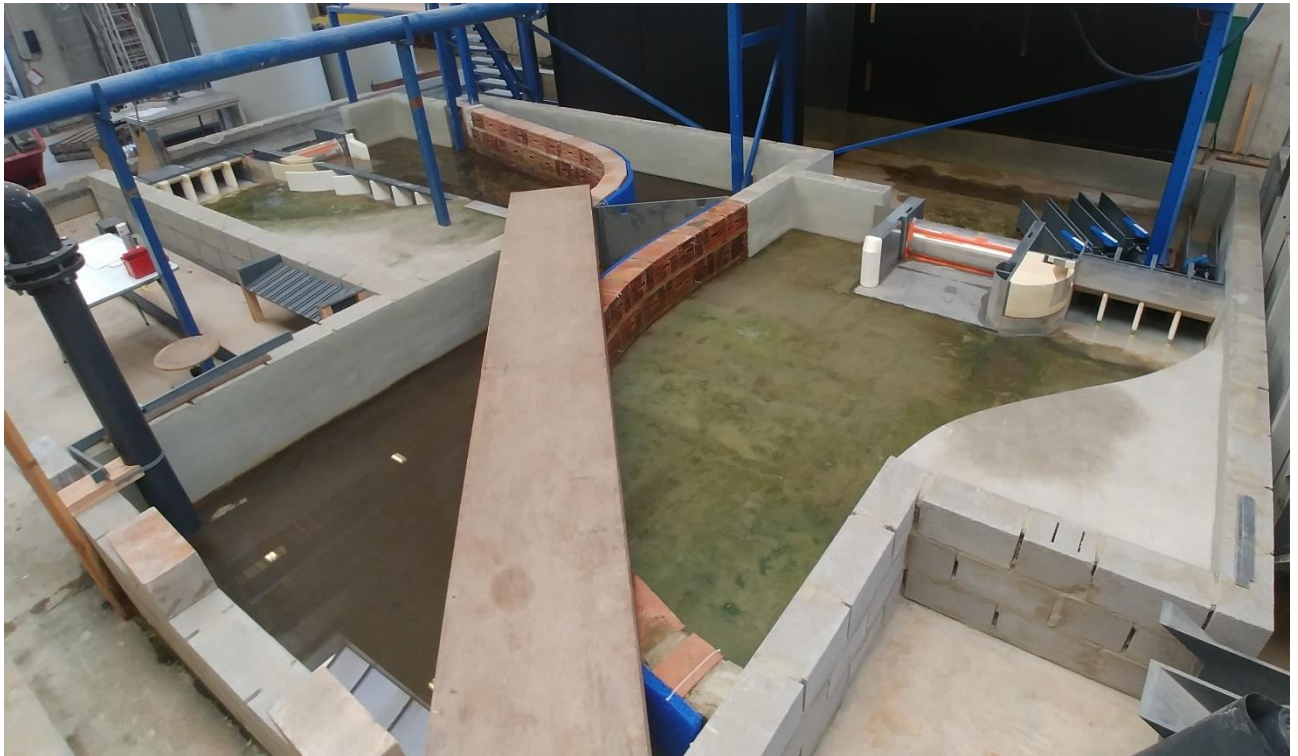


Figure VIII-12: General view of the scale models



Figure VIII-13: General view of Grands Malades scale model





Figure VIII-14: General view of Ivoz Ramet scale model

## IX. Geometry of the fish passages intakes

### IX.1 Methodology

The best general location of the fish passages intake has been defined for each pilot sites using the numerical models and smolts presence density maps (see chapter VII). After this analysis, a first geometry of the fish passages intake has been drawn by Arcadis and represented on the scale models (initial geometry). This first geometry respects literature criteria on water depth and flow velocity evolution along the structure to direct fishes downstream.

For this initial geometry, 3D velocity measurements have been done on the scale models to characterize the general flow conditions approaching the intakes. In a second step, the surface currents in the Meuse river have been studied by analysing the motion of 2 cm diameter floats released upstream of the models (Figure IX-1). Efficiency of the fish passages has been assessed considering the extent of the area of floats attraction by the fish passage, i.e. the ability of the fish passages to create surface currents directed towards the passage. Fish passages are thus dedicated to salmon smolts downstream migration.

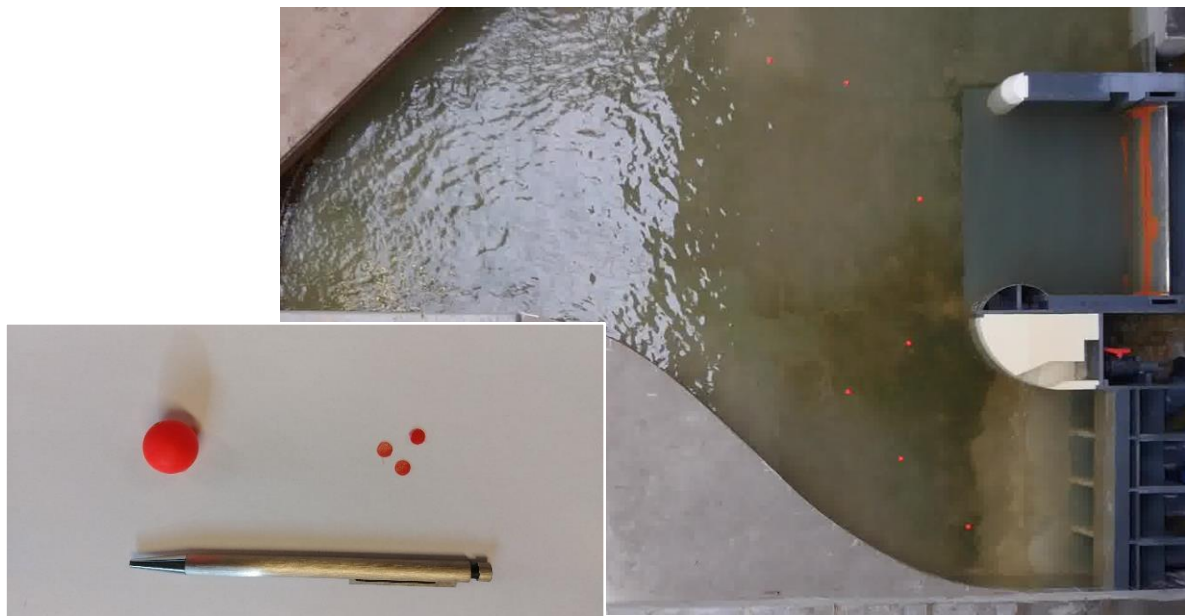


Figure IX-1: Floats used for surface currents characterization (left) and example of instantaneous location of floats in the Grands Malades model (right)

The operation condition of the HPP considered for each pilot site is the one of the equipment discharge through the turbines and no discharge released at the dam. As explained in chapter VII the discharge through the fish passage is 3.4 m<sup>3</sup>/s at Grands Malades and 7.1 m<sup>3</sup>/s at Ivoz Ramet.

In a second time, the initial geometry of the fish passages has been modified in concertation with Arcadis to increase the area of floats attraction and thus increase the efficiency of the structure regarding expected smolt attraction. Again, this increased efficiency has been verified by mean of floats tracking.

### IX.2 Grands Malades pilot site

#### IX.2.1 Initial geometry

The initial geometry of the fish passage intake at Grands Malades is shown on Figure IX-2. It is a 4.3 m wide intake located on the right side of the separation wall between the HPP and the dam, close to the HPP but still in the curve section of the wall. The entrance level is at elevation 76.40 m (2.0 m below the free surface elevation in the Meuse River). The intake bottom elevation increases

downstream to reach level 77.49 m. In the same time, the intake width decreases to 2.2 m. The intake diverts a discharge of 3.4 m<sup>3</sup>/s when Meuse elevation is at level 78.4 m.

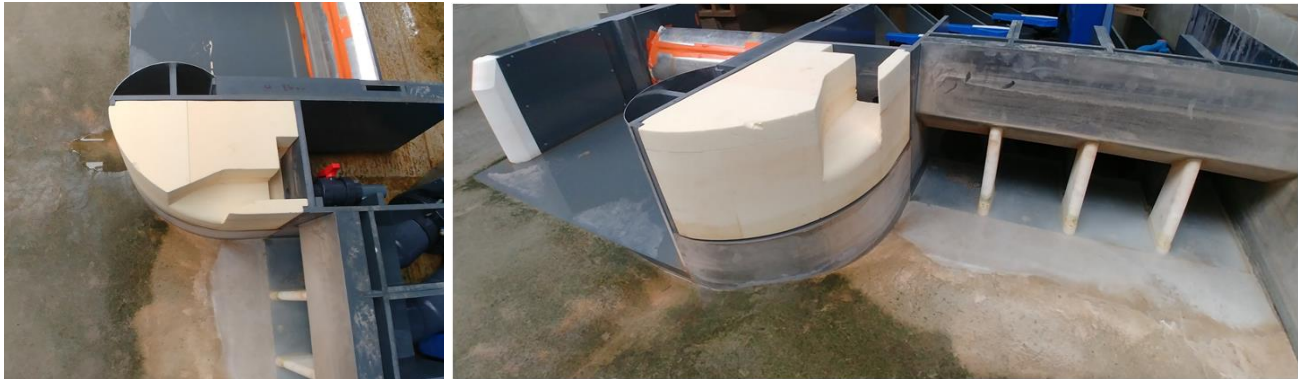


Figure IX-2: Initial geometry of fish passage intake at Grands Malades

The 3D flow velocities have been measured in front of the fish passage intake using an ADVP. Two elevations have been considered for the measurements (73.90 m and 75.70 m - Figure IX-3) with 17 locations (Figure IX-4). Velocities have been measured with the fish passage opened or closed.

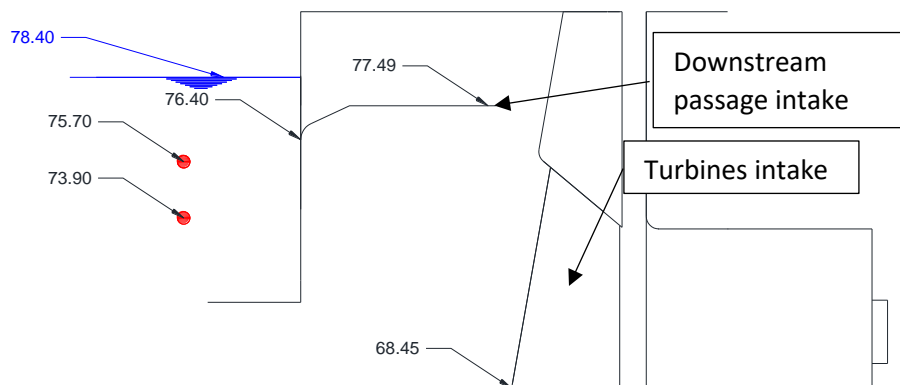


Figure IX-3: Elevations for 3D flow velocities measurement at Grands Malades

Figure IX-4 shows the horizontal flow velocity components measured on the Grands Malades site scale model. There is very small influence of the fish passage opening at the measurement locations, i.e. around the centre of the water column. Vertical velocity components at each measurement location is in the order of a few cm/s, i.e. negligible. These results suggest that the fish passage effect will probably be concentrated close to the free surface, as it will be shown with floats tracking.

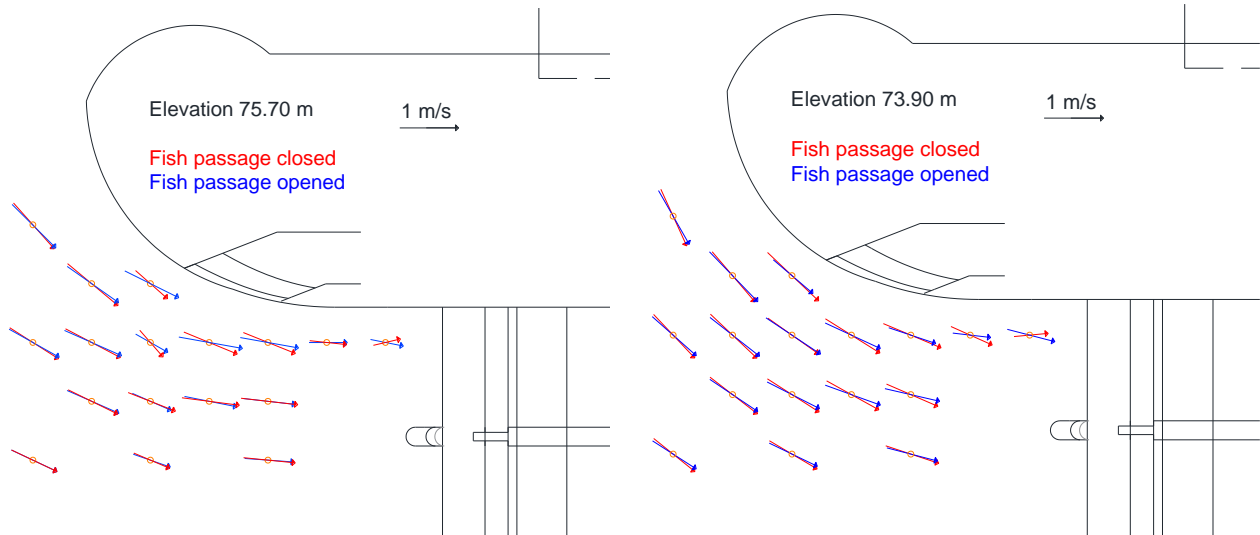


Figure IX-4: Horizontal flow velocity components on Grands Malades scale model

Results of float tracking are shown on Figure IX-5 with the fish passage closed and on Figure IX-6 with the fish passage opened.

With a closed fish passage, the floats are trapped in a recirculation area on the left side of the intake channel, in front of the turbines. This corresponds to a place of debris accumulation on the prototype. Given the extent of the recirculation, a few floats are stopped at the entrance of the fish passage.

When the fish passage is opened, the recirculation is still visible and it still traps most of the floats entering the intake channel. However, its extent is reduced. Floats entering the intake channel on the left side, along the separation wall, enter the fish passage.

Initial design of the fish passage can thus create significant surface currents and attracts floats, but on a very limited area on the left side of the intake channel.

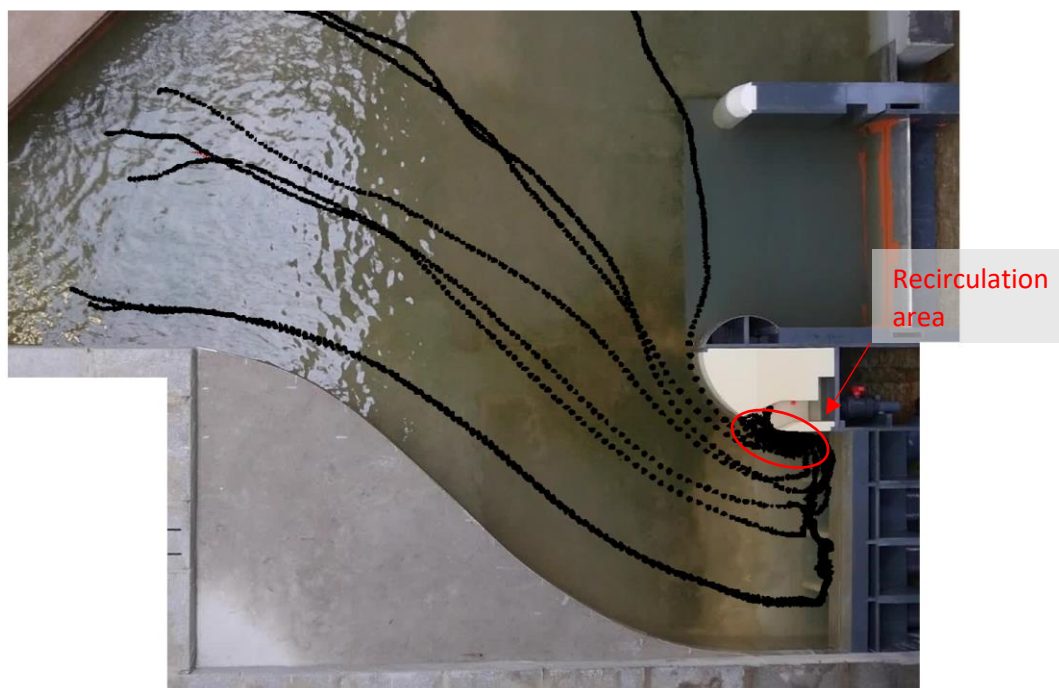


Figure IX-5: Floats trajectories without fish passage at Grands Malades (fish passage closed)



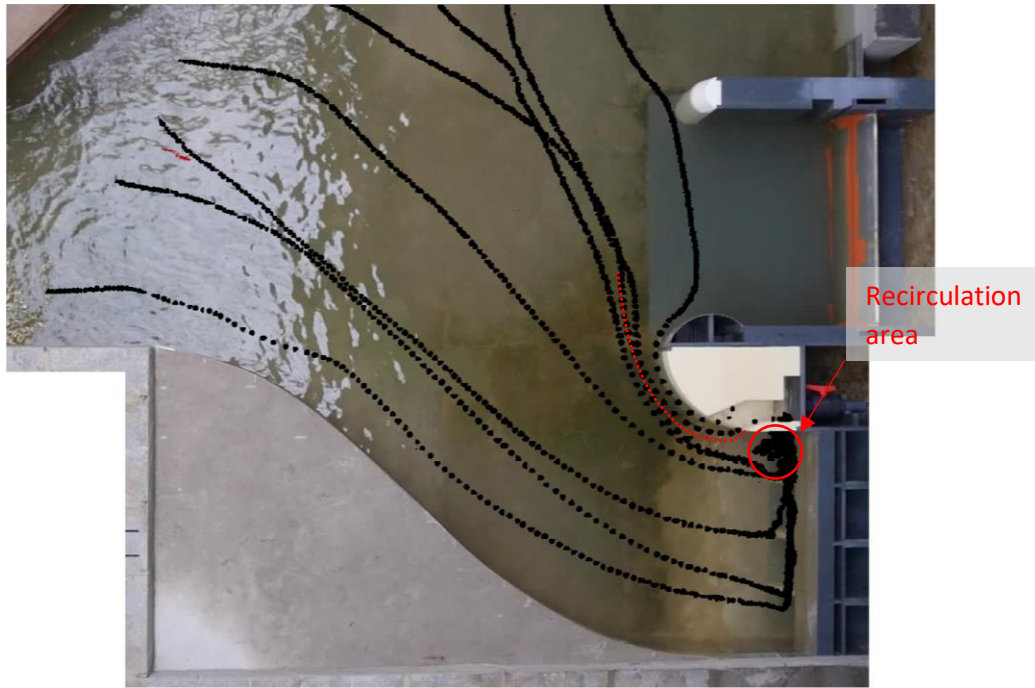


Figure IX-6: Floats trajectories for initial geometry of fish passage at Grands Malades (fish passage opened)

### IX.2.2 Optimized geometry

In order to increase the extent of the fish passage attraction area, the intake should be located at a place with lower flow velocities, i.e closer to the HPP. If we do so, the fish passage attraction will also act on the recirculation area and in particular decrease its extent. Looking carefully to the existing structures drawings with Arcadis, it has been found possible to locate the fish passage intake very close to the HPP mask wall. The elevations of the intake are the same as for the initial geometry. The intake is a little enlarged at 3 m. The modified geometry of the fish passage intake at Grands Malades is shown on Figure IX-7.



Figure IX-7: Modified geometry of fish passage at Grands Malades

Results of float tracking are shown on Figure IX-8 with the fish passage opened.

The recirculation on the left side of the intake channel is no more visible. All floats enter the fish passage either straight from the intake channel (first third of the channel width on the left side) either after blocking against the mask wall and low velocity translation along the wall. At the end of



the test, all the floats enter the fish passage except the one following the right bank of the channel, which is blocked on a stagnation area at the right side extremity of the mask wall.

Optimized geometry of the fish passage increases significantly the area with surface currents directed towards the passage and thus increase the floats attraction. This should improve significantly the attraction to the passage of smolts blocked in front of the mask wall.

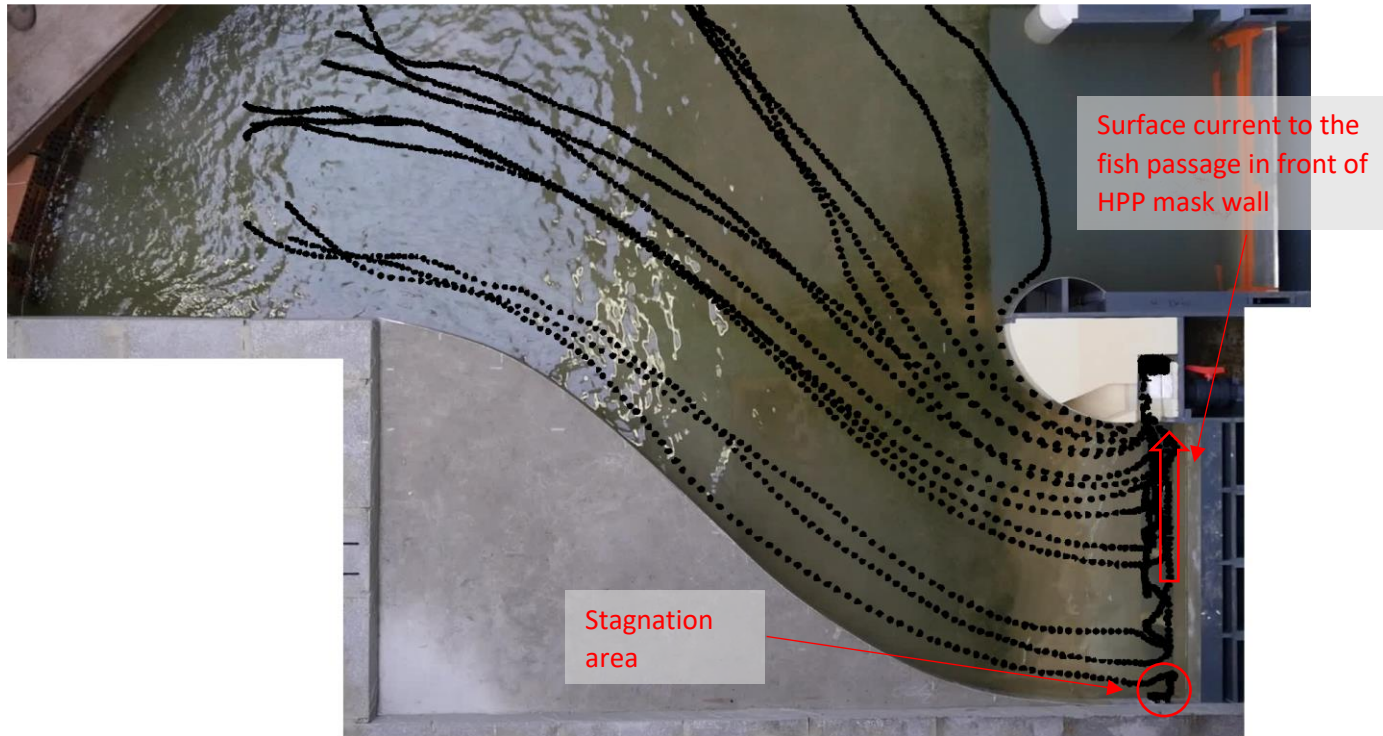


Figure IX-8: Floats trajectories for modified geometry of fish passage at Grands Malades

### IX.3 Ivoz Ramet pilot site

#### IX.3.1 Initial geometry

The initial geometry of the fish passage intake at Ivoz Ramet is shown on Figure IX-9. It is a 8.3 m wide opening intake located on the right side of the surface beam, close to the fish ladder outlet in the separation wall between the HPP and the dam. The entrance level is at elevation 62.45 m (2.0 m below the free surface elevation in the Meuse River). The intake bottom elevation increases downstream to reach elevation 63.55 m. The intake width perpendicular to the flow is 5.90 m. The intake diverts a discharge of 7.1 m<sup>3</sup>/s when Meuse elevation is at level 78.4 m.



Figure IX-9: Initial geometry of fish passage intake at Ivoz Ramet

The 3D flow velocities have been measured in front of the fish passage intake using an ADVP. Two elevations have been considered (61.45 m and 59.45 m - Figure IX-7) with 17 locations. As for Grands Malades, Velocities have been measured with the fish passage opened or closed.

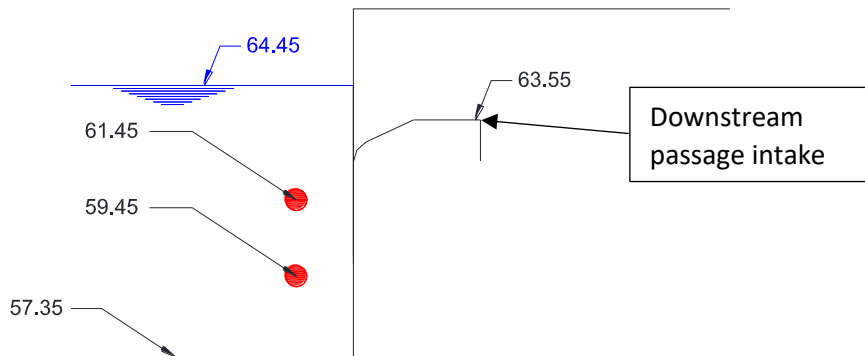


Figure IX-10: Elevations for 3D flow velocities measurement at Ivoz Ramet

Figure IX-11 shows the horizontal flow velocity components measured on the Ivoz Ramet site scale model. As for Grands Malades, there is very small influence of the fish passage opening at the measurement locations, i.e. around the centre of the water column. However, velocities amplitude is more than 2 times smaller than at Grands malades. Vertical velocity components at each measurement location is negligible, around 1 cm/s. Again, these results shows that the fish passage should have low attraction in the middle or at the bottom of the water column, and higher effect close to the free surface, where the smolts are expected to be.

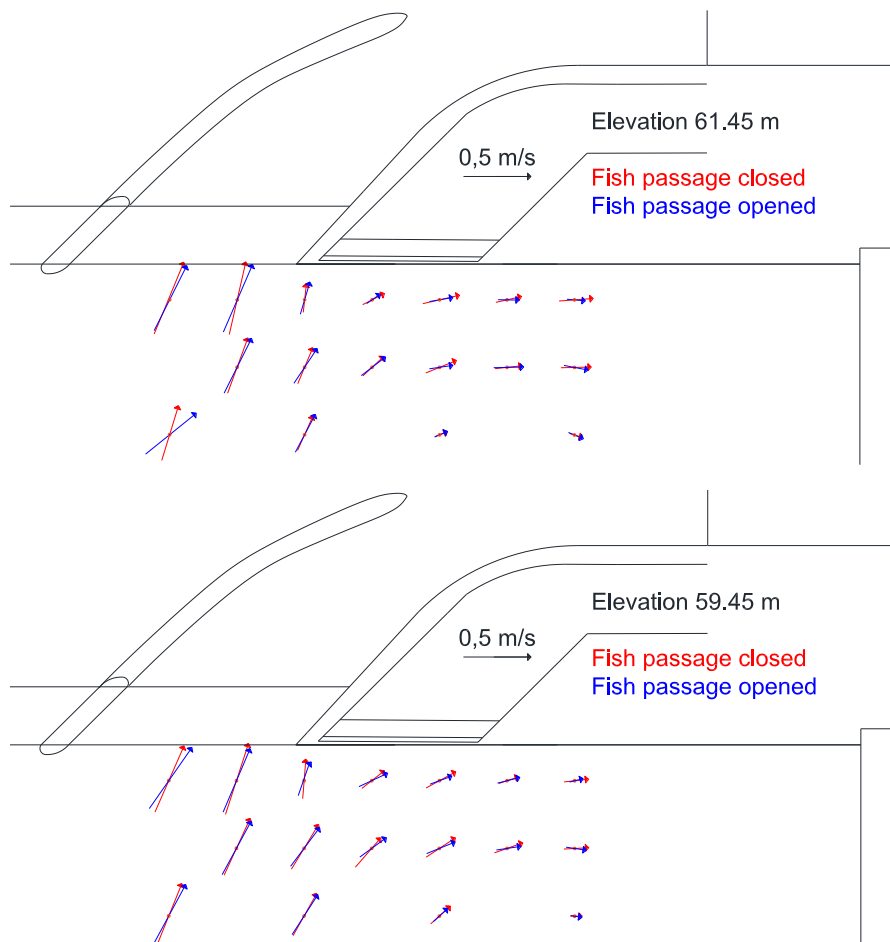


Figure IX-11: Horizontal flow velocity components on Ivoz Ramet scale model

Results of float tracking are shown on Figure IX-12 with the fish passage closed and on Figure IX-13 with the fish passage opened.

In both cases, all the floats going to the water intake are stopped by the surface beam and become motionless from this point. Floats launched on the right side of the intake channel are trapped in a large recirculating area taking place in front of the first gate on the left of the dam. When the fish passage is opened, the extend of the recirculation area decreases and a few floats are attracted into the passage. The attraction area is however limited in the Meuse river and floats blocked along the surface beam are never attracted to the passage.

Initial design of the fish passage is thus not effective to create significant surface currents in front of the surface beam and thus attracts floats blocked at this place.

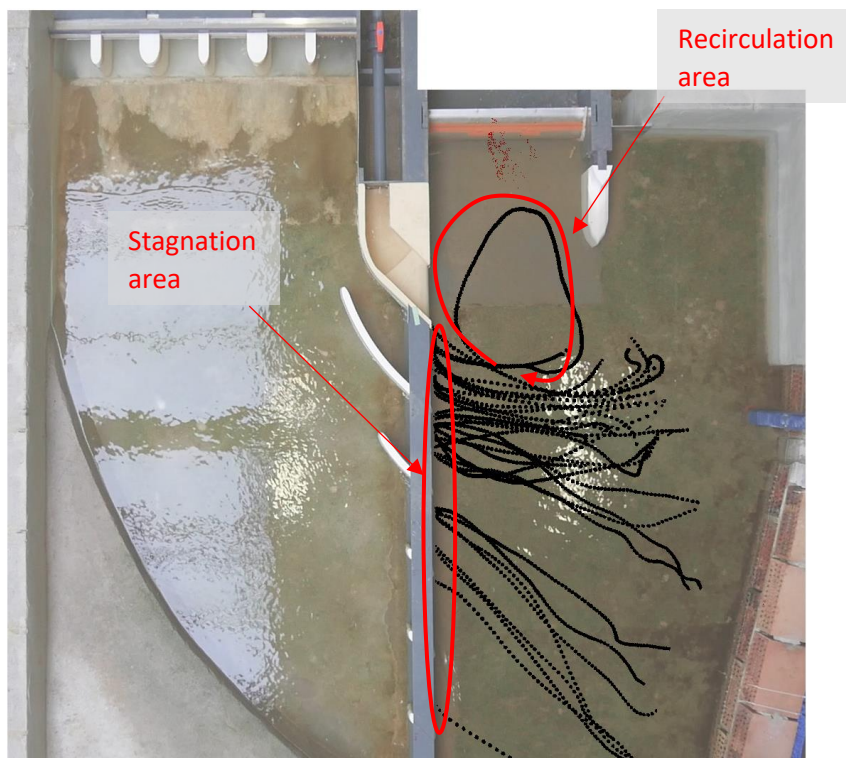


Figure IX-12: Floats trajectories without fish passage at Ivoz Ramet (fish passage closed)



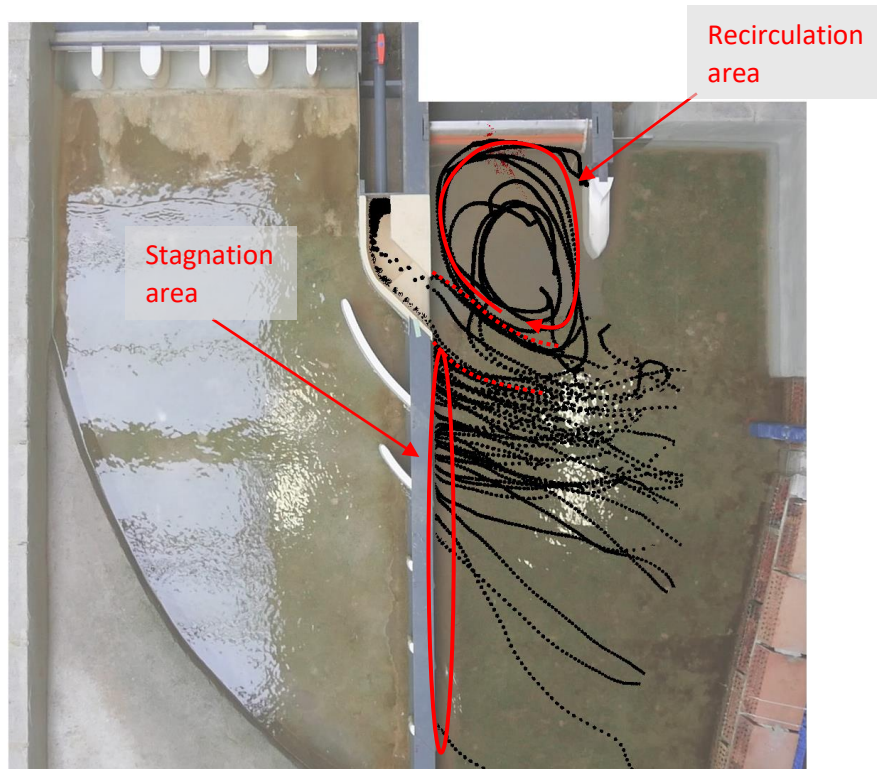


Figure IX-13: Floats trajectories for initial geometry of fish passage at Ivoz Ramet (fish passage opened)

### IX.3.2 Modified geometry

When looking closer to the feasibility of the proposed solution, and in particular when looking at support conditions for the surface beam, it appeared that the separation wall geometry was not exactly as presented on the available drawings. On-site inspection by divers confirmed a different geometry of the upstream extremity of the separation wall and thus of the surface beam supporting conditions. These new elements have been taken into account to modify the design of the intake of the fish passage on the model. This had significant impacts on the intake geometry, and in particular on the location of the intake weir, as well as on the HPP water intake area (Figure IX-14).

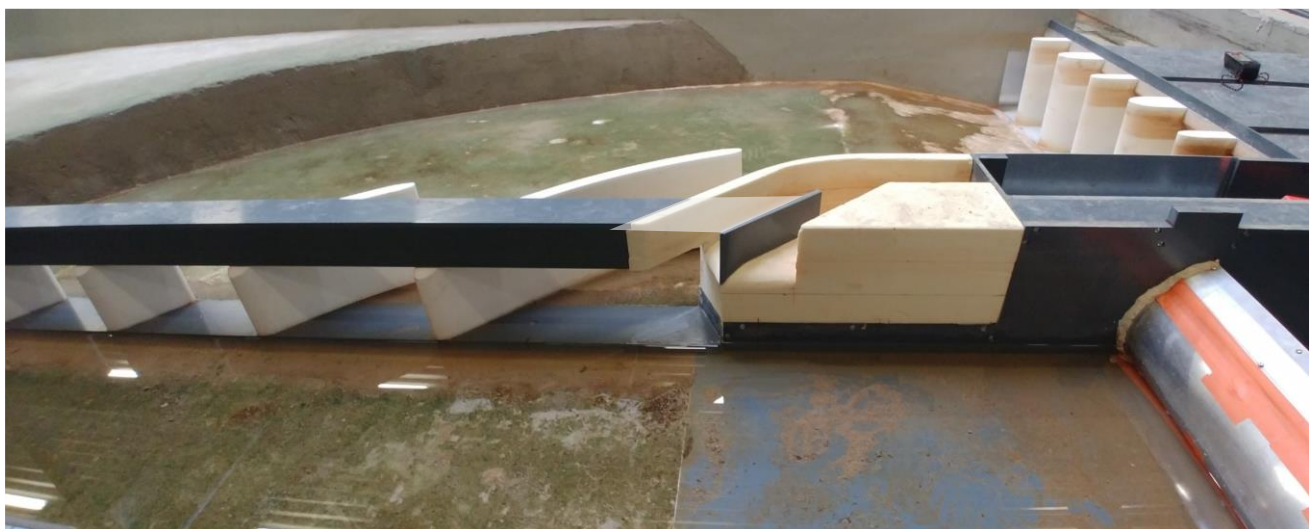


Figure IX-14: Modified geometry of fish passage intake at Ivoz Ramet

Results of float tracking are shown on Figure IX-15 with the fish passage opened.

Floats trajectories are similar to what has been observed with the initial design, except that now the floats stopped in front of the surface beam close to the fish passage are attracted to the passage. This obviously increases significantly the efficiency of the passage.

A further optimisation of the shape of the wall on the left side of the fish passage (connection with the surface beam) should enable to increase again the attraction of the passage.

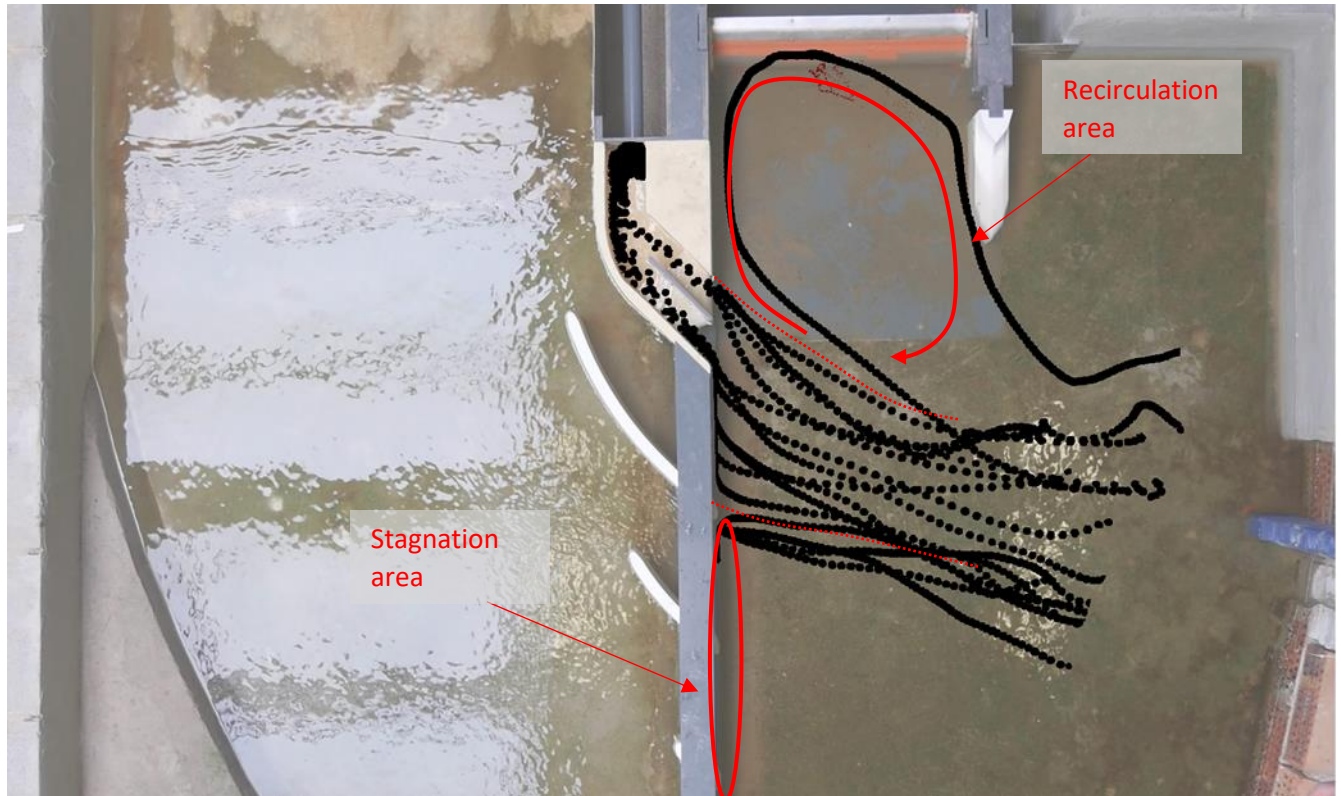


Figure IX-15: Floats trajectories for modified geometry of fish passage at Ivoz Ramet

#### IX.4 Conclusion

The preferred locations for fish passage intakes defined by means of numerical modelling have been validated and optimized on physical scale models. The geometry of these intakes has been modified/optimized in order to improve the system efficiency in terms of attraction. This attraction has been characterized by focusing on the free surface currents orientation around the fish passage in order to be most attractive for smolts.

As a result, for both pilot sites, considering constraints on diverted discharge and for the worst case of HPP operation, an optimized geometry of the fish passage intake able to create significant surface currents to the desired direction has been defined.



## X. General conclusions

The first part of the Action A3 of the Life for Fish project was dedicated to the hydraulic modelling of the two pilot sites (Grands Malades and Ivoz Ramet) in order to design solutions aiming at improving the safe downstream passage of fishes arriving upstream of the powerplants.

Hydraulic modelling of the sites has been done using the two complementary approaches of numerical and experimental modelling (hybrid modelling). Results of hydraulic modelling have been used to analyse the possible correlation between hydraulic parameters and fishes' behaviour as well as designing the downstream passage solutions.

Regarding salmon smolts, the monitoring extends over a low-flow period of the Meuse river during the months of April and May 2017. A new methodology for the filtering of the raw 2D coordinates was suggested, based on the removal of the coordinates leading to unrealistic fish velocities. The analysis of the characteristics of the Meuse river during the period of observation argues in favour of steady simulations in which the Meuse discharge is entirely evacuated through the turbines of the hydropower plant.

Correlations between the computed hydrodynamic variables (absolute velocity, absolute discharge, 2D turbulent viscosity and velocity gradient) and the measured 2D coordinates of smolts are analysed through the comparison of maps showing the spatial distributions and through the use of an original methodology based on probability density functions. This methodology consists in the comparison of the distribution of hydrodynamic variables in a given zone of interest with the distribution of these variables at the smolt locations. Hence, the attractiveness or repulsion of smolts is assessed by the identification of the range of values of the hydrodynamic parameters for which the probability density of smolts is higher than the probability density of the hydrodynamic values. At both sites, the results indicate an attractiveness of the smolts in areas with higher velocities. At Grands-Malades, smolts are mainly located along the left side of the water intake where the velocities are the highest, whatever the combination of turbine opening. At Ivoz-Ramet, the topographic step and the surface beam at the entrance of the water intake have a strong blockage effect on the smolts. Along this topographic step, the correlation analysis shows that the smolts are more prone to stay in areas with higher velocity values.

Regarding eels, only a limited fraction of the observed fishes is passing through the turbines (resp. 20% and 30% at Grands-Malades and Ivoz-Ramet). Most of the passages through the turbines occur in the absence of discharge at the dam after a residence time around 3 days. On contrary, the residence time of the eels passing through the dam is as low as around 1 minute. At Grands-Malades, eels are strongly attracted by the discharge at the dam even if the flow field is mainly controlled by the discharge at the turbines. At Ivoz-Ramet, some observations of eels passing through the turbines were done when the discharge at the dam is significantly higher than at the turbines, which can be explained by the velocity field in front of the surface beam.

Considering the conclusions about fishes behaviour at both pilot sites, downstream passage solutions have been designed to be effective mainly for smolts; i.e. to create attraction conditions in the upper part of the water column. Varied locations for the intake of a fish passage able to create significant attraction currents close to the free surface have been considered by mean of numerical modelling. These locations and the corresponding intake geometry have been defined with the project partners given local constraints and regarding flow conditions in the current situation (no fish passage). The analysis has been done considering the worst-case situation in terms of Meuse discharge, i.e. the maximum discharge which could be evacuated through the turbines of the hydropower plant without any discharge evacuated through the mobile dams or the locks. At Grands-Malades, the computations show that the best solution is to locate the fish pass on the left side of the water intake, close to the turbines, and to design it narrow. At Ivoz-Ramet, the best fish passage location is on the right side of the water intake entrance, upstream of the surface beam. In order to

maximize the fish passage attractiveness, the wider fish pass entrance coupled to the highest attraction discharge is preferred.

These preferred locations and the corresponding intake geometries have been validated and optimized by means of a physical scale model study for each pilot sites. Both scale models have been designed considering the numerical model results. They represent, for each pilot site, the two first bays of the mobile dam close to the HPP and the HPP intake channel. Tests have been performed on the models to assess the efficiency of the fish passage intakes in terms of attraction by means of free surface currents directed to the passage.

As a result, for both pilot sites, considering constraints on diverted discharge and for the worst case of HPP operation, an optimized geometry of the fish passage intake able to create significant surface currents to the desired direction has been defined using large scale numerical modelling and local physical scale models.

These solutions should be implemented on site as next steps of the project (actions C1 and C2).